EVALUATION OF POTENTIAL THERAPEUTICS FOR NON-SMALL CELL LUNG CANCER USING 3D TUMOR SPHEROID MODELS

By

Hayden Eric Stoub

A THESIS

Submitted to
Michigan State University
in partial fulfillment of the requirements
for the degree of

Physiology — Master of Science

2022

ABSTRACT

EVALUATION OF POTENTIAL THERAPEUTICS FOR NON-SMALL CELL LUNG CANCER USING 3D TUMOR SPHEROID MODELS

By

Hayden Eric Stoub

The development of novel and improved therapies for cancers requires robust means of investigation that both effectively recapitulate tumor biology while also utilizing resources efficiently. 3D tissue culture methods, namely spheroids and organoids, have emerged as an effective bridge between conventional *in vitro* methods and *in vivo* animal models in cancer research. This thesis provides background into lung cancer and the current landscape of 3D *in vitro* models of cancer, as well as detailing two studies in which multicellular tumor spheroids were used to investigate the therapeutic potential of candidate compounds.

The first study uses an NCI-H358 multicellular tumor spheroid to investigate three compounds: Apigenin, a plant derived flavonoid; MSU42011, a novel retinoid x receptor (RXR) agonist; and CEP-1347, a mixed lineage kinase (MLK) inhibitor. It was found that Apigenin alone decreased the viability of spheroids, and that the combination of Apigenin and CEP-1347 synergistically decreased viability and increased cell death within the spheroids.

The second study uses a murine lung adenocarcinoma tumor spheroid model to investigate the effects of MSU-71, a novel inhibitor of the nuclear factor erythroid 2-related factor (NRF2) pathway, on macrophage-induced invasion and migration. This compound blocked both migration in conventional experiments along with spheroid invasion, indicating its potential efficacy in preventing LUAD progression. This study also adapted the spheroid invasion model for use in multiple human LUAD cell lines and THP-1 conditioned medium. The findings presented herein demonstrate the versatility and value of 3D tumor spheroid models in the cancer drug development field.

Dedicated to **Traci Lynn Stoub** and **Elaine Joyce Stoub**
in honor of their incredible strength, resolve, and fortitude.

ACKNOWLEDGEMENTS

I first and foremost thank my mentor, Dr. Kathleen Gallo, for allowing me the opportunity to begin my career as a scientist in her lab. Thank you for your guidance and for encouraging my scientific creativity. I would also like to thank Dr. Rupali Das for her valuable advice and feedback on my research and writing. Thank you to Dr. Andrea Doseff and her team for inviting me to do science alongside them, a collaboration that ultimately led me to my interests in 3D tissue culture models of cancer. A very special thanks to Dr. Karen Liby for her indispensable advice and encouragement, and for sparking an interest in me for drug development. Finally, thank you to Dr. Gina Leinninger, whose passion for educating the next generation of physiologists has been evident in the classroom as well as in her role as interim director of the graduate program.

Thank you to my lab mates Summer, John, and Eva, with special thanks to Dr. Sean Misek and Brandon Llewellyn, whose hands-on training was an integral part of my graduate education. Many thanks also to Michael Ramirez-Para and Meenakshi Sudhakaran, who laid the groundwork for my research interest in tumor spheroids, and without whom this work would not be possible. I also wish to thank my colleagues in the Department of Pharmacology and Toxicology, namely Jess Moerland, Lyndsey Reich, and Chris Occhiuto for their collegial partnership and indispensable advice. Thank you to my excellent student-colleagues in the Department of Physiology and Cancer Research Network with special thanks to John Vusich and Nick Giaccobi for their refreshingly heterodox perspectives and insights. I also extend my deepest gratitude to Jasmine Jackson, who has saved countless times me from the administrative perils and bureaucratic nightmares typical of the graduate school experience; her heroism cannot be overstated.

Thank you to the amazing educators that I have taught in my tenure at MSU. Thank you to Drs. John Zubek, Nara Paramaswaran, and Susanna Moore, as well as my physiology teaching teammates for a thoroughly enjoyable experience teaching physiology. A special thank you to Dr. L. Karl Olson for helping me to shape my teaching strategy and tactics. Thank you to my teaching mentor Dr. Doug Luckie, who sparked my passion for teaching and who continually serves as an example of innovative and dynamic ways of increasing the probability that students will learn something of value. Thank you to the faculty at Lyman Briggs College, Dr. Jim Smith, Dr. Shahnaz Masani, Dr. Cassie Dresser-Briggs, and Dr. J.P. Lawrence, as well as all the wonderful GTAs and ULAs I had the opportunity to teach alongside of; I've come to appreciate that high quality and thoughtful teaching beats the newest facilities and equipment every time.

Finally thank you to my family for their unconditional love and support throughout my time at MSU. Thank you to my sister Callie for cultivating my well-rounded intellectual interests, and my brother Colton for serving as an example of leadership, duty, and responsibility, and to my parents, Eric and Traci for instilling in me a deep love of learning and encouraging me to ambitiously pursue my goals.

Gloria in excelsis Deo

TABLE OF CONTENTS

LIST OF TABLES

LIST OF FIGURES

KEY TO ABBREVIATIONS

ΔD	change in diameter (final–initial)
ABL	ABL proto-oncogene1
AIS	Adenocarcinoma *in situ*
ALK	Anaplastic lymphoma kinase
AP-1	Activator protein-1
ARE	Antioxidant response element
ASCL1	Acheate-Scrute family BHLH transcription factor 1
ATM	Ataxia telangiectasia mutated
ATP	Adenosine triphosphate
ATR	Ataxia telangiectasia and Rad-3-regulated protein
AXL	AXL receptor tyrosine kinase
BACH1	BTB domain and CNC homolog 1
Bax	BCL2 associated X, apoptosis regulator
Bcl	BCL apoptosis regulator
BRAF	B-raf oncogene, serine threonine kinase
CC10	Clara cell 10 kDa secretory protein
CCL	CC motif chemokine ligand
CD	cluster differentiation
CDKN2A	Cyclin dependent kinase inhibitor 2A
CHK2	Checkpoint kinase 2

CK	Cytokeratin
CLDN	Claudin
CM	Conditioned Medium
cMET	MET proto-oncogene, receptor tyrosine kinase
CREBBP	CREB binding protein
CRIPSR/Cas9	Clustered regularly interspaced short palindromic repeat/Cas9
CUL3	Cullin 3
CXCL	CXC motif ligand
CYP2E1	Cytochrome P540 family 2 subfamily E member 1
DAPI	4',6-diamidino-2-phenylindole
DMEM	Dulbecco's modified Eagle's medium
DNA-PK	Protein kinase, DNA-activated, catalytic subunit
EC	Ethyl carbamate
ECM	Extracellular matrix
EGF	Epidermal growth factor
EGFR	Epidermal growth factor receptor
EML4	EMAP like 4
EMT	Epithelial to mesenchymal transition
EP300	E1A binding protein P300
EPHA2	EPH receptor A2
ER	Estrogen receptor
ERBB2	HER2 gene

ERK	Extracellular signal-regulated kinase
FBS	Fetal bovine serum
FBXO22	F-box protein 22
FOXP3	Forkhead box P3
FTH1	Ferritin heavy chain 1
GAPDH	Glyceraldehyde-3-phosphate dehydrogenase
GEMM	Genetically engineered mouse model
GPCR	G protein coupled receptor
GSH	Glutathione
GTP	Guanine triphosphate
H&E	Hematoxylin and eosin
HER2	Human epidermal growth factor receptor 2
HK2	Hexokinase 2
HLA	Human leukocyte antigen
HMOX1	Heme oxygenase 1 gene
HO-1	Heme oxygenase 1 protein
HRAS	Harvey rat sarcoma viral oncogene homolog
ICDO	International classification of diseases, oncology
IHC	Immunohistochemistry
IL	Interleukin
iNOS	Inducible nitric oxide synthase
JAK	Janus kinase

JNK	C-jun N-terminus kinase 1
KEAP1	Kelch-like ECH associated protein 1
Ki67	Marker of proliferation Ki-67
KMT2	Lysine methyltransferase 2
KRAS	Kristen rat sarcoma viral oncogene homolog
LCC	Large cell carcinoma
LTK	Leukocyte receptor tyrosine kinase
LUAD	Lung adenocarcinoma
LXR	Liver X receptor
MAB	Monoclonal antibody
MAPK	Mitogen activated protein kinase
MDM2	MDM2 proto-oncogene
MFI	Mean fluorescence intensity
MHC	Major histocompatibility complex
MIA	Minimally invasive adenocarcinoma
MKK	MAP kinase kinase
MLK	Mixed lineage kinase
Mre11	MRE11 homolog, double stranded break repair nuclease
MSKCC	Memorial Sloan Kettering Cancer Center
MYCL1	MYCL oncogene, BHLH transcription factor
NADH	Nicotinamide adenine dinucleotide
NCCN	National Comprehensive Cancer Network

NCI	National Cancer Institute
NFE2L2	Nuclear factor-erythroid factor 2-related factor gene
NFκB	Nuclear factor kappa B
NIH	National Institutes of Health
NK	Natural killer cell
NOTCH1	Notch receptor 1
NOXA	Phorbol-12-myristate-13-acetate-induced protein1
NRAS	Neuroblastoma ras viral oncogene
NRF2	Nuclear factor-erythroid factor 2-related factor protein
NSCLC	Non-small cell lung cancer
P:A	Perimeter to area ratio
PBS	Phosphate buffered saline
PD-1	Programmed death 1
PD-L1	Programmed death ligand 1
PDAC	Pancreatic ductal adenocarcinoma
PDX	Patient derived xenograft
PDYN	Prodynorphin
PI	Propidium iodide
PI3K	Phosphoinositide 3 kinase
PLC	Phospholipase C
PMA	Phorbol-12myristate-13-acetate
PPAR	Peroxisome proliferator-activated receptor

PTEN	Phosphatase and tensin homolog
PUMA	p53-upregulated modulator of apoptosis
Rad50	RAD50 double stranded break repair protein
RAF	Murine sarcoma viral oncogene homolog B
RAS	Rat sarcoma virus gene
RB1	Retinoblastoma transcriptional co-repressor 1
RLF	Rearranged L-myc fusion protein
ROS1	ROS proto-oncogene 1, receptor tyrosine kinase
RPMI	Roswell Park Memorial Institute cell culture medium
RTK	Receptor tyrosine kinase
RXR	Retinoid X receptor
SCC	Squamous cell carcinoma
SCLC	Small cell lung cancer
siRNA	Small interfering RNA
SLC7A11	Solute carrier family 7 member 11
SLK	STE20 like kinase
SNAI2	Snail family transcriptional repressor 2
SREBP	Sterol regulatory element binding transcription factor 1
STAT	Signal transducer and activator of transcription
STK11	Serine threonine kinase 11
TAM	Tumor associated macrophage
TCGA	The Cancer Genome Atlas

TGFβ	Transforming growth factor beta
TLR	Toll-like receptor
TNBC	Triple negative breast cancer
TNFα	Tumor necrosis factor alpha
TNFR	Tumor necrosis factor receptor
TP53	Tumor protein p53
TPA	12- O-tetradecanoylphorbol-13-acetate
TRAIL	TNF related-apoptosis inducting ligand
TRKA	Neutrohilic receptor tyrosine kinase 1
TTF-1	Thyroid transcription factor 1
VC	Vinyl carbamate
VEGF	Vascular endothelial growth factor
WT	Wild type

CHAPTER 1. Literature review of lung cancer

Lung Cancer Epidemiology & Etiology

Lung cancer is the leading cause of cancer deaths globally and is the first and third most frequently diagnosed cancer for males and females, respectively, worldwide [GLOBOCAN 2020]. In the United States, lung cancer cases constitute the second most frequently diagnosed cancer and the leading cause of cancer deaths, with 235,760 new cases and 131,880 deaths in 2021 [SEER 2021].

While random errors during DNA replication constitute a substantial part of all cancer risk [Tomasetti & Vogelstein, 2015], lung cancer etiology is influenced by both semi-modifiable risk factors unique to lung tissue, as well as fully modifiable environmental risk factors [Wu et al. 2018]. Based on data from The Cancer Genome Atlas (TCGA) project, the mutational burden of lung cancer is only exceeded by that of melanoma [Castle et al. 2019]. This is understandable considering both sites experience high environmental exposure relative to other cancers. Most mutations in melanoma, for example, result from melanocyte exposure to ultraviolet radiation, whereas lung cancer mutations result primarily from inhaled carcinogens from smoking and pollution.

Tobacco smoke is the most well recognized lung cancer risk factor [Cummings & Proctor, 2014][CDC, 2014]. Tobacco smoke contains over 70 known carcinogens, including *N*-nitrosamides,   formed during nicotine combustion [Bade & Dela Cruz, 2020]. These compounds activate canonical cancer signaling pathways such as mitogen activated protein kinase (MAPK), phosphoinositide 3-kinase (PI3K) and nuclear factor κ B (NFκB) pathways, in addition to forming DNA adducts, resulting in mutations and subsequent tumorigenesis

[Akopyan & Bonavida, 2006]. The most recent statistics indicate that 21% of Americans use tobacco products, with 16.7% using combustible tobacco products [Cornelius et al. 2020].

As with all cancers, early detection correlates with improved lung cancer outcomes [Inage et al. 2018]. Upon initial radiological finding of a potential lung malignancy, patients are evaluated based on clinical risk factors including age, smoking history, previous medical history, family history, occupational exposure, and comorbidities, alongside radiological findings such as nodule size, shape, and density, any parenchymal abnormalities, as well as metabolic activity as assessed through positron emission tomography [NCCN, 2021]. Radiomic signatures, patterns observed in the radiographic studies of lung cancer patients, have increasingly been leveraged to predict molecular alterations [Li et al. 2019][Tu et al. 2019], as well as cancer dissemination [Dou et al. 2018][Coroller et al. 2017], and prognosis [Huang et al. 2018][Li et al. 2020][Bortorollo et al. 2021].

Histological Subtypes of Lung Cancer

Despite the increasing clinical utility of molecular diagnostics, lung tumor histology remains a key component of clinical decision making. Histologic characteristics of lung tumors indeed often correlate with molecular alterations as well as tumor phenotype and prognosis [Zheng 2016][Borczuk et al. 2003]. Upon radiological evidence of lung nodules ≥6mm, histological analysis is performed on samples collected through sputum cytology, non-invasive and image guided biopsies, thoracocentesis, or open surgical samples stained with hematoxylin and eosin (H&E) [NCCN, 2021]. Morphology of the H&E-stained specimens has conventionally served as the primary diagnostic criteria, but immunohistochemical staining is now used as a routine tool in forming differential diagnoses [Travis, 2020].

The World Health Organization 2015 guidelines for lung tumor classification list 77 distinct histological types and subtypes of lung cancer [Travis et al. 2015]; broadly, lung cancers are classified into small cell (SCLC), comprising 10% of lung tumors and non-small cell lung cancers (NSCLC), comprising about 90% of lung tumors [Zheng, 2016].

Adenocarcinoma

The largest subtype of NSCLC, lung adenocarcinomas (LUAD), accounts for approximately 50% of all US lung cancer cases [Travis, 2020]. LUAD histopathology is characterized by glandular growth pattern and immunohistochemistry (IHC) staining positive for thyroid transcription factor 1 (TTF-1) and negative for p40 [Yatabe et al. 2019]. Adenocarcinoma *in situ* (AIS) and minimally invasive adenocarcinoma (MIA) are typically treated surgically with no further intervention. In addition to surgical resection, patients with invasive adenocarcinoma may receive chemotherapies including cisplatin or carboplatin, combined with pemetrexed, or paclitaxel, and radiotherapy. Targeted therapies are used based on the presence of their oncogenic targets as indicated through immunohistochemistry [NCCN, 2021] and DNA sequencing. With complete surgical resection, AIS and MIA have a 100% five-year survival rate [Noguchi et al. 1995]. The five-year survival rate of all lung adenocarcinoma combined is 28.5%, ranging from 70% for localized disease to 8.4% for disease with distant metastases at time of diagnosis [SEER, 2021].

Prominent oncogenes in lung adenocarcinoma include *KRAS, EGFR, ALK, ERBB2,* and *BRAF*; alterations in these genes are, practically speaking, mutually exclusive among tumors [Greulich 2010]. Importantly, targeted therapies directed against oncogenic EGFR, ALK, HER2 and BRAF are available and used clinically. *TP53, KEAP1,* and *STK11* are prominent tumor suppressors that are deleted, mutated, or otherwise inactivated in LUAD [Inamura 2017] [Greulich 2010].

Relative to other NSCLC tumors, adenocarcinoma has a higher level of CD45+ immune cell infiltration, with increased CD3+ T-cell and CD19+ B-cell infiltration, and decreased infiltration of macrophages and monocytes [Stankovic et al. 2019]. Single-cell RNA sequencing has recently allowed for higher resolution analysis of cell-specific roles in tissue and vessel remodeling, lymphoid immune response, and tumor progression in lung adenocarcinoma [Kim et al. 2020].

Squamous Cell Carcinoma

Squamous cell carcinoma (SCC) represents roughly 25% of NSCLC cases in the United States, and is subdivided into keratinizing, non-keratinizing, and basaloid subtypes [Travis, 2020]. SCC is also confirmed through p40/TTF-1 differential IHC staining (SCC staining p40- and TTF-1+) [Yatabe et al. 2019], and exhibits positive cytokeratin (CK) 5, CK6, and p63 immunostaining based on level of differentiation [Zheng 2016]. TCGA analysis revealed statistically significant mutations in *TP53, CDKN2A, PTEN, PIK3CA, KEAP1, KMT2D, HLA-A, NFE2L2, NOTCH1, RB1,* and *PDYN.* Notably, *TP53* is mutated in 90% of tumors, and pathway analysis revealed enrichment in oxidative stress response pathways (34% of tumors), PI3K/

AKT signaling (47% of tumors), and cyclin dependent kinase inhibitor 2A (CDKN2A) downregulation (72% of tumors) [Inamura 2017].

Like adenocarcinoma, SCC resection is followed by treatment with cisplatin or carboplatin in combination with either gemcitabine or paclitaxel [NCCN, 2021]. SCC tumors rarely harbor actionable mutations in *EGFR, ALK, ERBB2,* and *BRAF*, limiting available targeted therapies [Chan & Hughes, 2015]. The five-year survival for all SCC is 21.7%, ranging from 46.8% for localized disease to 5.8% for disease with distant metastases at the time of diagnosis [SEER, 2021].

SCC is more heavily infiltrated by CD117+ mast cells and CD3+ T-cells than other histological subtypes [Banat et al. 2015]. Importantly, SCC maintains a high rate of *HLA-A* mutations [TCGA, 2012], increasing neoantigen recognition for natural killer (NK) and T-cell mediated killing. Whole tumor exome sequencing has also been used to develop clinically leverageable indices that predict responsiveness to immunotherapy in squamous cell carcinoma along with other histological subtypes. [Karasaki et al. 2017].

Small Cell Carcinoma

Small cell lung carcinoma (SCLC) constitutes 13% of all lung cancers, and is further subdivided into homogeneous SCLC tumors and heterogeneous SCLC/NSCLC tumors [Travis, 2020]. SCLC most often presents centrally as an invasive perihilar mass with substantial necrosis and hemorrhage [Travis, 2020].

SCLC cells are small in comparison to other lung tumor types. Relatively high numbers of mitotic cells are usually observed in SCLC, an important differentiator of SCLC from other neuroendocrine type tumors [Travis et al. 2015]. Assessment of tumor grade and overall diagnosis of SCLC can be performed through H&E staining, although relevant IHC markers include pankeratin and neuroendocrine markers CD56, chromogranin, and synaptophysin [Yatabe et al. 2019]. Owing to the high amount of cell division, robust Ki67 staining is also a hallmark of SCLC [Travis, 2020] [Zheng 2016]. Importantly, the adenocarcinoma marker TTF-1 expression is observed in 90% of SCLC, making it unsuitable for positive confirmation of SCLC [Zheng 2016].

SRY-box transcription factor 2 (SOX2) amplification has emerged as a hallmark molecular alteration in most SCLC [Rudin et al. 2012]. Both classic tumor suppressors *TP53* and *RB* are nearly universally inactivated in SCLC [George et al. 2015]. Other hallmark molecular alterations include *RLF-MYCL1* fusion protein as well as mutations in histone modifiers *CREBBP, EP300,* and *KMT2A* [Inamura 2017]. Finally, *NOTCH* signaling is repressed in 25% of SCLCs, downregulating neuroendocrine differentiation through *ASCL1* [Crabtree et al. 2016].

After initial evaluation, SCLC patients are clinically stratified into "limited" or "extensive" stage groups based on TNM characteristics. Surgical resection is only indicated for patients diagnosed with stage I-IIA disease, which comprise <5% of SCLC cases. Systemic therapy for limited stage SCLC consists of cisplatin and etoposide, with the option of carboplatin substitution if cisplatin is poorly tolerated. Primary therapy for extensive stage

SCLC consists of carboplatin and etoposide, with the addition of programmed death ligand 1 (PD-L1) checkpoint inhibitors atezolizumab or durvalumab. Radiotherapy concomitant with systemic chemotherapy is used for both limited and extensive stage groups, with a shorter delay of the start of radiotherapy associated with improved survival. Notably, because of the propensity for SCLC to metastasize to the brain, prophylactic intracranial radiotherapy protocols have been developed for extensive stage groups [NCCN, 2021]. The five-year survival for all SCLC is only 6.9%, owing to most diagnoses occurring in advanced stages of the disease. Five-year survival of localized disease is 29.3%, versus <3% for disease with distant metastases [SEER, 2021].

Because of the scarcity of resected tumors to study, the microenvironment of SCLC is not as well characterized as other lung cancer subtypes. Absolute counts of immune cell populations have been observed to be similar to other histological subtypes [Banat et al. 2015]. Genetically engineered mouse models of SCLC have shown lower numbers of tumor infiltrating leukocytes relative to other subtypes, and a low level of innate immune cell expansion. The main immune population is T-cells, with a notable increase in γδ-T cells [Busch et al. 2016]. Immune checkpoint molecules are frequently expressed by tumor infiltrating lymphocytes, and are associated with high forkhead box P3 (FoxP3) + T-cell presence, a cell population known to protect tumors [Rivalland et al. 2017]. Checkpoint inhibitors are routinely used in SCLC therapy regimens, due to the high mutational burden of the cancer, which results in higher levels of tumor neoantigen formation [Calles et al. 2019]. However, SCLC has long been known to harbor mutations in *HLA-A, B,* and *C*, along with β2-

microglobulin, preventing effective major histocompatibility complex formation and allowing tumors to evade immune surveillance [Doyle et al. 1985].

Large Cell Carcinoma

Large Cell Lung Cancer (LCC) constitutes 1.5-3% of lung cancers and is defined as a poorly differentiated carcinoma that is not otherwise classifiable as another histological subtype by light microscopy, IHC, or mucin staining [Travis 2020].

LCC is characterized by negative IHC staining for TTF-1 (excluding LUAD), p40 (excluding SCC), and mucin (excluding mucinous LUAD) [Travis 2020]. Given the small fraction of tumors LCC represents, many molecular analyses of histological subtypes do not focus expressly on the subtype. The pattern of molecular alterations in LCC closely resemble LUAD with frequent mutations in *TP53, EGFR, KRAS, STK11, KEAP1, BRAF,* and *PIK3CA, and* prominent *ALK* rearrangements [Hwang et al. 2014] [Rossi et al. 2014] [Jordan et al. 2017; via cBioPortal].

Treatment guidelines for LCC are identical to those for adenocarcinoma, with systemic cisplatin and pemetrexed chemotherapy along with radiotherapy indicated after surgical resection [NCCN, 2021]. The overall five-year survival of LCC is 18.3%, with localized disease survival at 53.6% and survival for disease with distant metastases at 5.4% [SEER, 2021]. Literature on the immune hallmarks of LCC is sparse; compared to LUAD and SCC, LCC tumors exhibit higher inducible nitric oxide synthase (iNOS), as well as the expression of interleukins IL-1β, IL-4, IL-6, and IL-8 [Almatroodi et al. 2015], cytokines indicative of a pro-inflammatory microenvironment.

Prominent Molecular Alterations in LUAD

All cancers maintain some level of genomic, genetic, and epigenetic aberrancy compared to otherwise healthy tissue; however, lung cancers are remarkable for their high mutational burden [Castle et al. 2019]. With the development of therapeutic resistance, a wider battery of available targeted therapies is necessary. This section provides details on the most common molecular alterations in LUAD: *TP53, EGFR, KRAS,* and *ALK* (Figure 1.1). Background on *KEAP1* and *STK11* can be found in Chapter 3.

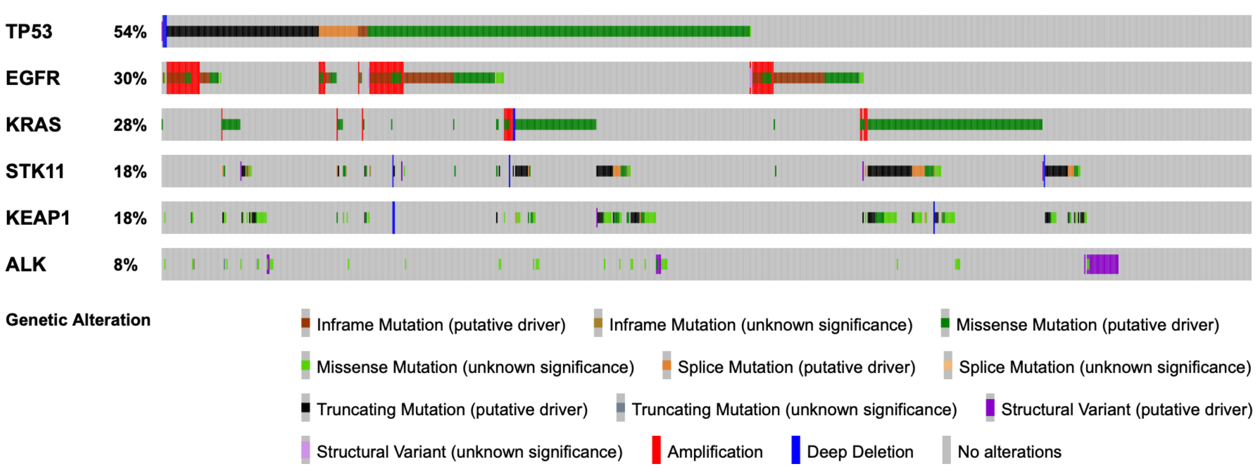

Figure 1.1 Prominent molecular alterations in LUAD. Genetic profiling of common genetic alterations in 915 LUAD tumor samples collected from 860 patients from [Jordan et al. 2016]; Figure generated from Non-Small Cell Lung Cancer (MSKCC, Cancer Discov. 2017) dataset [cBioPortal].

p53

The well characterized tumor-suppressor gene, p53, is often referred to as "the guardian of the genome", and is mutated in 50-70% of lung malignancies, with particularly high frequency in smokers and SCC [Gibbons et al. 2014] (Figure 1.1). p53 plays numerous roles as both a sensor of DNA damage, as well as an effector of tumor-suppressive processes. DNA damage specifically activates p53, which can in turn guide cellular responses ranging from apoptosis, cell cycle arrest, and senescence, to DNA repair and cell survival depending on the stimulus and extent of DNA damage [Vousden & Lane 2007].

DNA damage causes activation of three members of the PI3K-like kinase family: ataxia-telangectasia mutated (ATM), ataxia telangectasia and Rad3-related (ATR), and the DNA-protein kinase complex. ATM binds with MRE11 Homolog, Double Strand Break Repair Nuclease (Mre11), MRE11 Homolog, Double Strand Break Repair Nuclease (Rad50), and Nibrin to double-stranded DNA breaks. After autophosphorylation, ATM activates p53 by phosphorylating Ser15 and Ser20 (the latter mediated through CHK2). ATR is activated by single-strand DNA breaks, binding with the topoisomerase TOPBP1, replication protein a (RPA) family, and the 9-1-1 complex, and activates p53 by phosphorylation of Ser15. DNA-PK complex associates with the Ku70/80 heterodimer on double-stranded DNA breaks and phosphorylates p53 at Ser37. Phosphorylation of p53 at these sites prevents degradation by MDM2 and facilitates p53's activation of DNA repair mechanisms [Shi & Danson, 2020].

p53 plays a role in all major forms of DNA repair, which positions it as an important bulwark against the accumulation of mutations and more broadly against genomic instability [Williams & Schumacher, 2016]. Genomic instability, a hallmark of cancer, is increased when p53 is compromised, which can be due to loss of p53 function as well as gain of function p53 mutants. Whereas disruptions in the G1/S cell cycle checkpoint are observed in p53-null cells, p53 mutant cells also have perturbed M phase checkpoint, promoting aneuploidy [Hanel &

Moll, 2012]. As part of this M phase checkpoint, p53 transcriptional targets p21 and the mitotic checkpoint BubR1 activate and control centrosome homeostasis [Ho et al. 2020]. Additionally, p53 putatively plays a surveillance role for centrosomes as evidenced by direct association with the complex. p53 is also responsible for balancing homologous recombination and non-homologous end joining repair mechanisms, important repair mechanisms combatting genomic translocations and amplifications [Moureau et al. 2016][Ho et al. 2020].

When p53 is unable to successfully mediate DNA repair, its role switches to promote apoptosis guarding against the replication of abnormal cells. This is accomplished through transcriptional upregulation of pro-apoptotic factors such as BCL2-associated X (Bax), BCL2-binding component 3 (PUMA), and Phorbol-12-myristaate-13-acetate-induced protein 1 (NOXA), as well as direct activation of Bax by p53 and inhibition of anti-apoptotic factors Bcl-2 and Bcl-XL [Aubrey et al. 2017][Fridman & Lowe, 2003].

While clinically efficacious drugs targeting p53 have heretofore been unsuccessful, numerous tool compounds to restore p53 function have been developed or discovered. The primary mechanism by which these compounds act is by inducing conformational changes that stabilize the protein structure and restore DNA binding capabilities [Parrales & Iwakuma, 2016].

KRAS

The *RAS* family of genes–consisting of isoforms KRAS, NRAS, and HRAS–code for small guanine triphosphatases (GTPases) that, in their GTP bound form, activate numerous signaling pathways including MAPK and PI3K [Uprety & Adjei, 2020]. KRAS is mutated in approximately 30% of all lung cancers (Figure 1.1), with the majority of mutations resulting in the alteration of Gly12 which lies in the GTP binding domain [Campbell et al. 2016; accessed through cBioPortal]. These mutations "lock" KRAS in the GTP-bound conformation, disrupting GTP hydrolysis, resulting in constitutive activation of downstream signaling pathways [Zeitouni et al. 2016]. The degree to which various cancer cell lines with oncogenic KRAS are dependent on KRAS has recently been elucidated, revealing two molecular subtypes, KRAS-dependent and RSK-dependent cell lines with distinct morphological and metabolic phenotypes. The effectors which oncogenic KRAS engages are proposed to determine these phenotypes [Yuan et al. 2018].

KRAS has an emerging role as an important modulator of multiple elements of the tumor microenvironment [Carvalho et al. 2018][Dias Carvalho et al. 2020]. The tumor microenvironment of KRAS mutant mouse models of lung cancer is heavily infiltrated by myeloid cells, whereas the microenvironment of SCLC–predominantly $KRAS^{WT}$ tumors–are more infiltrated by CD3+ T-cells [Busch et al. 2016]. In a conditional $KRAS^{G12D}$ mouse model of lung cancer, using the chemokine 10 (CC10) promoter to localize KRAS mutation to club cells–a cell type exclusive to lung tissue and often the source of LUAD malignancy–KRAS mutation resulted in the elevation of the chemokines CCL2, CCL3, CXCL1, CXCL2, along with tumor necrosis factor α (TNFα), and vascular endothelial growth factor (VEGF) in bronchoalveolar lavage fluid [Ji et al. 2005]. KRAS also appears to drive Th17 T-cell infiltration and IL-17 upregulation [Chang 2015], which is a necessary step in lung cancer progression [Chang et al. 2014]. KRAS-mutant lung tumors also display upregulated IL-10 and transforming growth factor β (TGFβ), which directly inhibits NK cells along with suppressing CD8+ cytotoxic T cells through the activity of regulatory T-cells [Deng et al. 2020]. To what degree these suppressive factors are secreted from tumor cells directly or through M2-like tumor associated macrophages is still unclear. The effects of KRAS on the tumor microenvironment have also been researched in other KRAS-mutant malignancies such as pancreatic cancer [Hou et al. 2020], colorectal cancer [Park et al. 2021], and esophageal cancer [Essakly et al. 2020].

Translational research into KRAS-targeted therapy development has only recently been successful. Small molecule drugs have been investigated that bind to $KRAS^{G12C}$ by forming a covalent bond to the thiol group on the cysteine of the mutant protein [Lito et al. 2016]. This finding led to the development and US Food and Drug Administration (FDA) approval of the first targeted therapy for KRAS, sotorasib [Hong et al. 2020][Skoulidis et al. 2021]. While this represents a monumental advance in targeting a specific type of KRAS mutant found in lung cancers, therapeutic resistance can arise. Furthermore, there are still no clinically approved therapeutics that target KRAS mutant alleles other than $KRAS^{G12C}$.

EGFR

Epidermal growth factor receptor (EGFR) is a transmembrane receptor tyrosine kinase (RTK) and part of the broader ERBB family of RTKs. ERBB family members are commonly altered in lung cancer either through mutation (EGFR) or amplification (ERBB2) [Skoulidis & Heymach 2019]. These kinases are primarily known to activate MAPK signaling through the RAS/RAF/MEK axis, but can also activate other cancer-relevant pathways such as the PI3K/Akt axis, phospholipase C (PLC)-γ pathway, and signal transducer and activator of transcription (STAT) pathway signaling [Schlessinger 2004]. The activation of RTKs is mediated by the dimerization of individual RTKs, stabilized by the ligand EGF in the case of EGFR [da Cunha Santos et al. 2011].

EGFR is mutated in 14% of lung cancers (Figure 1.1) and has been successfully targeted therapeutically. The progress of EGFR inhibitor development is mainly attributable to the understanding of the protein structure and the structural impacts of specific mutations [Castellanos et al. 2017]. Perturbation of regulatory regions of the protein such as the αC-helix, activation loop, or adenosine triphosphate (ATP) binding regions are where mutations arise, and drugs bind selectively to mutant EGFR [Yun et al. 2007].

The L858R missense and E746-750 residue deletions represents 90% of the EGFR mutations. Gefitinib and erlotinib [Pao et al. 2004] were the first EGFR inhibitors to reach FDA approval for NSCLC treatment in 2003 and 2004, respectively [Roskoski 2019]. Ten years later, a second-generation inhibitor, afatinib, which binds covalently to the L858R mutant EGFR to inactivate it, was approved [Roskoski 2019]. This mechanism is shared by third generation inhibitor, osimertinib [Le & Gerber, 2019]. Resistance to these inhibitors, most notably through a T790M mutation [Kim et al. 2012a], has driven the development of third [Piotrowska et al. 2015] and fourth generation inhibitors [Wang et al. 2017] that inhibit the resistant EGFR variants. Small molecule tyrosine kinase inhibitors have the additional benefit of being orally available.

EGFR mutant lung cancer has also been successfully targeted with EGFR-directed monoclonal antibody therapies, namely cetuximab and panitumumab [Ciardiello & Tortora 2008]. Monoclonal antibodies (MABs) targeting oncogenes were first used against another RTK in breast cancer, HER2 [Cameron et al. 2017]; The HER2 antibody-chemotherapy drug conjugate Trastuzumab-deruxtecan has recently shown promise for relapsed HER2+ NSCLC [Li et al. 2021]. The ability for EGFR and HER2 to heterodimerize has spurred research into the efficacy of MAB combination therapies [Privitera et al. 2015] [Romaniello et al. 2018].

ALK

Rearrangements in the anaplastic lymphoma kinase (ALK) gene are present in approximately 8% of NSCLC patients (Figure 1.1) [Chia et al. 2014]. The most prominent ALK fusion partner is echinoderm microtubule-associated protein like-4 (EML4), which constitutes approximately 30% of all ALK rearrangements [Sasaki et al. 2010]. Apart from translocations, activating point mutations in the kinase domain of ALK are also seen in numerous cancers [Hallberg & Palmer, 2018]. Like EGFR, ALK fusion proteins activate numerous downstream oncogenic signalling pathways including MAPK, PLC-γ, JAK/STAT, and PI3K pathways [Della Corte et al. 2018].

The first ALK inhibitor to gain FDA approval–crizotinib–targets ROS1 and cMet in addition to ALK [Gristina et al. 2020]. So successful was the initial PROFILE 1001 that an expansion cohort was added to the dose escalation phase of the trial [Shaw et al. 2019]. Development of the second generation ALK inhibitors ceritinib and alectinib led to their approval as second-line therapies for crizotinib resistant NSCLC and later as first-line treatments [Gristina et al 2020]. Ensartinib is another second generation ALK inhibitor that has recently been developed with broader inhibitory activity against MET, AXL, ABL, EPHA2, LTK, ROS1, and SLK. Finally, entracitinib, a third generation ALK inhibitor with additional activity against TRKA-C and ROS1, was developed to combat intracranial metastases, owing to its ability to cross the blood brain barrier [Gristina et al 2020]. Like EGFR inhibitors, ALK inhibitors can be administered orally and are well tolerated compared to cytotoxic chemotherapies.

Models used in lung cancer research

One of the goals of cancer research[1] is to leverage basic biological knowledge to develop effective therapies that improve quality of life, length of survival, or preferably both. Drug discovery has evolved over time from a phenomenological and descriptive practice to evidence-driven discoveries of refined mechanisms and precision medicines. Critical to this empirical approach are models of cancer that allow investigators to better understand how drugs and drug-candidates affect biology at the various levels of organization. This section

[1] Some may argue this is indeed the *only* goal of cancer research as cancer is an objectively tragic phenomenon to befall a person. While I do not intend to thoroughly arbitrate the philosophy of science surrounding biomedical research, there are interpenetrating utilitarian and moral arguments to be made for the necessity of basic research to translate into findings that lift humanity. For the purposes of this thesis, I will define the *telos* of cancer research as a pursuit of a cure to this terrible set of diseases.

provides background on conventional preclinical cancer models (cell lines and mouse models) as well as the new generation of 3D tissue culture models that have enabled more productive drug discovery efforts to emerge.

Lung Cancer Cell Lines

The NCI-60 cell line panel, which was developed as an initiative for novel drug development in cancer research, includes nine human non-small cell lung cancer lines [Shoemaker 2006]. Starting in 2016, the National Cancer Institute (NCI) has begun to phase out the original NCI-60 in favor of cell lines generated from patient derived xenograft (PDX) tumors grown in nude mice with the idea that PDX lines are closer to the tumor of origin, rather than being grown *ex vivo* for extended periods of time [Ledford 2016]. The main strengths of tumor cell lines are their ease of use, affordability, and genetic fidelity to the original tumor [Gazdar et al. 2015]. Human cell lines can be xenografted for *in vivo* studies but require immunodeficient mice. Cell lines derived from mouse models of lung cancer are also useful in both *in vitro* applications and syngeneic *in vivo* applications, the Lewis Lung Carcinoma (LLC1) cell line, which harbors mutant NRAS, being the most prominent example [Bertram & Janik, 1980].

Mouse models

Injection of DNA adduct forming carcinogens such as vinyl carbamate (VC) or ethyl carbamate (EC) is a widely used model for spontaneous NSCLC generation. VC carcinogenesis is in part driven by hotspot mutations of KRAS, and can elicit lung tumor formation even in relatively resistant mouse strains such as C57BL6 [Massey et al. 1995]. A/J mice are frequently used as the higher CYP2E1 levels facilitate more bioactivation of VC, resulting in more efficient carcinogenesis [Forkert 2010]. Genetically engineered mouse models (GEMMs) of lung cancer are limited, and widespread use has been mostly restricted to SCLC [Rudin et al. 2019][Lorz et al. 2021] and SCC [Singh et al. 2018]. KRAS mutation is commonly used as a driver for LUAD oncogenesis and has been combined with mutations STK11 [Ji et al. 2007], p53 [Busch et al. 2016], and EGFR [Busch et al. 2016], while RB has been ablated in neuroendocrine GEMMs [Lázaro et al. 2017]. The ability to develop GEMM models of LUAD is hampered by mouse mortality rates prior to tumor formation, poor recapitulation of human pre-invasive disease, and lack of genetic disruption brought on by tobacco exposure [Gazdar et al. 2015].

3D in vitro models

The aim of three-dimensional culture methods is to recapitulate the biology of the system being modeled more accurately. With varying degrees of sophistication, 3D cultures more accurately emulate cell-cell and cell-matrix interactions, metabolic and pharmacological spatial gradients, tissue differentiation and architecture, and multicellular systems. The two main classes of 3D culture systems are multicellular spheroids and organoids. While there is some semantic overlap of the two, spheroids are usually generated from established cancer cell lines, do not retain the architecture of the tissue of origin, and are genetically clonal in contrast to organoids that are either derived from stem cells or resected tumor tissue, and often retain histological integrity, and are genetically heterogeneous [Gunti et al. 2021].

Multicellular Spheroids

Multicellular spheroids are 3D structures that are generated from cancer cell lines. Numerous methods to generate spheroids have been developed; multi-cell aggregates can be formed either through centrifugation or through the hanging drop method wherein a small drop containing cells are inverted allowing cells to aggregate at the bottom of the drop via gravity. These methods are relatively low cost in resources and time, and yield spheroids of consistent size and quality. Spinning bioreactor and rotating wall cultures allow for high numbers of spheroids to be generated, but yield a range of spheroid sizes and cannot be used for cells with low cohesion [Gunti et al. 2021]. Other methods of spheroid generation have been developed utilizing microfluidics, magnetic levitation, or 3D printing, However the cost and scalability for these methods are prohibitive for large scale use [Lv et al. 2017].

In extracellular matrix (ECM)-supplemented spheroid culture, integrin expression by the cells allows for the loose aggregation of spheroids, followed by an upregulation of cadherins. Once sufficient E-cadherin expression is achieved, spheroids take on a smooth epithelium-like outer surface [Lin et al. 2006]. Large (≥500μm) spheroids also exhibit nutrient/waste gradients and display a continuum of proliferating, quiescent, and necrotic cells [Nunes et al. 2018]. Finally, 3D tumor spheroids also exhibit gradation in penetrance of drugs and demonstrate the shortcomings of 2D cultures in modeling biological responses to therapies [Nunes et al. 2018][Ekert et al. 2018].

Experiments using tumor spheroids to investigate migration and invasion fall into two general categories. In planar surface experiments, the behavior of 3D tumor spheroids is characterized as they interact with a 2D surface. This method has been used to investigate ECM-tumor cell interactions, specifically the effects of matrix substrates with different biophysical characteristics such as collagen I and Matrigel [Vinci et al. 2012] [Leggett et al. 2017]. Embedded multicellular spheroids allow for visual characterization of invasion through a matrix-like collagen or Matrigel [Lim et al. 2020] [Leggett et al. 2017]. The unique advantages of this technique over conventional migration and invasion experiments such as wound healing and transwell assays are manifold; wound healing assays and unmodified transwells do not test the ability of cancer cells to remodel ECM, and transwell assays bias results toward single-cell migration due to the small pore size. Spheroid invasion assays using Matrigel, or a similar substrate have the added advantage of more accurately recapitulating the cellular changes along the epithelial-mesenchymal spectrum that are present *in vivo* [Leggett et al. 2017].

Tumor organoids

Organoids are distinct from tumor spheroids in that they are derived either from stem cells or tumor tissue rather than established cell lines. Similar to many spheroid culture methods, organoids require supplementation with laminin and collagen rich basement membrane extract [Schutgens & Clevers, 2020]. In stem cell derived organoids, careful control of growth factor cocktails drives differentiation[2] and organization of the organoids. These organoids generated from untransformed cells, are genetically editable with systems like clustered regularly interspaced palindromic repeat/Cas9 (CRISPR/Cas9) and have been

[2] The imperfect differentiation process can produce interesting, even if unintended, results, an example being neural lineage cells being produced when differentiating kidney organoids [Wu et al. 2018].

used to model the impact of early mutations on tumorigenesis [Gunti et al. 2021]. Chemical carcinogenesis has also been investigated using lung organoids grown *ex vivo* and re-implanted into mice [Naruse et al. 2020].

Organoids can also be generated directly from tumor tissue and subsequently expanded [Sato et al. 2011]. Tumor derived organoids better capture tumor heterogeneity than cell line-derived counterparts, with one study showing that tumor derived organoids generated from single cells had significant genetic heterogeneity as well as diversity in DNA methylation and the transcriptome [Roerink et al. 2018]. Promising advances have also been made in the commercial development of tumor-derived organoids for personalized oncology [Ding et al. 2022].

3D tumor models in drug development

A major limitation to 3D culture methods in drug development is scalability for both resources and time; cultivation and expansion of organoids and some spheroids requires basement membrane extract that is costly to generate. High throughput applications of 3D culture models are therefore necessary for use in drug development.

Multicellular tumor spheroids exhibit gradients in both nutrients and waste products. Similarly, drug penetration is not homogenous throughout tumor spheroids, which allows for more accurate modeling of pharmacodynamics for drug development [Sant & Johnson 2017]. Indeed, 3D culture models have been shown to be less sensitive to certain compounds than 2D monolayers [Nath & Devi 2016][Lovitt et al. 2015]. However, some compounds have exhibited increased potency in tumor spheroids, such as trastuzumab in HER2+ breast cancer [Pickl et al. 2009] and MAPK pathway inhibitors blocking thyroid cancer invasion [Ingeson-Carlsson et al. 2015]. The specific change in sensitivity to these compounds is attributable to metabolic, proliferative/cell cycle, and oxidative stress conditions present in the spheroid.

Both tumor spheroids and organoids are valuable tools for studying cancer stem cells. Spheroid media can be refined to select for cancer stem cells through growth factor addition and serum deprivation, and these spheroids can closely resemble tumor derived organoids when grown in agar coated vessels [Ryu et al. 2019]. Organoids, often derived from pluripotent stem cells, are similarly able to be enriched for cancer stem cells, and have been used to investigate their effects on metastasis *in vivo* [Schutgens & Clevers 2020].

The ability to characterize toxicity *ex vivo* has been advanced by "body on a chip" organoid technology, combining multiple tissue types of organoids to mimic drug metabolism and tolerability, even demonstrating drug transporter expression in intestinal organoids [Gunti et al. 2021] [Onozato et al. 2018].

Drug screening studies performed in tumor derived organoid platforms can be used as a predictor for clinical response [Vlachogiannis et al. 2018], an attribute being increasingly leveraged in personalized medicine [Wang et al. 2021a][Hsu et al. 2021]. Using conventional luminescence-based viability assays, high throughput drugs screening platforms using organoids have been used to correlate IC_{50} values of potential therapeutics to oncogenic mutations [van de Watering et al. 2015]. Chemotherapy resistance has been studied in both spheroids [Nunes et al. 2019] and organoids with clonal analysis of organoids revealing the presence of therapeutic resistance, even in organoids derived from treatment naïve tumor samples [Roerink et al. 2018].

Biobanks of genetically and histologically characterized organoids, alongside matched healthy tissue, have been generated for colorectal, pancreatic, liver, bladder, prostate, ovarian, and breast cancer [Schutgens & Clevers 2020]. While one biobank of mixed tissue types contains one lung organoid line [Pauli et al 2017], as of 2021 there are currently no open access organoid banks of exclusively lung tumor derived organoids. Additionally, lung cancer organoids have yet to be characterized into molecular subtypes as has been done with breast cancer and PDAC organoids [Schutgens & Clevers 2020].

3D tumor culture models are powerful tools that bridge the gap between traditional 2D cell culture methods and *in vivo* methods of investigation. This thesis details two spheroid models to investigate compounds with potential therapeutic use in LUAD. The study in Chapter Two uses multi-parameter analysis of an NCI-H358 spheroid model to determine the effects of three exemplar compounds on LUAD viability. Chapter Three details the use of a 3D tumor spheroid invasion assay to test the novel NRF2 pathway inhibitor MSU-71 for its effects in blocking invasion. Both models demonstrate advancements in drug development that help bridge the gap between *in vitro* experimental methods and *in vivo* models of cancer.

REFERENCES

REFERENCES

Akopyan, Gohar, and Benjamin Bonavida. "Understanding tobacco smoke carcinogen NNK and lung tumorigenesis." *International journal of oncology* 29, no. 4 (2006): 745-752.

Aubrey, Brandon J., Gemma L. Kelly, Ana Janic, Marco J. Herold, and Andreas Strasser. "How does p53 induce apoptosis and how does this relate to p53-mediated tumour suppression?." *Cell Death & Differentiation* 25, no. 1 (2018): 104-113.

Bade, Brett C., and Charles S. Dela Cruz. "Lung cancer 2020: epidemiology, etiology, and prevention." *Clinics in chest medicine* 41, no. 1 (2020): 1-24.

Banat, G-Andre, Aleksandra Tretyn, Soni Savai Pullamsetti, Jochen Wilhelm, Andreas Weigert, Catherine Olesch, Katharina Ebel et al. "Immune and inflammatory cell composition of human lung cancer stroma." *PLoS one* 10, no. 9 (2015): e0139073.

Bertram, John S., and Przemyslaw Janik. "Establishment of a cloned line of Lewis Lung Carcinoma cells adapted to cell culture." *Cancer letters* 11, no. 1 (1980): 63-73.

Borczuk, Alain C., Lyall Gorenstein, Kristin L. Walter, Adel A. Assaad, Liqun Wang, and Charles A. Powell. "Non-small-cell lung cancer molecular signatures recapitulate lung developmental pathways." *The American journal of pathology* 163, no. 5 (2003): 1949-1960.

Bortolotto, Chandra, Andrea Lancia, Chiara Stelitano, Marianna Montesano, Elisa Merizzoli, Francesco Agustoni, Giulia Stella, Lorenzo Preda, and Andrea Riccardo Filippi. "Radiomics features as predictive and prognostic biomarkers in NSCLC." *Expert Review of Anticancer Therapy* 21, no. 3 (2021): 257-266.

Busch, Stephanie E., Mark L. Hanke, Julia Kargl, Heather E. Metz, David MacPherson, and A. McGarry Houghton. "Lung cancer subtypes generate unique immune responses." *The Journal of Immunology* 197, no. 11 (2016): 4493-4503.

Calles, Antonio, G. Aguado, C. Sandoval, and R. Álvarez. "The role of immunotherapy in small cell lung cancer." *Clinical and Translational Oncology* (2019): 1-16.

Cameron, David, Martine J. Piccart-Gebhart, Richard D. Gelber, Marion Procter, Aron Goldhirsch, Evandro de Azambuja, Gilberto Castro Jr et al. "11 years' follow-up of trastuzumab after adjuvant chemotherapy in HER2-positive early breast cancer: final analysis of the HERceptin Adjuvant (HERA) trial." *The Lancet* 389, no. 10075 (2017): 1195-1205.

Carvalho, Patrícia Dias, Carlos F. Guimaraes, Ana P. Cardoso, Susana Mendonça, Ângela M. Costa, Maria J. Oliveira, and Sérgia Velho. "KRAS oncogenic signaling extends beyond cancer cells to orchestrate the microenvironment." *Cancer research* 78, no. 1 (2018): 7-14.

Castellanos, Emily, Emily Feld, and Leora Horn. "Driven by mutations: the predictive value of mutation subtype in EGFR-mutated non–small cell lung cancer." *Journal of thoracic oncology* 12, no. 4 (2017): 612-623.

Castle, John C., Mohamed Uduman, Simarjot Pabla, Robert B. Stein, and Jennifer S. Buell. "Mutation-derived neoantigens for cancer immunotherapy." *Frontiers in immunology* 10 (2019): 1856.

US Department of Health and Human Services. "The health consequences of smoking—50 years of progress: a report of the Surgeon General." (2014).

Chan, Bryan A., and Brett GM Hughes. "Targeted therapy for non-small cell lung cancer: current standards and the promise of the future." *Translational lung cancer research* 4, no. 1 (2015): 36.

Chang, Seon Hee. "Tumorigenic Th17 cells in oncogenic Kras-driven and inflammation-accelerated lung cancer." *Oncoimmunology* 4, no. 1 (2015): e955704.

Chang, Seon Hee, Seyedeh Golsar Mirabolfathinejad, Harshadadevi Katta, Amber M. Cumpian, Lei Gong, Mauricio S. Caetano, Seyed Javad Moghaddam, and Chen Dong. "T helper 17 cells play a critical pathogenic role in lung cancer." *Proceedings of the National Academy of Sciences* 111, no. 15 (2014): 5664-5669.

Chia, Puey Ling, Paul Mitchell, Alexander Dobrovic, and Thomas John. "Prevalence and natural history of ALK positive non-small-cell lung cancer and the clinical impact of targeted therapy with ALK inhibitors." *Clinical epidemiology* 6 (2014): 423.

Ciardiello, Fortunato, and Giampaolo Tortora. "EGFR antagonists in cancer treatment." *New England Journal of Medicine* 358, no. 11 (2008): 1160-1174.

Coroller, Thibaud P., Vishesh Agrawal, Elizabeth Huynh, Vivek Narayan, Stephanie W. Lee, Raymond H. Mak, and Hugo JWL Aerts. "Radiomic-based pathological response prediction from primary tumors and lymph nodes in NSCLC." *Journal of Thoracic Oncology* 12, no. 3 (2017): 467-476.

Crabtree, Judy S., Ciera S. Singleton, and Lucio Miele. "Notch signaling in neuroendocrine tumors." *Frontiers in oncology* 6 (2016): 94.

Cummings, K. Michael, and Robert N. Proctor. "The changing public image of smoking in the United States: 1964–2014." *Cancer Epidemiology and Prevention Biomarkers* 23, no. 1 (2014): 32-36.

da Cunha Santos, Gilda, Frances A. Shepherd, and Ming Sound Tsao. "EGFR mutations and lung cancer." *Annual Review of Pathology: Mechanisms of Disease* 6 (2011): 49-69.

Della Corte, Carminia Maria, Giuseppe Viscardi, Raimondo Di Liello, Morena Fasano, Erika Martinelli, Teresa Troiani, Fortunato Ciardiello, and Floriana Morgillo. "Role and targeting of anaplastic lymphoma kinase in cancer." *Molecular cancer* 17, no. 1 (2018): 1-9.

Deng, Shanshan, Michael J. Clowers, Walter V. Velasco, Marco Ramos-Castaneda, and Seyed Javad Moghaddam. "Understanding the complexity of the tumor microenvironment in K-ras mutant lung cancer: finding an alternative path to prevention and treatment." *Frontiers in oncology* 9 (2020): 1556.

Dias Carvalho, Patrícia, Ana Luísa Machado, Flávia Martins, Raquel Seruca, and Sérgia Velho. "Targeting the tumor microenvironment: an unexplored strategy for mutant KRAS tumors." *Cancers* 11, no. 12 (2019): 2010.

Ding, Shengli, Carolyn Hsu, Zhaohui Wang, Naveen R. Natesh, Rosemary Millen, Marcos Negrete, Nicholas Giroux et al. "Patient-derived micro-organospheres enable clinical precision oncology." *Cell Stem Cell* (2022).

Dou, Tai H., Thibaud P. Coroller, Joost JM van Griethuysen, Raymond H. Mak, and Hugo JWL Aerts. "Peritumoral radiomics features predict distant metastasis in locally advanced NSCLC." *PloS one* 13, no. 11 (2018): e0206108.

Doyle, Austin, W. John Martin, Keiko Funa, A. Gazdar, D. Carney, S. E. Martin, I. Linnoila, F. Cuttitta, J. Mulshine, and P. Bunn. "Markedly decreased expression of class I histocompatibility antigens, protein, and mRNA in human small-cell lung cancer." *The Journal of experimental medicine* 161, no. 5 (1985): 1135-1151.

Ekert, Jason E., Kjell Johnson, Brandy Strake, Jose Pardinas, Stephen Jarantow, Robert Perkinson, and David C. Colter. "Three-dimensional lung tumor microenvironment modulates therapeutic compound responsiveness in vitro–implication for drug development." *PloS one* 9, no. 3 (2014): e92248.

Essakly, Ahlem, Heike Loeser, Max Kraemer, Hakan Alakus, Seung-Hun Chon, Thomas Zander, Reinhard Buettner et al. "PIK3CA and KRAS amplification in esophageal adenocarcinoma and their impact on the inflammatory tumor microenvironment and prognosis." *Translational oncology* 13, no. 2 (2020): 157-164.

Forkert, Poh-Gek. "Mechanisms of lung tumorigenesis by ethyl carbamate and vinyl carbamate." *Drug metabolism reviews* 42, no. 2 (2010): 355-378.

Fridman, Jordan S., and Scott W. Lowe. "Control of apoptosis by p53." *Oncogene* 22, no. 56 (2003): 9030-9040.

Gazdar, Adi F., Fred R. Hirsch, and John D. Minna. "From mice to men and back: an assessment of preclinical model systems for the study of lung cancers." *Journal of Thoracic Oncology* 11, no. 3 (2016): 287-299.

George, Julie, Jing Shan Lim, Se Jin Jang, Yupeng Cun, Luka Ozretić, Gu Kong, Frauke Leenders et al. "Comprehensive genomic profiles of small cell lung cancer." *Nature* 524, no. 7563 (2015): 47-53.

Greulich, Heidi. "The genomics of lung adenocarcinoma: opportunities for targeted therapies." *Genes & cancer* 1, no. 12 (2010): 1200-1210.

Gibbons, Don L., Lauren A. Byers, and Jonathan M. Kurie. "Smoking, p53 mutation, and lung cancer." *Molecular cancer research* 12, no. 1 (2014): 3-13.

Sung, Hyuna, Jacques Ferlay, Rebecca L. Siegel, Mathieu Laversanne, Isabelle Soerjomataram, Ahmedin Jemal, and Freddie Bray. "Global cancer statistics 2020: GLOBOCAN estimates of incidence and mortality worldwide r 36 cancers in 185 countries." *CA: a cancer journal for clinicians* 71, no. 3 (2021): 209-249.

Gristina, Valerio, Maria La Mantia, Federica Iacono, Antonio Galvano, Antonio Russo, and Viviana Bazan. "The emerging therapeutic landscape of alk inhibitors in non-small cell lung cancer." *Pharmaceuticals* 13, no. 12 (2020): 474.

Gunti, Sreenivasulu, Austin TK Hoke, Kenny P. Vu, and Nyall R. London. "Organoid and spheroid tumor models: techniques and applications." *Cancers* 13, no. 4 (2021): 874.

Hallberg, B., and R. H. Palmer. "The role of the ALK receptor in cancer biology." *Annals of Oncology* 27 (2016): iii4-iii15.

Hanel, Walter, and Ute M. Moll. "Links between mutant p53 and genomic instability." *Journal of cellular biochemistry* 113, no. 2 (2012): 433-439.

Ho, Teresa, Ban Xiong Tan, and David Lane. "How the other half lives: what p53 does when it is not being a transcription factor." *International journal of molecular sciences* 21, no. 1 (2020): 13.

Hong, David S., Marwan G. Fakih, John H. Strickler, Jayesh Desai, Gregory A. Durm, Geoffrey I. Shapiro, Gerald S. Falchook et al. "KRASG12C inhibition with sotorasib in advanced solid tumors." *New England Journal of Medicine* 383, no. 13 (2020): 1207-1217.

Hou, Pingping, Avnish Kapoor, Qiang Zhang, Jiexi Li, Chang-Jiun Wu, Jun Li, Zhengdao Lan et al. "Tumor microenvironment remodeling enables bypass of oncogenic KRAS dependency in pancreatic cancer." *Cancer discovery* 10, no. 7 (2020): 1058-1077.

Hsu, CH-T., Z. Wang, S. Oh, G. Rupprecht, D. Delubac, X. Shen, and D. Hsu. "1782P Micro-organospheres as a novel precision oncology platform in colorectal cancer." *Annals of Oncology* 32 (2021): S1219.

Huang, Lyu, Jiayan Chen, Weigang Hu, Xinyan Xu, Di Liu, Junmiao Wen, Jiayu Lu et al. "Assessment of a radiomic signature developed in a general NSCLC cohort for predicting overall survival of ALK-positive patients with different treatment types." *Clinical lung cancer* 20, no. 6 (2019): e638-e651.

Hwang, David H., David P. Szeto, Anthony S. Perry, Jacqueline L. Bruce, and Lynette M. Sholl. "Pulmonary large cell carcinoma lacking squamous differentiation is clinicopathologically indistinguishable from solid-subtype adenocarcinoma." *Archives of Pathology and Laboratory Medicine* 138, no. 5 (2014): 626-635.

Inage, Terunaga, Takahiro Nakajima, Ichiro Yoshino, and Kazuhiro Yasufuku. "Early lung cancer detection." *Clinics in chest medicine* 39, no. 1 (2018): 45-55.

Inamura, Kentaro. "Lung cancer: understanding its molecular pathology and the 2015 WHO classification." *Frontiers in oncology* 7 (2017): 193.

Ingeson-Carlsson, Camilla, Angela Martinez-Monleon, and Mikael Nilsson. "Differential effects of MAPK pathway inhibitors on migration and invasiveness of BRAFV600E mutant thyroid cancer cells in 2D and 3D culture." E*xperimental cell research* 338, no. 2 (2015): 127-135.

Ji, H., A. M. Houghton, T. J. Mariani, S. Perera, C. B. Kim, R. Padera, G. Tonon et al. "K-ras activation generates an inflammatory response in lung tumors." *Oncogene* 25, no. 14 (2006): 2105-2112.

Ji, Hongbin, Matthew R. Ramsey, D. Neil Hayes, Cheng Fan, Kate McNamara, Piotr Kozlowski, Chad Torrice et al. "LKB1 modulates lung cancer differentiation and metastasis." *Nature* 448, no. 7155 (2007): 807-810.

Jordan, Emmet J., Hyunjae R. Kim, Maria E. Arcila, David Barron, Debyani Chakravarty, JianJiong Gao, Matthew T. Chang et al. "Prospective comprehensive molecular characterization of lung adenocarcinomas for efficient patient matching to approved and emerging therapies." *Cancer discovery* 7, no. 6 (2017): 596-609; Accessed through cBioPortal

Karasaki, Takahiro, Kazuhiro Nagayama, Hideki Kuwano, Jun-ichi Nitadori, Masaaki Sato, Masaki Anraku, Akihiro Hosoi et al. "An immunogram for the cancer-immunity cycle: towards personalized immunotherapy of lung cancer." *Journal of Thoracic Oncology* 12, no. 5 (2017): 791-803.

Kim, Youngwook, Jeonghun Ko, ZhengYun Cui, Amir Abolhoda, Jin Seok Ahn, Sai-Hong Ou, Myung-Ju Ahn, and Keunchil Park. "The EGFR T790M mutation in acquired resistance to an irreversible second-generation EGFR inhibitor." *Molecular cancer therapeutics* 11, no. 3 (2012): 784-791.

Kim, Nayoung, Hong Kwan Kim, Kyungjong Lee, Yourae Hong, Jong Ho Cho, Jung Won Choi, Jung-Il Lee et al. "Single-cell RNA sequencing demonstrates the molecular and cellular reprogramming of metastatic lung adenocarcinoma." *Nature communications* 11, no. 1 (2020): 1-15.

Lázaro, Sara, Miriam Pérez-Crespo, Ana Belén Enguita, Pilar Hernández, Jesús Martínez-Palacio, Marta Oteo, Julien Sage, Jesús M. Paramio, and Mirentxu Santos. "Ablating all three retinoblastoma family members in mouse lung leads to neuroendocrine tumor formation." *Oncotarget* 8, no. 3 (2017): 4373.

Le, Tri, and David E. Gerber. "Newer-generation EGFR inhibitors in lung cancer: how are they best used?." *Cancers* 11, no. 3 (2019): 366.

Ledford, Heidi. "US cancer institute to overhaul tumour cell lines." *Nature News* 530, no. 7591 (2016): 391.

Li, Xiaofeng, Guotao Yin, Yufan Zhang, Dong Dai, Jianjing Liu, Peihe Chen, Lei Zhu, Wenjuan Ma, and Wengui Xu. "Predictive power of a radiomic signature based on 18F-FDG PET/CT images for EGFR mutational status in NSCLC." *Frontiers in oncology* 9 (2019): 1062.

Li, Hailin, Rui Zhang, Siwen Wang, Mengjie Fang, Yongbei Zhu, Zhenhua Hu, Di Dong, Jingyun Shi, and Jie Tian. "CT-based radiomic signature as a prognostic factor in stage IV ALK-positive non-small-cell lung cancer treated with TKI crizotinib: A Proof-of-Concept Study." *Frontiers in oncology* 10 (2020): 57.

Li, Bob T., Egbert F. Smit, Yasushi Goto, Kazuhiko Nakagawa, Hibiki Udagawa, Julien Mazières, Misako Nagasaka et al. "Trastuzumab deruxtecan in HER2-mutant non–small-cell lung cancer." *New England Journal of Medicine* (2021).

Lin, Ruei-Zeng, Li-Fang Chou, Chi-Chen Michael Chien, and Hwan-You Chang. "Dynamic analysis of hepatoma spheroid formation: roles of E-cadherin and β1-integrin." *Cell and tissue research* 324, no. 3 (2006): 411-422.

Lito, Piro, Martha Solomon, Lian-Sheng Li, Rasmus Hansen, and Neal Rosen. "Allele-specific inhibitors inactivate mutant KRAS G12C by a trapping mechanism." *Science* 351, no. 6273 (2016): 604-608.

Lorz, Corina, Marta Oteo, and Mirentxu Santos. "Neuroendocrine Lung Cancer Mouse Models: An Overview." *Cancers* 13, no. 1 (2021): 14.

Lovitt, Carrie J., Todd B. Shelper, and Vicky M. Avery. "Evaluation of chemotherapeutics in a three-dimensional breast cancer model." *Journal of cancer research and clinical oncology* 141, no. 5 (2015): 951-959.

Lv, Donglai, Zongtao Hu, Lin Lu, Husheng Lu, and Xiuli Xu. "Three‑dimensional cell culture: A powerful tool in tumor research and drug discovery." *Oncology letters* 14, no. 6 (2017): 6999-7010.

Massey, Thomas E., Theodora R. Devereux, Robert R. Maronpot, Julie F. Foley, and Marshall W. Anderson. "High frequency of K-ras mutations in spontaneous and vinyl carbamate-induced lung tumors of relatively resistant B6CF1 (C57BL/6J× BALB/cJ) mice." *Carcinogenesis* 16, no. 5 (1995): 1065-1069.

Moureau, Sylvie, Janna Luessing, Emma Christina Harte, Muriel Voisin, and Noel Francis Lowndes. "A role for the p53 tumour suppressor in regulating the balance between homologous recombination and non-homologous end joining." *Open biology* 6, no. 9 (2016): 160225.

Naruse, Mie, Ryoichi Masui, Masako Ochiai, Yoshiaki Maru, Yoshitaka Hippo, and Toshio Imai. "An organoid-based carcinogenesis model induced by in vitro chemical treatment." *Carcinogenesis* 41, no. 10 (2020): 1444-1453.

Nath, Sritama, and Gayathri R. Devi. "Three-dimensional culture systems in cancer research: Focus on tumor spheroid model." *Pharmacology & therapeutics* 163 (2016): 94-108.

National Comprehensive Cancer Network. "NCCN Guidelines Version 1.2022 Non-Small Cell Lung Cancer" (2021).

Noguchi, Masayuki, Akio Morikawa, Masanori Kawasaki, Yoshihiro Matsuno, Tesshi Yamada, Setsuo Hirohashi, Haruhiko Kondo, and Yukio Shimosato. "Small adenocarcinoma of the lung. Histologic characteristics and prognosis." *Cancer* 75, no. 12 (1995): 2844-2852.

Nunes, Ana S., Andreia S. Barros, Elisabete C. Costa, André F. Moreira, and Ilidio J. Correia. "3D tumor spheroids as in vitro models to mimic in vivo human solid tumors resistance to therapeutic drugs." *Biotechnology and bioengineering* 116, no. 1 (2019): 206-226.

Nunes, Ana S., Andreia S. Barros, Elisabete C. Costa, André F. Moreira, and Ilidio J. Correia. "3D tumor spheroids as in vitro models to mimic in vivo human solid tumors resistance to therapeutic drugs." *Biotechnology and bioengineering* 116, no. 1 (2019): 206-226.

Onozato, Daichi, Misaki Yamashita, Anna Nakanishi, Takumi Akagawa, Yuriko Kida, Isamu Ogawa, Tadahiro Hashita, Takahiro Iwao, and Tamihide Matsunaga. "Generation of intestinal organoids suitable for pharmacokinetic studies from human induced pluripotent stem cells." *Drug Metabolism and Disposition* 46, no. 11 (2018): 1572-1580.

Pao, William, Vincent Miller, Maureen Zakowski, Jennifer Doherty, Katerina Politi, Inderpal Sarkaria, Bhuvanesh Singh et al. "EGF receptor gene mutations are common in lung cancers from “never smokers” and are associated with sensitivity of tumors to gefitinib and erlotinib." *Proceedings of the National Academy of Sciences* 101, no. 36 (2004): 13306-13311.

Park, Hye Eun, Seung-Yeon Yoo, Nam-Yun Cho, Jeong Mo Bae, Sae-Won Han, Hye Seung Lee, Kyu Joo Park, Tae-You Kim, and Gyeong Hoon Kang. "Tumor microenvironment-adjusted prognostic implications of the KRAS mutation subtype in patients with stage III colorectal cancer treated with adjuvant FOLFOX." *Scientific reports* 11, no. 1 (2021): 1-10.

Parrales, Alejandro, and Tomoo Iwakuma. "Targeting oncogenic mutant p53 for cancer therapy." *Frontiers in oncology* 5 (2015): 288.

Pauli, Chantal, Benjamin D. Hopkins, Davide Prandi, Reid Shaw, Tarcisio Fedrizzi, Andrea Sboner, Verena Sailer et al. "Personalized in vitro and in vivo cancer models to guide precision medicine." C*ancer discovery* 7, no. 5 (2017): 462-477.

Pickl, M., and C. H. Ries. "Comparison of 3D and 2D tumor models reveals enhanced HER2 activation in 3D associated with an increased response to trastuzumab." *Oncogene* 28, no. 3 (2009): 461-468.

Piotrowska, Zofia, Matthew J. Niederst, Chris A. Karlovich, Heather A. Wakelee, Joel W. Neal, Mari Mino-Kenudson, Linnea Fulton et al. "Heterogeneity underlies the emergence of EGFRT790 wild-type clones following treatment of T790M-positive cancers with a third-generation EGFR inhibitor." *Cancer discovery* 5, no. 7 (2015): 713-722.

Privitera, G., T. Luca, N. Musso, C. Vancheri, N. Crimi, V. Barresi, D. Condorelli, and S. Castorina. "In vitro antiproliferative effect of trastuzumab (Herceptin®) combined with cetuximab (Erbitux®) in a model of human non-small cell lung cancer expressing EGFR and HER2." *Clinical and experimental medicine* 16, no. 2 (2016): 161-168.

Rivalland, Gareth, Marzena Walkiewicz, Gavin Michael Wright, and Thomas John. "Small cell lung cancer: The immune microenvironment and prognostic impact of checkpoint expression." (2017): 8569-8569.

Roerink, Sophie F., Nobuo Sasaki, Henry Lee-Six, Matthew D. Young, Ludmil B. Alexandrov, Sam Behjati, Thomas J. Mitchell et al. "Intra-tumour diversification in colorectal cancer at the single-cell level." *Nature* 556, no. 7702 (2018): 457-462.

Romaniello, Donatella, Luigi Mazzeo, Maicol Mancini, Ilaria Marrocco, Ashish Noronha, Matthew Kreitman, Swati Srivastava et al. "A combination of approved antibodies overcomes resistance of lung cancer to osimertinib by blocking bypass pathways." *Clinical Cancer Research* 24, no. 22 (2018): 5610-5621.

Roskoski Jr, Robert. "Small molecule inhibitors targeting the EGFR/ErbB family of protein-tyrosine kinases in human cancers." *Pharmacological research* 139 (2019): 395-411.

Rossi, G., M. C. Mengoli, Alessia Cavazza, D. Nicoli, M. Barbareschi, C. Cantaloni, M. Papotti et al. "Large cell carcinoma of the lung: clinically oriented classification integrating immunohistochemistry and molecular biology." *Virchow's Archive* 464, no. 1 (2014): 61-68.

Rudin, Charles M., Steffen Durinck, Eric W. Stawiski, John T. Poirier, Zora Modrusan, David S. Shames, Emily A. Bergbower et al. "Comprehensive genomic analysis identifies SOX2 as a frequently amplified gene in small-cell lung cancer." *Nature genetics* 44, no. 10 (2012): 1111-1116.

Rudin, Charles M., John T. Poirier, Lauren Averett Byers, Caroline Dive, Afshin Dowlati, Julie George, John V. Heymach et al. "Molecular subtypes of small cell lung cancer: a synthesis of human and mouse model data." *Nature Reviews Cancer* 19, no. 5 (2019): 289-297.

Ryu, Na-Eun, Soo-Hong Lee, and Hansoo Park. "Spheroid culture system methods and applications for mesenchymal stem cells." *Cells* 8, no. 12 (2019): 1620.

Sant, Shilpa, and Paul A. Johnston. "The production of 3D tumor spheroids for cancer drug discovery." *Drug Discovery Today: Technologies* 23 (2017): 27-36.

Sasaki, Takaaki, Scott J. Rodig, Lucian R. Chirieac, and Pasi A. Jänne. "The biology and treatment of EML4-ALK non-small cell lung cancer." *European journal of cancer* 46, no. 10 (2010): 1773-1780.

Sato, Toshiro, Daniel E. Stange, Marc Ferrante, Robert GJ Vries, Johan H. Van Es, Stieneke Van Den Brink, Winan J. Van Houdt et al. "Long-term expansion of epithelial organoids from human colon, adenoma, adenocarcinoma, and Barrett's epithelium." *Gastroenterology* 141, no. 5 (2011): 1762-1772.

Schlessinger, Joseph. "Common and distinct elements in cellular signaling via EGF and FGF receptors." *Science* 306, no. 5701 (2004): 1506-1507.

Schutgens, Frans, and Hans Clevers. "Human organoids: tools for understanding biology and treating diseases." *Annual Review of Pathology: Mechanisms of Disease* 15 (2020): 211-234.

SEER*Explorer: An interactive website for SEER cancer statistics [Internet]. Surveillance Research Program, National Cancer Institute. [Cited 2021 September 27]. Available from https://seer.cancer.gov/explorer/

Shaw, Alice Tsang, Gregory J. Riely, Y-J. Bang, D-W. Kim, David Ross Camidge, Benjamin J. Solomon, Marileila Varella-Garcia et al. "Crizotinib in ROS1-rearranged advanced non-small-cell lung cancer (NSCLC): updated results, including overall survival, from PROFILE 1001." *Annals of Oncology* 30, no. 7 (2019): 1121-1126.

Shi, Tao, and Tobias B. Dansen. "Reactive oxygen species induced p53 activation: DNA damage, redox signaling, or both?." *Antioxidants & redox signaling* 33, no. 12 (2020): 839-859.

Shoemaker, Robert H. "The NCI60 human tumour cell line anticancer drug screen." *Nature Reviews Cancer* 6, no. 10 (2006): 813-823.

Singh, Aditi P., Diego Adrianzen Herrera, Yifei Zhang, Roman Perez-Soler, and Haiying Cheng. "Mouse models in squamous cell lung cancer: impact for drug discovery." *Expert opinion on drug discovery* 13, no. 4 (2018): 347-358.

Skoulidis, Ferdinandos, and John V. Heymach. "Co-occurring genomic alterations in non-small-cell lung cancer biology and therapy." *Nature Reviews Cancer* 19, no. 9 (2019): 495-509.

Skoulidis, Ferdinandos, Bob T. Li, Grace K. Dy, Timothy J. Price, Gerald S. Falchook, Jürgen Wolf, Antoine Italiano et al. "Sotorasib for Lung Cancers with KRAS p. G12C Mutation." *New England Journal of Medicine* (2021).

Stankovic, Branislava, Heidi Anine Korsmo Bjørhovde, Renate Skarshaug, Henrik Aamodt, Astri Frafjord, Elisabeth Müller, Clara Hammarström et al. "Immune cell composition in human non-small cell lung cancer." *Frontiers in immunology* 9 (2019): 3101.

Cancer Genome Atlas Research Network, 2012. Comprehensive genomic characterization of squamous cell lung cancers. *Nature*, 489(7417), p.519.

Tomasetti, Cristian, and Bert Vogelstein. "Variation in cancer risk among tissues can be explained by the number of stem cell divisions." *Science* 347, no. 6217 (2015): 78-81.

Travis, William D. "Lung cancer pathology: current concepts." *Clinics in chest medicine* 41, no. 1 (2020): 67-85.

Travis, William D., Elisabeth Brambilla, Andrew G. Nicholson, Yasushi Yatabe, John HM Austin, Mary Beth Beasley, Lucian R. Chirieac et al. "The 2015 World Health Organization classification of lung tumors: impact of genetic, clinical and radiologic advances since the 2004 classification." *Journal of thoracic oncology* 10, no. 9 (2015): 1243-1260.

Tu, Wenting, Guangyuan Sun, L. I. Fan, Yun Wang, Yi Xia, Yu Guan, Qiong Li, Di Zhang, Shiyuan Liu, and Zhaobin Li. "Radiomics signature: a potential and incremental predictor for EGFR mutation status in NSCLC patients, comparison with CT morphology." *Lung Cancer* 132 (2019): 28-35.

Uprety, Dipesh, and Alex A. Adjei. "KRAS: From undruggable to a druggable Cancer Target." *Cancer Treatment Reviews* 89 (2020).

van de Wetering, Marc, Hayley E. Francies, Joshua M. Francis, Gergana Bounova, Francesco Iorio, Apollo Pronk, Winan van Houdt et al. "Prospective derivation of a living organoid biobank of colorectal cancer patients." *Cell* 161, no. 4 (2015): 933-945.

Vlachogiannis, Georgios, Somaieh Hedayat, Alexandra Vatsiou, Yann Jamin, Javier Fernández-Mateos, Khurum Khan, Andrea Lampis et al. "Patient-derived organoids model treatment response of metastatic gastrointestinal cancers." *Science* 359, no. 6378 (2018): 920-926.

Vousden, Karen H., and David P. Lane. "p53 in health and disease." *Nature reviews Molecular cell biology* 8, no. 4 (2007): 275-283.

Wang, Shuhang, Yongping Song, and Delong Liu. "EAI045: The fourth-generation EGFR inhibitor overcoming T790M and C797S resistance." *Cancer letters* 385 (2017): 51-54.

Wang, Z., E. Cortes-Sanchez, C. H. Yang, D. Nelson, C. Keating, A. Smith, D. Hsu, B. Welm, A. Welm, and X. Shen. "1149P An automated platform for rapid drug screening in patient-derived micro-organospheres." *Annals of Oncology* 32 (2021): S929.

Williams, Ashley B., and Björn Schumacher. "p53 in the DNA-damage-repair process." *Cold Spring Harbor perspectives in medicine* 6, no. 5 (2016): a026070.

Wu, Song, Wei Zhu, Patricia Thompson, and Yusuf A. Hannun. "Evaluating intrinsic and non-intrinsic cancer risk factors." *Nature communications* 9, no. 1 (2018): 1-12.

Yatabe, Yasushi, Sanja Dacic, Alain C. Borczuk, Arne Warth, Prudence A. Russell, Sylvie Lantuejoul, Mary Beth Beasley et al. "Best practices recommendations for diagnostic immunohistochemistry in lung cancer." *Journal of Thoracic Oncology* 14, no. 3 (2019): 377-407.

Yuan, Tina L., Arnaud Amzallag, Rachel Bagni, Ming Yi, Shervin Afghani, William Burgan, Nicole Fer et al. "Differential effector engagement by oncogenic KRAS." *Cell reports* 22, no. 7 (2018): 1889-1902.

Yun, Cai-Hong, Titus J. Boggon, Yiqun Li, Michele S. Woo, Heidi Greulich, Matthew Meyerson, and Michael J. Eck. "Structures of lung cancer-derived EGFR mutants and inhibitor complexes: mechanism of activation and insights into differential inhibitor sensitivity." *Cancer cell* 11, no. 3 (2007): 217-227.

Zeitouni, Daniel, Yuliya Pylayeva-Gupta, Channing J. Der, and Kirsten L. Bryant. "KRAS mutant pancreatic cancer: no lone path to an effective treatment." *Cancers* 8, no. 4 (2016): 45.

Zheng, Min. "Classification and pathology of lung cancer." *Surgical Oncology Clinics* 25, no. 3 (2016): 447-468.

CHAPTER 2. Apigenin and CEP-1347 synergize to prohibit growth and reduce LUAD viability in a 3D tumor spheroid model

Introduction

One of the perennial challenges of drug research and development in cancer is balancing efficacy with collateral damage to healthy tissue. Targeted therapies have shown major promise in this area, aiming at the molecular characteristics of tumor cells that set them apart from the surrounding tissue. In the case of LUAD, the EGFR inhibitors gefitinib and erlotinib have shown efficacy in cancers with EGFR alterations that drive progression [Castellanos et al. 2017]. Recently, the FDA has approved the first therapeutic targeted at inhibiting KRAS^{G12C} found in LUAD [FDA 2020], with multiple other approaches other KRAS mutants in development [Moore et al. 2020]. However, the G12C mutation represents only the specific molecular alteration is not ubiquitous across patients (or even within tumors [Lim & Ma, 2019]), and resistance can often quickly develop, highlighting a continued need for new therapeutic options.

This Chapter describes the development of a 3D LUAD tumor spheroid model and its application to testing compounds of potential therapeutic utility. These compounds represent three areas of small molecule drug development, each with specific advantages: dietary components, which are regulated with substantially less complexity[3] than mainstream pharmaceuticals and are more easily deliverable to consumers; novel compounds, which can be patented and offer commercial incentive for development; and repurposed drugs, which are uniquely able to leverage prior safety validation from early phase clinical trials, putting them at lower risk for failure in later stages of drug development.

[3] Dietary supplements do not need FDA approval. “Complexity” in this context translates to “expenditure of time and capital”.

Flavonoids & Apigenin

Apigenin is part of the broader flavonoid family of phytochemicals, which are found in fruits, vegetables, especially Chinese celery, and herbs such as parsley [Ahmed et al. 2021]. Apigenin is also available as a commercially sold dietary supplement. Apigenin has emerged as a compound of interest for both cancer prevention [Shukla & Gupta 2020] and treatment [Imran et al 2020][Ahmed et al. 2021].

Apigenin's anti-cancer effects are multi-faceted and differ across cancer types. In breast cancer, apigenin has been shown to potentiate or elicit apoptosis in estrogen receptor positive (ER+) breast cancer cells [Madunić et al. 2015], HER2+ breast cancer [Way et al. 2004] [Seo et al. 2014], and triple negative breast cancer (TNBC) [Sudhakaran et al. 2020]. Apigenin has been shown to prevent melanoma migration, invasion, and metastasis [Piantelli et al. 2005], an effect mediated through inhibition of the STAT3 signaling pathway [Cao et al. 2016]. In ovarian cancer, apigenin was shown to inhibit migration and invasion by increasing the rate of focal adhesion kinase degradation [Hu et al. 2008]. Apigenin also targets multiple Akt signaling axes, such as the CD26/Akt/Snail-Slug axis to prevent NSCLC migration *in vitro* and tumor progression *in vivo* [Chang et al. 2018]. In multiple cancer cell lines, including A549 (lung), SK-Hep1 (Liver), and MDA-MB-231 (TNBC) cells apigenin prevents HGF-mediated Akt phosphorylation, and through the PI3K/Akt pathways inhibit integrin β4 function, prevents MDA-MB-231 invasive growth *in vivo* [Lee et al. 2008].

In lung cancer, apigenin has been shown to decrease viability through multiple mechanisms. Apigenin has a well-defined role in promoting apoptosis through caspase 8 activation and subsequent mitochondrial- and caspase 3-dependent apoptosis programs in NSCLC cell lines [Lu et al. 2010][Lu et al. 2011]. However, the concentrations of apigenin alone that elicit apoptosis (40 μM-120 μM) are far higher than what is achievable *in vivo.*

Apigenin has been shown to be an effective sensitizer to traditional chemotherapies. In the context of TNBC, apigenin sensitized 3D spheroid and organoid models to doxorubicin by downregulating efflux pumps ABCC4 and ABCG2 [Sudhakaran et al. 2020]. In lung cancer, apigenin has been shown to re-sensitize cisplatin resistant A549 cells in a p53 dependent manner [Li et al. 2021]. Also, in a p53 dependent manner, apigenin enhances tumor-necrosis factor related apoptosis-inducing ligand (TRAIL)-induced apoptosis of NSCLC cell lines by upregulating the expression of TRAIL receptors DR4 and DR5 [Chen et al. 2016]. Mechanistically, apigenin potentiates DR5-initiated apoptosis by inhibiting heat shock protein 70 (Hsp70), a negative regulator of DR5. This involves a shift in splice variants of cellular FLICE inhibitory protein (c-FLIP) away from c-FLIP$_S$, in favor of c-FLIP$_L$ which also negatively regulates DR5, and directly promotion DR5a splicing [Voss et al. 2021]. Finally, apigenin has been shown to sensitize lung cancer cells to radiotherapy in both 2D and 3D cultures [Watanabe et al. 2007]. The radiosensitizing effects of apigenin appear to be mediated through both glycolytic pathways and inhibition of AKT signaling [Bao et al. 2015] [Zhao et al. 2021].

In addition to its effects directly on tumor cells, apigenin has recently shown promise as a modulator of the tumor microenvironment. In lung cancer, apigenin has been shown to downregulate programmed death 1 (PD-1) expression through STAT3 inhibition [Jiang et al. 2021]. PD-L1 is downregulated by apigenin in melanoma cells and tumor associated dendritic cells [Xu et al. 2018]. In a mouse model of pancreatic cancer, apigenin increased expression of master myeloid regulator SH2 Domain-Containing Inositol 5'-Phosphatase 1 (SHIP-1), decreased myeloid derived suppressor cells, and increased tumoricidal M1 macrophages in the tumor microenvironment, resulting in a reduced tumor burden of the mice [Villalobos-Ayela et al. 2020]. Apigenin also inhibits the secretion of a wide range of pro-inflammatory factors from tumor cells [Patil et al. 2015], many of which are deeply interconnected with the tumor immune microenvironment. While there is an increasingly robust literature on apigenin's effects on myeloid cells *per se*, the potential of apigenin as a modulator of immune components within the tumor microenvironment remains a largely unexplored research niche.

Apigenin's therapeutic relevance extends to include other lung pathologies such as reversing pulmonary fibrosis caused by paraquat immunotoxicity [Liu et al. 2018]. In a rat model of bleomycin-induced pulmonary fibrosis, apigenin delivered via nanoparticle was effective in reducing IL-8, TNFα, and TGFβ in addition to lowering collagen IA transcript levels [Zhang et al. 2017]. A similar study demonstrated that this effect may be mediated through upregulation of PPARγ [Zhou et al. 2016]. Quercetin, a 3-hydroxyflavone structurally like apigenin, has been investigated for therapeutic potential in treating SARS-CoV-2 infection [Colunga Biancatelli et al. 2020] and ensuing inflammatory complications [Diniz et al 2020].

Rexinoids

Rexinoids are a class of both endogenous and synthetic compounds that act as selective agonists of the retinoid X receptor (RXR) [Leal et al. 2021]. As type II nuclear receptors, RXRs are bound to their respective sites on DNA. Transcriptional regulation occurs when the ligand for RXR binds, which allows for dissociation of corepressors and their replacement with coactivators—often histone acetyltransferases—which allow DNA to open making sites more available for transcription [Sever & Glass, 2013].

Early research into nuclear receptors revealed a multitude of "orphan" nuclear receptor proteins–including RXR for which no ligand was readily apparent. Identification of the ligands for these receptors began with 9-*cis* retinoic acid, the ligand for RXR. With further research in ligand identification for orphan receptors, rapid progress has been made in the development of compounds targeting them. [Evans & Mangelsdorf, 2014]. Another key discovery was the finding that RXR can heterodimerize with a multitude of other nuclear receptors including the retinoid acid receptor (RAR), liver x receptor (LXR), peroxisome proliferator-activated receptor (PPAR), thyroid hormone receptor (TR), and vitamin D receptor (VDR), pregnane x receptor (PXR), and constitutive androstane receptor (CAR) family proteins [Leal et al. 2021][Delfosse et al. 2021].

RXR mediates many cancer-relevant processes which has generated interest in the drug development realm. Much of the early work on RXR agonists demonstrated the effectiveness of the compounds at inducing differentiation in myeloid leukemia, mainly through RXR:RAR heterodimerization [Shiohara et al. 1999][Mehta et al. 1996][Dawson et al 1994]. Differentiation and growth arrest through RXR:RAR heterodimerization has also been shown in the context of neuroblastoma [Giannini et al. 1997]. Combinations of pharmacological agonists for RXR (bexarotene) and PPARγ (rosiglitazone) inhibited cell proliferation and induced differentiation of human colorectal cancer cells *in vitro*, and slowed growth of colorectal cancer cell xenografts *in vivo* [Cesario et al. 2006]. The efficacy of combining these therapies is notable considering RXR:PPAR heterodimers are “permissive” heterodimers insofar as they only require one ligand to either partner, in contrast to “non-permissive” heterodimers that require both ligands to initiate transcription [Pérez et al. 2011].

Two hallmarks of cancer–evasion from immune detection and tumor-associated inflammation–highlight how tumor cells sculpt and interact with the microenvironment and vice versa [Hanahan & Weinberg 2011]. The rexinoids LG100268 and LG101506 were shown to decrease inflammatory cytokine release from lipopolysaccharide (LPS) stimulated RAW264.7. cells [Cao et al. 2016]. Another study revealed bexarotene, LG100268, and pyrimidine derivatives of the two compounds suppress nitric oxide synthesis as well as downregulate LPS-induced release of cytokines and chemokines, IL1b, IL6, and CCL9 in RAW264.7 cells [Zhang et al. 2019]. In addition to their *in vitro* anti-inflammatory properties, rexinoids have shown *in vivo* efficacy in modulating the tumor microenvironment. In an MMTV-neu mouse model of HER2+ breast cancer, LG100268 decreased infiltration of myeloid derived suppressor cells (MDSCs), increased cytotoxic CD8+/helper CD4+ T-cell ratios, decreased *ex vivo* expression of T_{reg} marker FOXP3 in CD4+ T-cells, and elicited a 50% increase in PD-L1 expression in tumors [Leal et al. 2019].

Bexarotene is the only rexinoid clinically in use, with FDA and European Medicines Agency (EMA) approval as a second-line treatment in cutaneous T-cell lymphoma [Gniadecki et al 2007]. A 2003 Phase II clinical trial of patients with metastatic breast cancer showed limited clinical benefits in 20% of patients [Esteva et al 2003]. In a proof-of-concept clinical study, bexarotene reduced biomarkers cyclin D1, Ki67, and EGFR in patient tumors, an effect that correlated with drug penetrance into the tumor [Dragnev et al. 2007]. Another Phase II trial in advanced NSCLC showed limited survival benefits when bexarotene was combined with the EGFR inhibitor erlotinib. This survival benefit was notably correlated with the presence of hypertriglyceridemia [Dragnev et al. 2011]. Indeed, elevated plasma triglycerides have remained a canonical side-effect of bexarotene. In Phase I clinical trials, hypertriglyceridemia was controlled with the HMG-CoA reductase inhibitor atorvastatin [Assaf et al 2006]. RXR:LXR heterodimer-mediated transcription of SREBP has emerged as the likely culprit of the hyperlipidemic side effects in rexinoids [Marshall et al. 2015]. A major aim of new rexinoid development is the mitigation of these adverse metabolic side effects.

MSU42011 is a novel rexinoid that has comparable anti-inflammatory properties to bexarotene but results in significantly lower levels of plasma cholesterol and triglycerides in preclinical models. In a vinyl-carbamate induced murine lung cancer model, MSU42011 was more effective than bexarotene in reducing tumor burden and modulating tumor myeloid populations as both a single agent and in combination with cytotoxic chemotherapy [Moreland et al. 2020].

MLK Inhibitors

Mixed lineage kinases (MLKs) are a subset of the mitogen activated protein kinase kinase kinases (MAP3Ks). As components of MAPK signaling, MLKs have been shown to be activated by receptor tyrosine kinases (RTKs), Toll-like receptors (TLRs), G-protein coupled receptors (GPCRs), chemokine and cytokine receptors including tumor necrosis factor rectors (TNFRs) [Gallo et al. 2020]. Naturally, MAP3Ks are kinases that phosphorylate, as their name indicates, MAP2Ks. MLK3, encoded by the *MAP3K11* gene, is the most well characterized MLK family member and engages the three main MAPK pathways. MLK3 activates c-jun N terminus kinase (JNK) through phosphorylation of MKK4/7 [Rana et al. 1996] [Tibbles et al. 1996], p38 through phosphorylation of MKK3/6 [Tibbles et al. 1996][Kim et al. 2004], and extracellular signal-related kinase (ERK) by either direct phosphorylation of MKK1/2 [Chadee & Kyriakis 2004], or by acting as a scaffold for MKK1/2 induced ERK activation [Chadee et al. 2006]. MLK3 has also been shown to activate the NFkB pathway [Hehner et al. 2000].

MLKs play multifaceted roles in cancer. Pan-MLK inhibitors CEP-1347 and CEP-11004 have been shown to inhibit the growth of HRAS mutated NIH-3T3 cells [Nehu et al. 2002] and HeLa cells [Cha et al 2006], without affecting untransformed cells. The generality of this finding was confirmed in studies showing that CEP-1347 decreased viability ER+ breast cancer cells but not normal mammary epithelial cells [Wang et al 2013]. This decrease in viability from CEP-1347 is attributable to G2/M arrest; and induction of apoptosis was accompanied by an increase in Bax expression [Wang et al 2013]. Mitotic catastrophe has emerged as a possible link between cell cycle arrest and programmed cell death, wherein aneuploid cells undergo apoptosis to prevent proliferation of potentially problematic polyploid populations of cells [McGee, 2015]. Considering the pan-MLK nature of CEP-1347 and CEP-11004, it remains unclear as to which MLK(s) are the most critical target(s) in cancer.

Apart from effects on viability, MLK3 plays important roles in cancer cell invasion, migration, and metastasis [Gallo et al. 2020]. MLK3 activates JNK, which in turn phosphorylates paxillin, promoting focal adhesion turnover, a necessary step in cell migration [Chen & Gallo, 2012]. Through both JNK and ERK, MLK3 activate AP-1 family transcription factors, notably fos-related antigen 1 (Fra-1), to upregulate matrix metalloprotease (MMP) expression and modulate epithelial to mesenchymal transition (EMT) [Rattanasinchai et al. 2017]. Furthermore, CEP-1347 has been shown to inhibit migration in a gastric cancer wound healing model [Mishra et al. 2010] and in a 3D tumor spheroid model of glioblastoma [Misek et al. 2017].

CEP-1347 was previously investigated for therapeutic potential for Parkinsons disease, but failed to garner approval due to lack of efficacy [PRECEPT 2007]. Nevertheless, the validated safety profile of CEP-1347 [Parkinson Study Group, 2004] makes it a valuable candidate compound for drug repurposing in other diseases [Okada et al. 2015]. Other MLK inhibitors such as URMC-099 are better able to cross the blood-brain barrier [Goodfellow et al. 2013], and are under active investigation for neuroprotective effects in the neurological complications of acquired immunodeficiency syndrome (neuro-AIDS) [Eggert et al. 2010], autoimmune encephalitis [Bellizi et al. 2018], and traumatic neurocognitive disorders [Miller-Rhodes et al. 2019]. Like apigenin, MLK inhibitors have a robust literature on their effects on tumor cells and a growing body of work on their effects in immune cells, yet the effects of MLK inhibitors, and indeed the role of MLKs themselves, in the tumor microenvironment remains an underexplored frontier.

Accurate characterization of candidate therapeutics for their anti-tumor properties is an important step in the drug development pipeline. This chapter details the optimization of a 3D multicellular KRAS mutant LUAD spheroid platform that combines image-based growth analysis with physiological and biochemical measures of viability. Apigenin, MSU42011, and CEP-1347, representing three classes of compounds with therapeutic potential, were tested both as single agents and in combination for their impacts.

Materials & Methods

Compounds Cell lines

Apigenin was purchased from Sigma (St. Louis, MO); MSU42011 was obtained from the lab of Karen Liby (Michigan State University); CEP-1347 was purchased from Cephalon, Inc. (North Wales, PA). NCI-H358 human lung adenocarcinoma cells were purchased from American Tissue Culture Collection (ATCC). ATCC lung adenocarcinoma cell lines NCI-H23 and A549 cells were a gift from the lab of Eran Andrechek (Michigan State University). All cell lines were grown in complete growth medium consisting of RPMI (Gibco cat. 21875034) supplemented with 10% FBS (Gibco cat. 26140079) and 500U/ml penicillin/streptomycin (Gibco cat. 15070063) at 37°C and 5% CO_2.

3D Tumor Spheroids & Imaging

Spheroids were generated by seeding dissociated cells in a v-bottom 96-well plate (Greiner bio-one, cat. 651101) with NCI-H358 cells at a density of 2000/well. Plates were then centrifuged at 500*g* for 5 min and supplemented with 2% Matrigel (Corning cat. 356231). Spheroids were grown for 4 days at which time treatments were initiated (day 0). Brightfield images of individual spheroids were taken with a BZ-X-800E All-in-one fluorescence microscopy system (Keyence, Osaka, Japan) on day 0, as well as 3- and 6-days post treatment. Images were analyzed with Fiji (NIH, Bethesda, MD) by converting images to 8-bit, converting images to binary, removing outliers, and analyzing for Feret diameter (longest continuous segment between two points on edge of spheroid). Change in diameter (spheroid ΔD) of spheroids were calculated as spheroid $\Delta D = D_{final} - D_{initial}$.

Viability Assays

Viability in 2D culture was determined using a metabolite-coupled viability assay with 1000 cells/well seeded in a 96-well plate. Once cells had adhered overnight, treatments were administered, and plates were incubated for 48 h. At endpoint, 30 µl CellTiter AQueous One Solution Cell Proliferation Assay (MTS, Promega cat. G3580) was added and plates were incubated for 30 min, at which point the absorbance at 490nm was read using a Synergy Neo2 Multi-Mode Microplate Reader (BioTek Instruments Inc., Winooski, VT).

Cell viability of spheroids was assayed by transferring spheroids into a black-walled 96-well plate and using CellTiter-Glo 3D Cell Viability Assay (Promega cat. G9681) at 3- and 6-days post-treatment per manufacturer's protocol. After visually confirming successful spheroid dissociation and lysis, luminescence was read using the Synergy Neo2 Multi-Mode Microplate Reader.

Live/Dead Staining

Spheroids at 6-days post treatment were co-stained with 2µM CalceinAM (Thermo Fisher cat. C3100MP) to visualize live cells and 2µg/ml propidium iodide (PI) to visualize PIpermeable dead cells (Molecular Probes cat. AAJ66764MC). After incubation at 37°C for 1h, spheroids were washed with PBS and transferred to a flat-bottom 96 well plate and imaged with a BZ-X-800E All-in-one fluorescence microscopy system (Keyence, Osaka, Japan). Exposure levels were set for each experiment by auto-exposing the spheroid with the highest fluorescence intensity and maintaining a consistent exposure level throughout the imaging session. Z-planes through the entire spheroid were taken and a max intensity projection was generated using the full-focus feature. Images were analyzed with Fiji by calculating the spheroid mean fluorescence intensity (MFI) and normalizing to spheroid area of max intensity projection.

TNBC Organoids

Tumor organoids were generated from human TNBC patient-derived xenografts grown in NOD-SCID-γ (NSG) female mice as previously described [Sudhakaran et al. 2020]. Organoids were generated from primary tumors and peritoneal metastases and embedded in type I rat tail collagen (Corning cat. 354236) and grown for 3 days with treatments or vehicle. Organoids were then fixed with 3.7% formaldehyde and stained with rhodamine phalloidin-Alexa546 (Thermo cat. R415) and 4′,6-diamidino-2-phenylindole (DAPI) (Sigma cat. D9542). Organoids were then imaged on the Olympus FluoView 1000 confocal laser scanning microscope system, configured on an Olympus IX81 inverted microscope with Olympus FluoView 1000 Advanced Software (Olympus America, Inc., Center Valley, PA). A z-series of 17-24 images were taken and max-intensity projections and merged images were generated in Fiji.

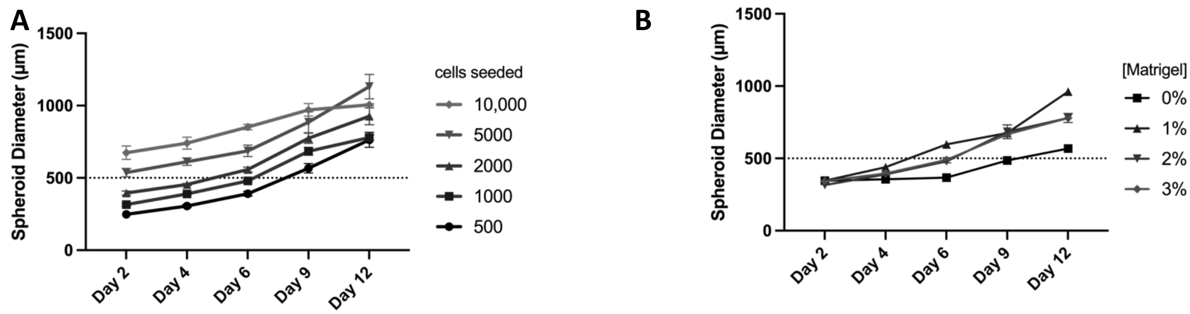

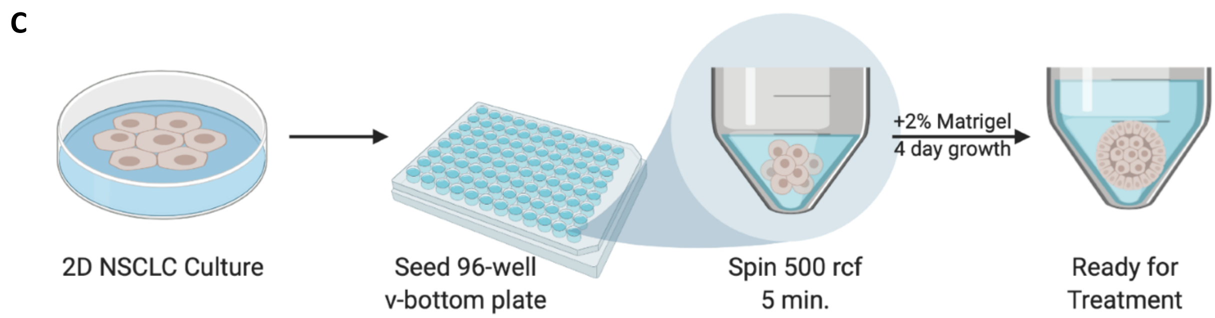

Figure 2.1. Optimization of conditions for generation and growth of NCI-H358 spheroids. To generate spheroids with initial size of <500µm diameters, NCI-H358 cells ranging from 500-10,000 cells per well (**A**) were seeded into the wells of 96-well v-bottom plate, aggregated by centrifugation at 500 *g* and supplemented with Matrigel, ranging in concentration from 0-3% (**B**). Growth was tracked for 12 days by imaging spheroids and measuring diameter. The final spheroid generation scheme is shown in panel (**C**).

Optimization of NCI-H358 spheroid model

To adapt the previously used spheroid viability model [Dubois et al. 2017] for non-small cell lung cancer, cell lines were screened to determine the best candidate cell line for the model. The NCI-H358 cell line was selected for its prior use in 3D tumor spheroid models [Kim et al. 2012b][Meenach et al. 2016] and its status as a $KRAS^{G12C}$ mutant, the most common KRAS mutation in NSCLC. NCI-H358 is notably p53-null, and WT for EGFR, ALK, KEAP1 and STK11

To optimize conditions for spheroid growth, NCI-H358 cells were seeded at various densities and spheroid growth was monitored over 12 days (Figure 2.1A). A treatment threshold of 500μm diameter after 4 days was desired to allow for sufficient room for further growth after treatment. Based upon these spheroid growth rate data, the optimal seeding density was determined to be 2000 cells/well. Differing concentrations of Matrigel were also tested for effects on spheroid growth rate, with 2% Matrigel final concentration being selected (Figure 2.1B). A schematic for optimized NCI-H358 spheroid generation is shown in Figure 2.1C.

Spheroid treatment timeline and analysis pipeline

To evaluate spheroid viability in response to treatments with compounds, images were taken at the time of treatment (t=0), at 3 days post-treatment, and at 6 days post-treatment. Six spheroids per treatment group were generated on day 4, grown until time of treatment

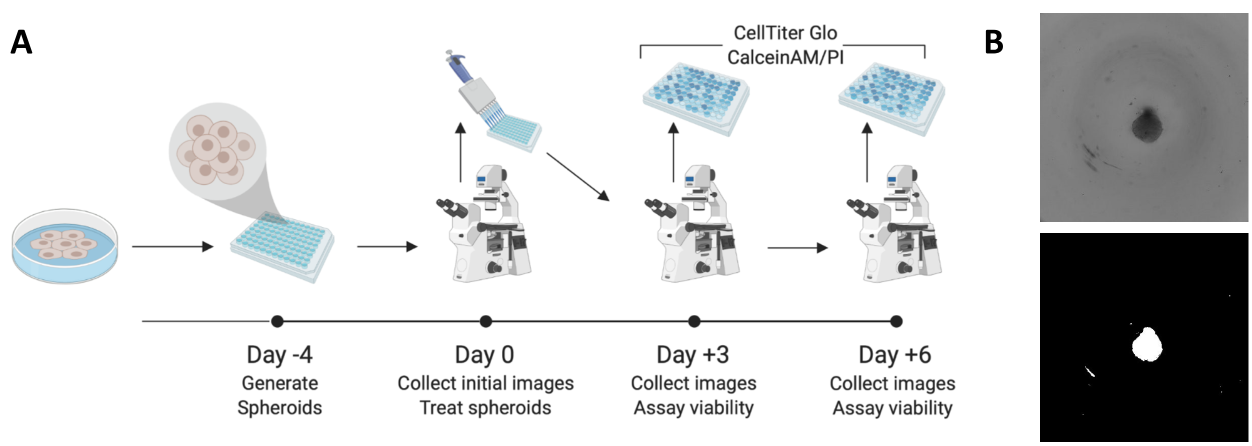

Figure 2.2. Treatment and analysis timeline of NCI-H358 spheroid viability experiments. (**A**) Spheroids (n=6) were generated over four days to allow for growth and spheroid coalescence. On Day 0, images were taken of spheroids and treatments were administered. At Day 3, images were taken of all spheroids, and endpoint analysis was performed on half (n=3) of the spheroids. Differential live/dead cell staining was performed using CalceinAM and propidium iodide. After lysis of spheroids, viability was assessed with CellTiter Glo 3D. Images and endpoint analyses of the remaining spheroids were repeated on Day 6 (n=3). (**B**) Representative image at day 0 (top). Fiji was used to convert to binary image and after removing outliers (bottom), area and Feret diameter were quantified (see methods for details).

(day 0) and imaged on day 3. Three of the spheroids were lysed for viability analysis and the remaining 3 spheroids were imaged on day 6 prior to lysis for viability assay (Figure 2A). This allowed for image-based analysis of all six spheroid on day 3 and three spheroids on day 6, leading to a larger number of replicates for spheroid ΔD at day 3.

To assess spheroid ΔD, spheroids were imaged and analyzed with ImageJ (Figure 2.2B). As a visual readout of viability/death, spheroids at their endpoint (day 3 or 6) were first stained with CalceinAM (viable) or propidium iodide (PI; dead), transferred to a flat bottomed 96-well plate, appropriate for fluorescence imaging, and once imaged, dissociated, lysed, and assayed with CellTiter Glo.

Assaying viability in 2D Culture

To determine the appropriate concentrations of each compound to test in the 3D model, NCI-H358 along with A549 and NCI-H23 cells were treated with apigenin (Figure 2.3A), MSU42011 (Figure 2.3B), or CEP-1347 (Figure 2.3C) for 48h. NCI-H358 and A549 cells showed significant decreases in viability when treated with 50μM Apigenin (45.65% reduction for NCI-H358; 22.36% reduction for A549), and no significant effects from CEP-1347 or MSU42011 at the indicated concentrations (Figure 2.3D). NCI-H23 cells showed no significant changes in viability with the three compounds.

Effects on viability in 3D Culture

Apigenin. After generation and growth over four days, NCI-H358 spheroids were treated with 50μM, 25μM or 12.5μM apigenin or vehicle. At day 3, the spheroid ΔD of DMSO spheroids was 141.4μm. A significant reduction in spheroid growth was observed upon

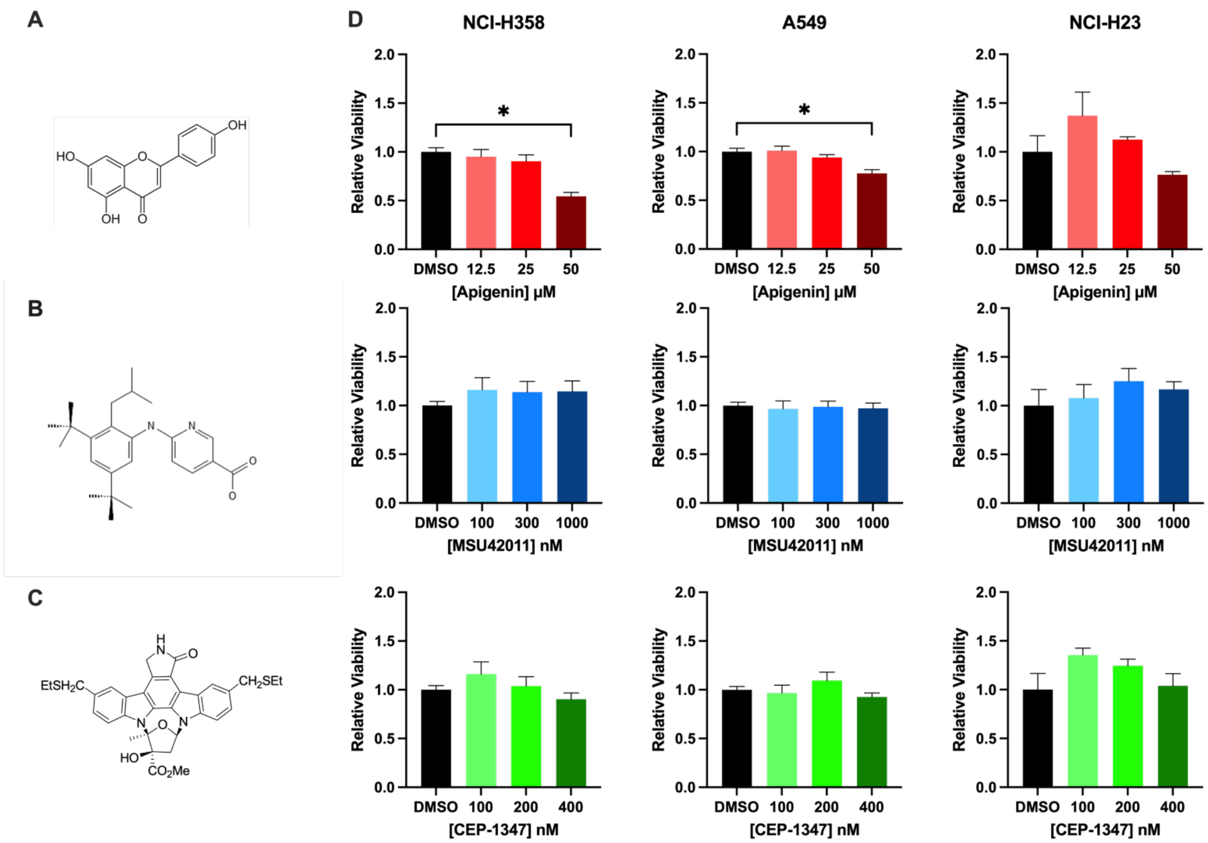

Figure 2.3. Compound structures and 2D viability measurements. Chemical structures of (**A**) apigenin, (**B**) MSU42011 and (**C**) CEP-1347. NSCLC lines NCI-H358, A549, and NCI-H23 were seeded in 2D culture in triplicate and treated with compounds or vehicle (DMSO) at indicated concentrations for 48h and assayed for viability with MTS reagent (**D**). Relative viability was quantitated as A_{490} of selected well ÷ mean A_{490} of DMSO wells. N=3 biological replicates. Statistical analysis via one-way ANOVA with Dunnett post-test; * $p<0.05$.

treatment with 25μM, as measured by spheroid ΔD. Notably, 50 μm apigenin induced spheroids regression, (spheroid ΔD -41.97μm) at day 3 compared with day 0 (Figure 2.4A). A decrease in viability as measured by CellTiter Glo was also observed in the 50 μM treatment group (38% reduction) (Figure 2.4C).

At day 6, vehicle treated spheroid ΔD was 237.2μm. A negative spheroid ΔD, indicating spheroid regression was again seen in the 50μM apigenin group (-56.11μm) and reduced growth was observed in the 25μM apigenin group (75.77μm) (Figure 2.4B). Spheroid

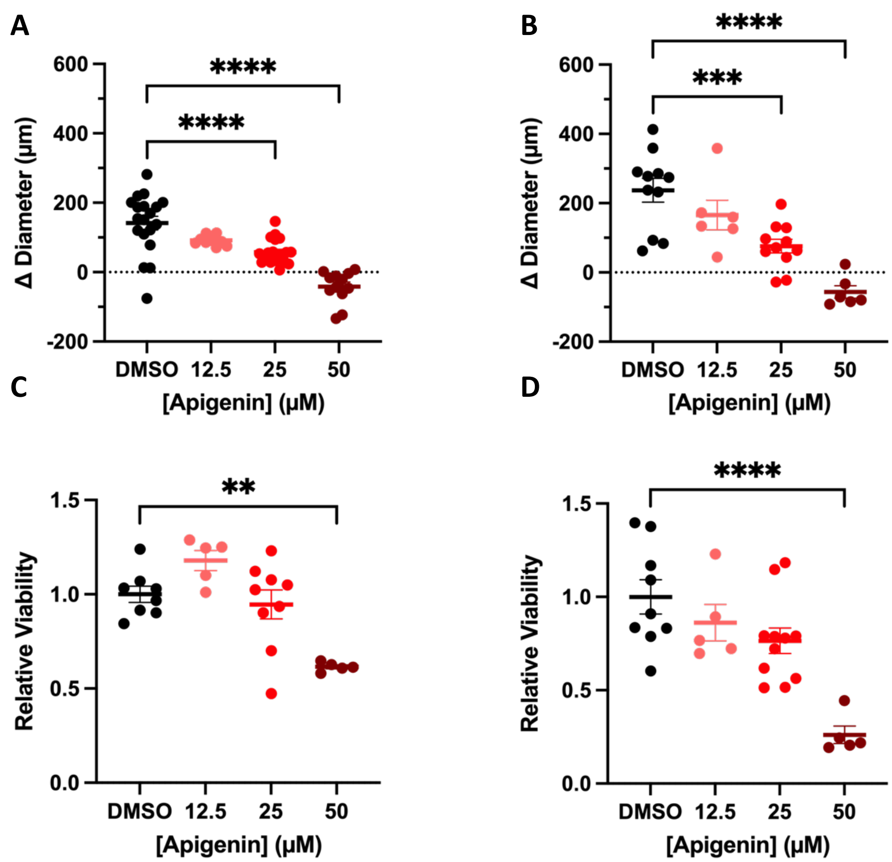

Figure 2.4. Apigenin reduces size and viability of NCI-H358 spheroids. NCI-H358 spheroids were generated and treated with apigenin at indicated concentrations. Spheroids were imaged and analyzed for change in diameter at day 3 (**A**) and day 6 (**B**) and assayed for relative viability with CellTiter Glo 3D at day 3 (**C**) and day 6 (**D**). Each data point corresponds to an individual spheroid. For each experiment n=2-6 spheroids, N=2-3 biological replicates. Statistical analysis by one-way ANOVA with Tukey post-test; ** $p<0.01$, *** $p<0.005$, **** $p<0.001$.

viability measured by CellTiter Glo was also further decreased in the 50μM apigenin treated spheroids on day 6 with a 74% decrease in viability compared to vehicle (Figure 2.4D). Taken together, these data demonstrate apigenin's ability to inhibit the growth of NCI-H358 spheroids and at high concentrations to promote regression of spheroids. This is consistent with the idea that high concentrations of apigenin can promote apoptosis.

MSU42011. To assess effects of the rexinoid MSU42011 on viability in the 3D model, NCI-H358 spheroids were treated with 1000nM, 250nM, or 62.5nM MSU42011 or vehicle control (DMSO). No significant effects on Δ diameter or viability were observed on day 3 (Figure 2.5A, 2.5C).

At day 6, spheroids treated with 1000nM MSU42011 had a larger Δ diameter of 363.3μm compared to vehicle-treated spheroids which only had a Δ diameter of 218.7μm (Figure 5B). Also at day 6, 250nM MSU42011 displayed a 54.6% increase in viability compared to vehicle. Notably, viability of spheroids treated with 1000nM MSU42011 was not

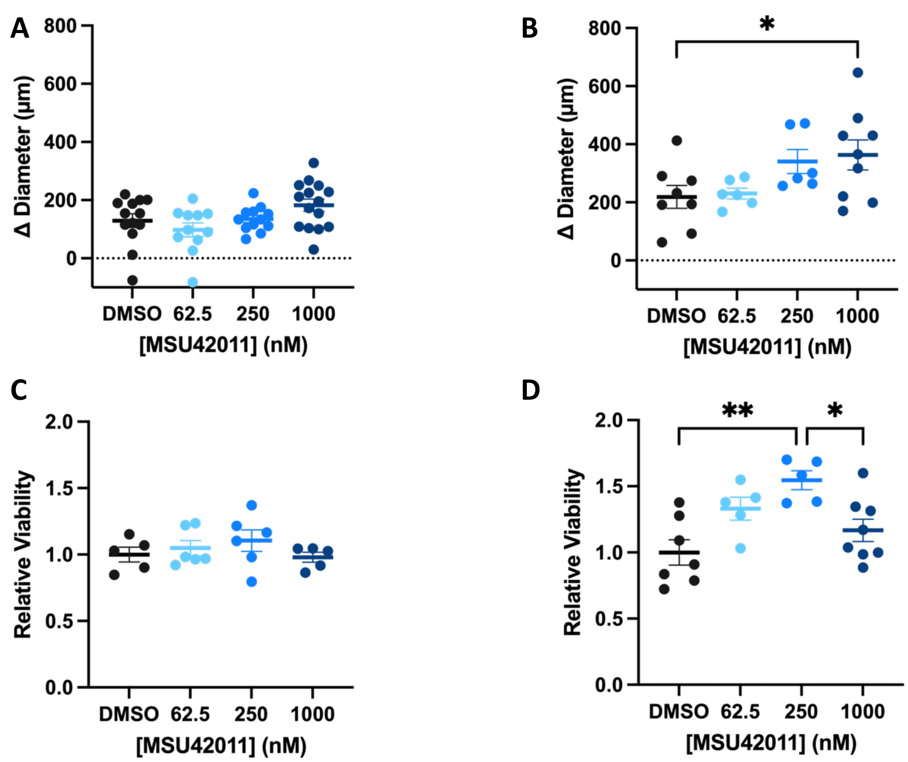

Figure 2.5. MSU42011 does not reduce growth or viability of NCI-H358 spheroids. NCI-H358 spheroids were generated and treated with the rexinoid MSU42011 at the indicated concentrations. Spheroids were imaged and analyzed for spheroid ΔD (**A-B**) and assayed for relative viability with CellTiter Glo 3D (**C-D**). Each datapoint corresponds to a spheroid. For each experiment n=2-6 spheroids, N=2-3 experiments. Statistical analysis via one-way ANOVA with Tukey post-test; * $p<0.05$, ** $p<0.01$

significantly from vehicle treated spheroids (Figure 2.5D). These data indicate that MSU42011 does not inhibit the growth of NCI-H358 spheroids and may in fact modestly promote spheroid growth under these experimental conditions.

Combination treatments in 3D culture

Apigenin + MSU42011. In a prior *in vivo* lung cancer prevention study, mice treated with a combination of celery-based apigenin-rich (CEBAR) diet and MSU42011 had significantly reduced tumor burden compared to control (Liby and Doseff labs, unpublished). Stemming from this result, NCI-H358 spheroids were treated with a combination of apigenin and MSU42011; growth was quantified by spheroid spheroid ΔD, and viability was assessed using CellTiter Glo. Relative cell death was quantified by staining with propidium iodide (PI), along with the cell viability counterstain CalceinAM. On day 3, both single agent and combination treated spheroids showed similar viability, and only 25μM apigenin concentration showed a decrease in Δ diameter. Spheroids treated with 25μM apigenin and 1μM MSU42011 in combination were not significantly different from either of the two single-agent groups (Figure 2.6A, C).

On day 6, viability of combination treated spheroids did not differ significantly from control. However, combination treated spheroids had significantly lower viability compared to MSU42011 alone, but it was not statistically different from treatment with apigenin alone (Figure 2.6B). The growth of spheroids measured as Δ diameter (105μm) in response to combination apigenin and MSU42011 was also significantly lower than that of spheroids treated with MSU42011 alone (361.3μm) (Figure 2.6D). Despite the finding that addition of

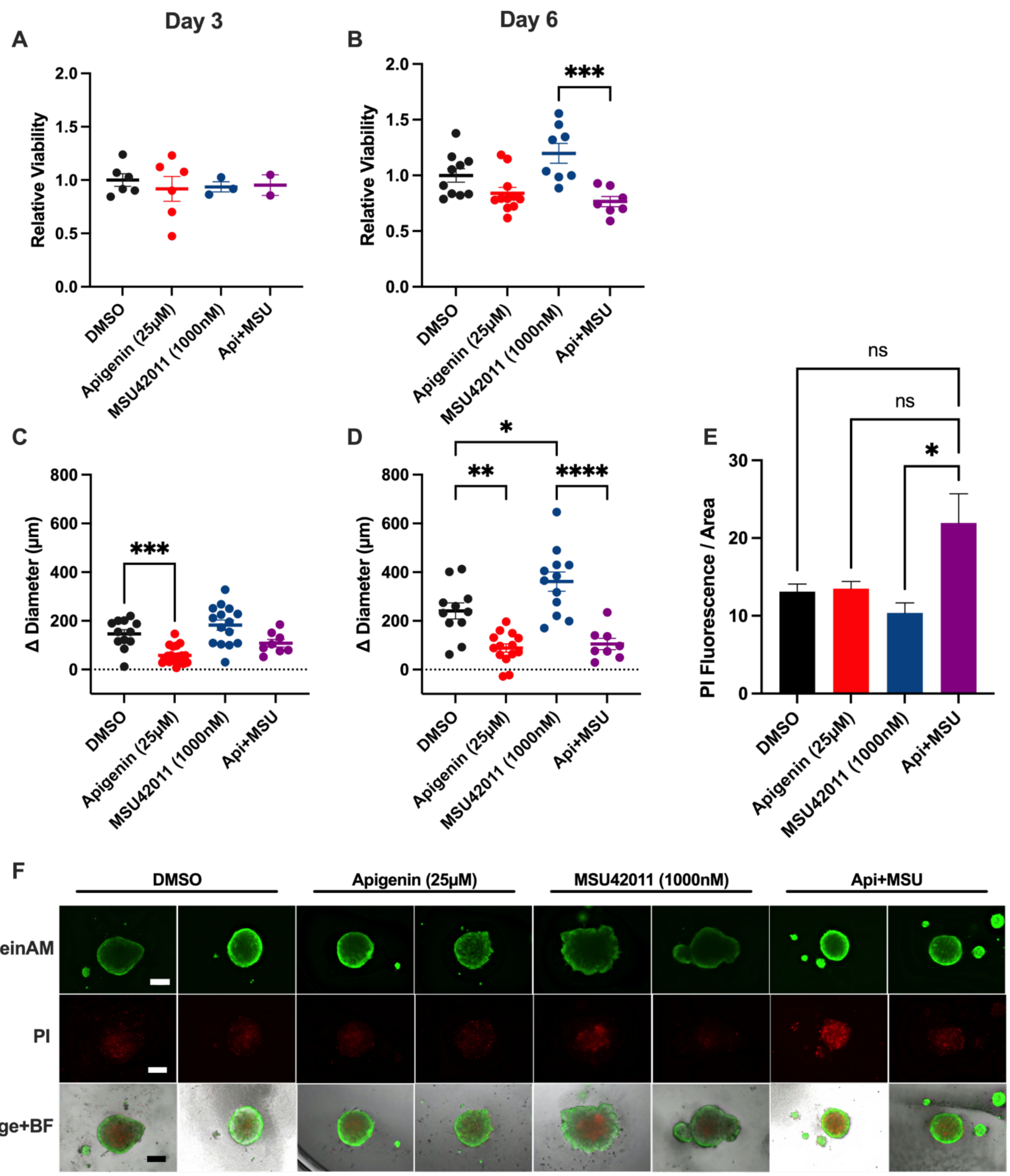

Figure 2.6. Lack of synergy of apigenin and MSU42011 in NCI-H358 spheroids. Spheroids were generated as previously described, treated, and assayed for viability (**A-B**) and imaged in brightfield (BF) to determine spheroid ΔD (**C-D**) on post-treatment days 3 and 6. Spheroids were also stained with CalceinAM (*green) and* propidium iodide (PI, *red*), as indicators of viability and death, respectively. PI fluorescence intensity was quantified and normalized to spheroid area (**F**). Two representatives shown, N=3 spheroid experiments with n=2-6 spheroids per experiment. Scalebar = 200µm. (**E**) Statistical analysis via one-way ANOVA with Tukey post-test, * $p<0.05$, ** $p<0.01$, *** $p<0.005$, **** $p<0.001$.

MSU42011 did not impact efficacy of apigenin in reducing tumor spheroid growth, the combination treatment significantly increased cell death, as measured by fluorescence intensity of propidium iodide (PI), when compared to treatment with MSU 42011 alone.

The combination treatment trended toward increased cell death over treatment with apigenin alone, but this did not reach statistical significance (Figure 2.6E-F). In summary, the combination of apigenin and MSU42011 does not synergize to inhibit spheroid growth. However, apigenin did effectively suppress both tumor spheroid growth and the increased viability induced by MSU42011.

It should be noted that small Calcein AM staining spheroid-like bodies were observed in the vicinity of the H358 spheroids, which were more prominent in the combination treatment group. This observation is difficult to interpret as spheroids are transferred from their original plate to a flat-bottomed 96-well plate for imaging. These bodies may be fragments from the original spheroid sheared off by pipetting or could alternatively be smaller spheroids that formed from incomplete aggregation during spheroid generation.

Apigenin+CEP-1347 The effects of apigenin, CEP-1347 and the combination thereof were investigated in a tumor organoid invasion pilot experiment. In brief, human TNBC xenografts were grown in NSG mice, and subsequently harvested to generate organoids as described [Sudhakaran et al. 2020]. In a pilot experiment presented here, lymph node metastases were harvested and used to generate spheroids which were subsequently embedded in 3D collagen and treated with vehicle, apigenin (25 μM), CEP-1347 (400 nM), or combination for 3 days. Compared to untreated organoids, the apigenin or CEP-1347 treated

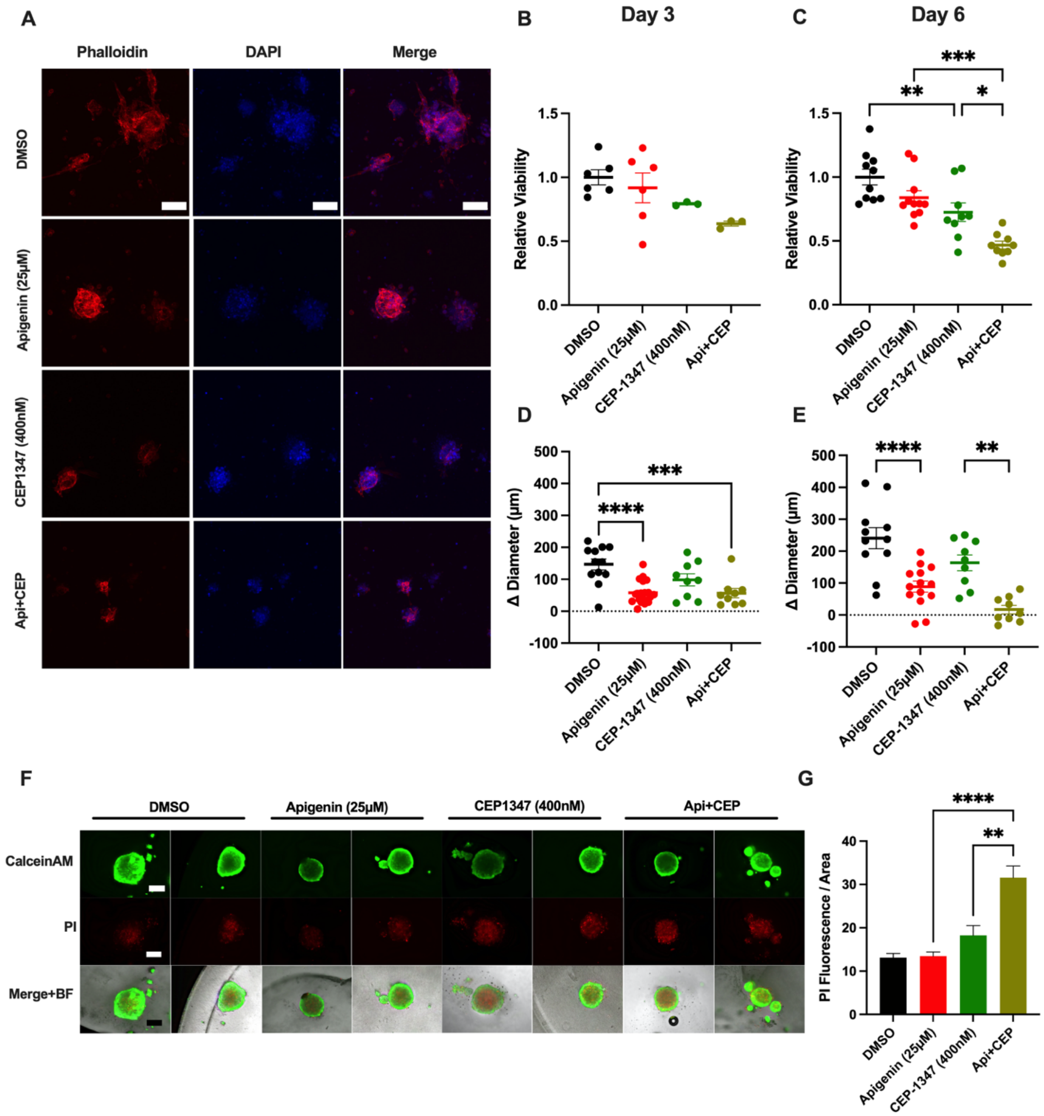

Figure 2.7. Apigenin and CEP-1347 synergize to decrease viability in NCI-H358 spheroids. (**A**) Organoids generated from triple-negative breast cancer xenografts (see text for details) were stained with DAPI (*blue*) and phalloidin (*red*) and showed marked reductions in size and invasiveness when treated with apigenin, CEP-1347, and in combination (scalebar = 100μm). N=1 experiment with n=3 image fields per treatment group. NCI-H358 spheroids were generated as previously described, treated, and assayed for viability (**B-C**) and imaged in brightfield (BF) to determine spheroid ΔD (**D-E**) on post-treatment days 3 and 6. (**F**) Spheroids were stained with CalceinAM (*green*) and propidium iodide (PI, *red*) (two representatives shown, scalebar = 200μm). (**G**) PI fluorescence intensity was quantified and normalized to spheroid area. N=3 spheroid experiments with n=2-6 spheroids per experiment. Statistical analysis via one-way ANOVA with Tukey post-test, * $p<0.05$, ** $p<0.01$, *** $p<0.005$, **** $p<0.001$

spheroids appeared less invasive, and organoids treated with the combination were substantially smaller than the untreated group (Figure 2.7A). The apparent regression observed in combination treatment of CEP-1347 and apigenin prompted investigation into the effects of the combination in the 3D LUAD spheroid model.

Thus, the combination of apigenin and CEP-1347 was investigated using the NCI-H358 spheroid model. At day 3, no significant differences in viability were observed between control and 25μM apigenin, 400nM CEP-1347, or the combination (Figure 2.7B). At day 3 spheroid ΔD was diminished by 25μM apigenin (57.57μm), but not by 400nM CEP-1347 treatments (96.36μm) compared to control (146.58μm). Spheroid ΔD upon combination treatment at 3 days was comparable to apigenin treatment alone (56.49μm) (Figure 2.7D).

At day 6, spheroids treated with 400nM CEP-1347 alone had a significant reduction in viability of 26% measured through CTG. When combined with 25μM apigenin, the viability was further reduced to 53% of control (Figure 2.7C). Contrastingly, spheroid ΔD at day 6 of CEP-1347 treatment was not significantly different from vehicle (163.5μm for CEP-1347, 240.8μm for vehicle) (Figure 2.7E). Finally, PI fluorescence of combination spheroids (31.57) was significantly higher than CEP-1347 alone (18.26) or apigenin alone (13.48, SEM±0.928) (Figure 2.7F-G).

Taken together, these data indicate that apigenin can decrease spheroid growth as measured by spheroid ΔD while CEP-1347 is effective in decreasing viability as measured by CTG. The combination of apigenin and CEP-1347 synergizes to decrease both measures of viability and increases cell death as measured by PI staining.

Discussion

The revolution in targeted cancer therapies has led to the development of more efficacious treatments with improvements in side-effects. However, whether by tumor cell-intrinsic mechanisms mitigating cytotoxic chemotherapy and radiation or through target alteration or pathway circumvention in targeted therapy, most lung cancers develop resistance [Wang et al. 2021b]. The development of novel therapies is necessary to overcome this challenge.

In the initial viability study with 2D culture, apigenin significantly decreased the viability of NCI-H358 and A549, but not NCI-H23 cells. One potential explanation for this difference between these KRAS mutant cell lines is the differential engagement KRAS effectors. Yuan et al [2018] used an siRNA screen to determine the dependency of KRAS mutant cancer cell lines and identified the KRAS-subtype which is dependent on KRAS and the RSK-subtype which are dependent upon RSK rather than KRAS. Interestingly, A549 and NCI-H358 cell lines are classified as KRAS-subtype, while NCI-H23 is an RSK-subtype cell line. The findings from the 2D viability experiments suggest that these subtypes may be important to apigenin's effects on viability. Testing other cell lines that have known KRAS or RSK dependency may clarify whether KRAS dependency is necessary for apigenin to exert its effects on viability.

Comparison of 2D viability assays and 3D spheroid viability assays reveal differences between the two methods. For 2D viability, the MTS assay which measures the substrate reduction by NADH, typically correlates with the number of cells, but can also be modulated by metabolic processes independent of cell number [McGowan et al. 2011]. The 3D approach addresses this by measuring multiple dimensions of viability including a metabolic equivalent (ATP through CellTiter Glo 3D), a physical growth dimension (spheroid ΔD), and testing membrane permeability (PI penetrance). Concordance between these measurements can confirm results, and discordance between them can aid in determining mechanisms by which compounds are acting. Whereas there was no significant change in spheroid ΔD, CEP-1347 treatment did elicit a remarkable decrease in CTG viability and increased cell death stain PI, albeit non-significantly (Figure 2.7). This effect was robustly amplified with the addition of Apigenin, which underscores the potential for effective combined use of these two compounds.

The combination treatment with MSU42011 and Apigenin was initiated by data from a prior *in vivo* study that indicated potential benefit for lung cancer prevention from the combination of MSU42011 and CEBAR, a dietary formulation of apigenin (data not shown). In the tumor spheroid model, it did not appear that these drugs were beneficial in combination, and the effect of 25μM apigenin seemed to outweigh any effect from 1μM MSU42011 (Figure 2.6). The spheroid model, however, lacks input from immune components, which both compounds have been shown to modulate *in vivo*.

The combination treatment with CEP-1347 and Apigenin was prompted by data from a prior collaborative study examining the effects of apigenin on TNBC PDX-derived organoids [Sudhakaran et al. 2020]. In a pilot study, lymph node metastases from the orthotopic PDX TNBC model were used to generate organoids and investigate the impact of

CEP-1347 and apigenin on organoid invasion in 3D collagen (Figure 2.7A). These organoids were used to investigate the effects of compounds on invasion. Both single agent apigenin and CEP-1347 decreased the invasive phenotype as well as spheroid size. A substantial reduction in organoid size was observed in the apigenin+CEP-1347 combination treatment. The combination treatment in this spheroid model resulted in a reduction in viability greater than the sum of the individual effect sizes at day 6 (Figure 2.7C, E, & G).

All three of the compounds used in this chapter also have potential anti-tumor immunomodulatory activity. Apigenin downregulates inducible PD-L1 expression [Jian et al. 2021], giving the compound potential as a sensitizer for checkpoint inhibitors. Lung cancers are generally considered good candidates for immunotherapy, stemming from their high mutational burden [Castle et al. 2019]. Rexinoids, and specifically MSU42011, have been shown in other cancers to increase the level of CD8+ cytotoxic T-cells, and enhance the efficacy of anti-PD-L1 and –PD1 checkpoint inhibitors [Leal et al. 2021]. Finally, CEP-1347 has been shown to re-educate macrophage-like cells in neuroinflammation and liver inflammation contexts [Gallo et al. 2020], indicating potential use of the compound in re-educating tumor associated macrophages.

In summary, the 3D tumor spheroid model adapted here was able to capture effects on viability from compounds that were not readily apparent in a traditional 2D viability assay. The incorporation of immune components into this assay may shed more light on compounds with immunomodulatory mechanisms. Finally, deeper mechanistic investigations are merited for the apigenin+CEP-1347 combination treatment, as this combination showed synergistic decreases in all viability dimensions.

REFERENCES

REFERENCES

Ahmed, Semim Akhtar, Dey Parama, Enush Daimari, Sosmitha Girisa, Kishore Banik, Choudhary Harsha, Uma Dutta, and Ajaikumar B. Kunnumakkara. "Rationalizing the therapeutic potential of apigenin against cancer." *Life Sciences* 267 (2021): 118814.

Assaf, C., M. Bagot, R. Dummer, Madeleine Duvic, R. Gniadecki, R. Knobler, A. Ranki, P. Schwandt, and S. Whittaker. "Minimizing adverse side‐effects of oral bexarotene in cutaneous T‐cell lymphoma: an expert opinion." *British Journal of Dermatology* 155, no. 2 (2006): 261-266.

Bao, Yang‐Yang, Shui‐Hong Zhou, Zhong‐Jie Lu, Jun Fan, and Ya‐Ping Huang. "Inhibiting GLUT-1 expression and PI3K/Akt signaling using apigenin improves the radiosensitivity of laryngeal carcinoma in vivo." *Oncology reports* 34, no. 4 (2015): 1805-1814.

Bellizzi, Matthew J., Jennetta W. Hammond, Herman Li, Mary A. Gantz Marker, Daniel F. Marker, Robert S. Freeman, and Harris A. Gelbard. "The mixed-lineage kinase inhibitor URMC-099 protects hippocampal synapses in experimental autoimmune encephalomyelitis." *eNeuro* 5, no. 6 (2018).

Cao, Hui-Hui, Jian-Hong Chu, Hiu-Yee Kwan, Tao Su, Hua Yu, Chi-Yan Cheng, Xiu-Qiong Fu et al. "Inhibition of the STAT3 signaling pathway contributes to apigenin-mediated anti-metastatic effect in melanoma." *Scientific reports* 6, no. 1 (2016): 1-12.

Cao, Martine, Darlene B. Royce, Renee Risingsong, Charlotte R. Williams, Michael B. Sporn, and Karen T. Liby. "The rexinoids LG100268 and LG101506 inhibit inflammation and suppress lung carcinogenesis in A/J mice." *Cancer Prevention Research* 9, no. 1 (2016): 105-114.

Castellanos, Emily, Emily Feld, and Leora Horn. "Driven by mutations: the predictive value of mutation subtype in EGFR-mutated non–small cell lung cancer." *Journal of thoracic oncology* 12, no. 4 (2017): 612-623.

Cesario, Rosemary M., Jessica Stone, Wan-Ching Yen, Reid P. Bissonnette, and William W. Lamph. "Differentiation and growth inhibition mediated via the RXR: PPARγ heterodimer in colon cancer." *Cancer letters* 240, no. 2 (2006): 225-233.

Cha, Hyukjin, Surabhi Dangi, Carolyn E. Machamer, and Paul Shapiro. "Inhibition of mixed-lineage kinase (MLK) activity during G2-phase disrupts microtubule formation and mitotic progression in HeLa cells." *Cellular signalling* 18, no. 1 (2006): 93-104.

Chadee, Deborah N., and John M. Kyriakis. "MLK3 is required for mitogen activation of B-Raf, ERK and cell proliferation." *Nature cell biology* 6, no. 8 (2004): 770-776.

Chadee, Deborah N., Dazhong Xu, Gene Hung, Ali Andalibi, David J. Lim, Zhijun Luo, David H. Gutmann, and John M. Kyriakis. "Mixed-lineage kinase 3 regulates B-Raf through maintenance of the B-Raf/Raf-1 complex and inhibition by the NF2 tumor suppressor protein." *Proceedings of the National Academy of Sciences* 103, no. 12 (2006): 4463-4468.

Chang, Jer-Hwa, Chao-Wen Cheng, Yi-Chieh Yang, Wan-Shen Chen, Wen-Yueh Hung, Jyh-Ming Chow, Pai-Sheng Chen, Michael Hsiao, Wei-Jiunn Lee, and Ming-Hsien Chien. "Downregulating CD26/DPPIV by apigenin modulates the interplay between Akt and Snail/Slug signaling to restrain metastasis of lung cancer with multiple EGFR statuses." *Journal of Experimental & Clinical Cancer Research* 37, no. 1 (2018): 1-16.

Chen, Jian, and Kathleen A. Gallo. "MLK3 regulates paxillin phosphorylation in chemokine-mediated breast cancer cell migration and invasion to drive metastasis." *Cancer research* 72, no. 16 (2012): 4130-4140.

Chen, Minghui, Xueshi Wang, Daolong Zha, Fangfang Cai, Wenjing Zhang, Yan He, Qilai Huang, Hongqin Zhuang, and Zi-Chun Hua. "Apigenin potentiates TRAIL therapy of non-small cell lung cancer via upregulating DR4/DR5 expression in a p53-dependent manner." *Scientific reports* 6, no. 1 (2016): 1-17.

Colunga Biancatelli, Ruben Manuel Luciano, Max Berrill, John D. Catravas, and Paul E. Marik. "Quercetin and vitamin C: an experimental, synergistic therapy for the prevention and treatment of SARS-CoV-2 related disease (COVID-19)." *Frontiers in immunology* 11 (2020): 1451.

Dawson, Marcia I., Elena Elstner, Masahiro Kizaki, Dan-Lin Chen, Seppo Pakkala, Berit Kerner, and H. Phillip Koeffler. "Myeloid differentiation mediated through retinoic acid receptor/retinoic X receptor (RXR) not RXR/RXR pathway." *Blood* (1994): 446-452.

Delfosse, Vanessa, Tiphaine Huet, Deborah Harrus, Meritxell Granell, Maxime Bourguet, Caroline Gardia-Parège, Barbara Chiavarina et al. "Mechanistic insights into the synergistic activation of the RXR–PXR heterodimer by endocrine disruptor mixtures." *Proceedings of the National Academy of Sciences* 118, no. 1 (2021).

Diniz, Lúcio Ricardo Leite, Marilia Trindade de Santana Souza, Allana Brunna Sucupira Duarte, and Damião Pergentino de Sousa. "Mechanistic aspects and therapeutic potential of quercetin against COVID-19-associated acute kidney injury." *Molecules* 25, no. 23 (2020): 5772.

Dragnev, Konstantin H., W. Jeffrey Petty, Sumit J. Shah, Lionel D. Lewis, Candice C. Black, Vincent Memoli, William C. Nugent et al. "A proof-of-principle clinical trial of bexarotene in patients with non–small cell lung cancer." *Clinical Cancer Research* 13, no. 6 (2007): 1794-1800.

Dragnev, Konstantin H., Tian Ma, Jobin Cyrus, Fabrizio Galimberti, Vincent Memoli, Alexander M. Busch, Gregory J. Tsongalis et al. "Bexarotene plus erlotinib suppress lung carcinogenesis independent of KRAS mutations in two clinical trials and transgenic models." *Cancer Prevention Research* 4, no. 6 (2011): 818-828.

Dubois, Clémence, Robin Dufour, Pierre Daumar, Corinne Aubel, Claire Szczepaniak, Christelle Blavignac, Emmanuelle Mounetou, Frédérique Penault-Llorca, and Mahchid Bamdad. "Development and cytotoxic response of two proliferative MDA-MB-231 and non-proliferative SUM1315 three-dimensional cell culture models of triple-negative basal-like breast cancer cell lines." *Oncotarget* 8, no. 56 (2017): 95316.

Eggert, Dawn, Prasanta K. Dash, Santhi Gorantla, Huanyu Dou, Giovanni Schifitto, Sanjay B. Maggirwar, Stephen Dewhurst, Larisa Poluektova, Harris A. Gelbard, and Howard E. Gendelman. "Neuroprotective activities of CEP-1347 in models of neuroAIDS." *The journal of immunology* 184, no. 2 (2010): 746-756.

Esteva, Francisco J., John Glaspy, Said Baidas, Leslie Laufman, Laura Hutchins, Maura Dickler, Debu Tripathy et al. "Multicenter phase II study of oral bexarotene for patients with metastatic breast cancer." *Journal of clinical oncology* 21, no. 6 (2003): 999-1006.

Evans, Ronald M., and David J. Mangelsdorf. "Nuclear receptors, RXR, and the big bang." *Cell* 157, no. 1 (2014): 255-266.

US Food & Drug Administration. "NDA/BLA Multi-disciplinary Review and Evaluation: LUMAKRAS™ (sotorasib)" https://www.accessdata.fda.gov/drugsatfda_docs/nda/2021/214665Orig1s000MultidisciplineR.pdf

Gallo, Kathleen A., Edmund Ellsworth, Hayden Stoub, and Susan E. Conrad. "Therapeutic potential of targeting mixed lineage kinases in cancer and inflammation." *Pharmacology & therapeutics* 207 (2020): 107457.

Giannini, Giuseppe, Marcia I. Dawson, Xiao-kun Zhang, and Carol J. Thiele. "Activation of three distinct RXR/RAR heterodimers induces growth arrest and differentiation of neuroblastoma cells." *Journal of Biological Chemistry* 272, no. 42 (1997): 26693-26701.

Gniadecki, R., C. Assaf, M. Bagot, R. Dummer, M. Duvic, R. Knobler, Annamari Ranki, P. Schwandt, and S. Whittaker. "The optimal use of bexarotene in cutaneous T‐cell lymphoma." *British Journal of Dermatology* 157, no. 3 (2007): 433-440.

Goodfellow, Val S., Colin J. Loweth, Satheesh B. Ravula, Torsten Wiemann, Thong Nguyen, Yang Xu, Daniel E. Todd et al. "Discovery, synthesis, and characterization of an orally bioavailable, brain penetrant inhibitor of mixed lineage kinase 3." *Journal of medicinal chemistry* 56, no. 20 (2013): 8032-8048.

Hanahan, Douglas, and Robert A. Weinberg. "Hallmarks of cancer: the next generation." *Cell* 144, no. 5 (2011): 646-674.

Hehner, Steffen P., Thomas G. Hofmann, Alexej Ushmorov, Oliver Dienz, Irene Wing-Lan Leung, Norman Lassam, Claus Scheidereit, Wulf Dröge, and M. Lienhard Schmitz. "Mixed-lineage kinase 3 delivers CD3/CD28-derived signals into the IκB kinase complex." *Molecular and Cellular Biology* 20, no. 7 (2000): 2556-2568.

Hu, Xiao-Wen, Dan Meng, and Jing Fang. "Apigenin inhibited migration and invasion of human ovarian cancer A2780 cells through focal adhesion kinase." *Carcinogenesis* 29, no. 12 (2008): 2369-2376.

Jiang, Ze-Bo, Wen-Jun Wang, Cong Xu, Ya-Jia Xie, Xuan-Run Wang, Yi-Zhong Zhang, Ju-Min Huang et al. "Luteolin and its derivative apigenin suppress the inducible PD-L1 expression to improve anti-tumor immunity in KRAS-mutant lung cancer." *Cancer Letters* (2021).

Kim, Ki-Yong, Byung-Chul Kim, Zhiheng Xu, and Seong-Jin Kim. "Mixed lineage kinase 3 (MLK3)-activated p38 MAP kinase mediates transforming growth factor-β-induced apoptosis in hepatoma cells." *Journal of Biological Chemistry* 279, no. 28 (2004): 29478-29484.

Kim, Taeyoon, Il Doh, and Young-Ho Cho. "A 3D tumor spheroid chip with the pharmacokinetic drug elimination model developed by balanced droplet dispensing." Sensors and Actuators B: *Chemical* 174 (2012): 436-440.

Leal, Ana S., Kayla Zydeck, Sarah Carapellucci, Lyndsey A. Reich, Di Zhang, Jessica A. Moerland, Michael B. Sporn, and Karen T. Liby. "Retinoid X receptor agonist LG100268 modulates the immune microenvironment in preclinical breast cancer models." *NPJ breast cancer* 5, no. 1 (2019): 1-15.

Leal, Ana S., Lyndsey A. Reich, Jessica A. Moerland, Di Zhang, and Karen T. Liby. "Potential therapeutic uses of rexinoids." *Advances in Pharmacology* 91 (2021): 141-183.

Lee, Wei-Jiunn, Wen-Kang Chen, Chau-Jong Wang, Wea-Lung Lin, and Tsui-Hwa Tseng. "Apigenin inhibits HGF-promoted invasive growth and metastasis involving blocking PI3K/Akt pathway and β4 integrin function in MDA-MB-231 breast cancer cells." *Toxicology and applied pharmacology* 226, no. 2 (2008): 178-191.

Li, Yunxia, Xin Chen, Wei He, Shuyue Xia, Xiaochuan Jiang, Xiaoyang Li, Jiayu Bai, Nan Li, Lei Chen, and Biao Yang. "Apigenin enhanced antitumor effect of cisplatin in lung cancer via inhibition of cancer stem cells." *Nutrition and cancer* 73, no. 8 (2021): 1489-1497.

Lim, Zuan-Fu, and Patrick C. Ma. "Emerging insights of tumor heterogeneity and drug resistance mechanisms in lung cancer targeted therapy." *Journal of hematology & oncology* 12, no. 1 (2019): 1-18.

Liu, Yifei, Zhengyi Li, Xiaoxu Xue, Yong Wang, Yijie Zhang, and Junpeng Wang. "Apigenin reverses lung injury and immunotoxicity in paraquat-treated mice." *International immunopharmacology* 65 (2018): 531-538.

Lu, Hsu-Feng, Yu-Jie Chie, Ming-Sung Yang, Ching-Sung Lee, Jene-John Fu, Jai-Sing Yang, Tzu-Wei Tan et al. "Apigenin induces caspase-dependent apoptosis in human lung cancer A549 cells through Bax-and Bcl-2-triggered mitochondrial pathway." I*nternational journal of oncology* 36, no. 6 (2010): 1477-1484.

Lu, Hsu-Feng, Yu-Jie Chie, Ming-Sung Yang, Kung-Wen Lu, Jene-John Fu, Jai-Sing Yang, Hung-Yi Chen et al. "Apigenin induces apoptosis in human lung cancer H460 cells through caspase-and mitochondria-dependent pathways." *Human & experimental toxicology* 30, no. 8 (2011): 1053-1061.

Madunić, Ivana Vrhovac, Josip Madunić, Maja Antunović, Mladen Paradžik, Vera Garaj-Vrhovac, Davorka Breljak, Inga Marijanović, and Goran Gajski. "Apigenin, a dietary flavonoid, induces apoptosis, DNA damage, and oxidative stress in human breast cancer MCF-7 and MDA MB-231 cells." *Naunyn-Schmiedeberg's archives of pharmacology* 391, no. 5 (2018): 537-550.

Mc Gee, Margaret M. "Targeting the mitotic catastrophe signaling pathway in cancer." *Mediators of inflammation* 2015 (2015).

McGowan, Eileen M., Nikki Alling, Elise A. Jackson, Daniel Yagoub, Nikolas K. Haass, John D. Allen, and Rosetta Martinello-Wilks. "Evaluation of cell cycle arrest in estrogen responsive MCF-7 breast cancer cells: pitfalls of the MTS assay." *PloS one* 6, no. 6 (2011): e20623.

Meenach, Samantha A., Alexandra N. Tsoras, Ronald C. McGarry, Heidi M. Mansour, J. Zach Hilt, and Kimberly W. Anderson. "Development of three-dimensional lung multicellular spheroids in air-and liquid-interface culture for the evaluation of anticancer therapeutics." *International journal of oncology* 48, no. 4 (2016): 1701-1709.

Mehta, Kapil, Teresa McQueen, Nouri Neamati, Steven Collins, and Michael Andreeff. "Activation of retinoid receptors RAR alpha and RXR alpha induces differentiation and apoptosis, respectively, in HL-60 cells." *Cell growth & differentiation: the molecular biology journal of the American Association for Cancer Research* 7, no. 2 (1996): 179-186.

Miller-Rhodes, Patrick, Cuicui Kong, Gurpreet S. Baht, Priyanka Saminathan, Ramona M. Rodriguiz, William C. Wetsel, Harris A. Gelbard, and Niccolò Terrando. "The broad spectrum mixed-lineage kinase 3 inhibitor URMC-099 prevents acute microgliosis and cognitive decline in a mouse model of perioperative neurocognitive disorders." *Journal of neuroinflammation* 16, no. 1 (2019): 1-15.

Misek, Sean A., Jian Chen, Laura Schroeder, Chotirat Rattanasinchai, Ashley Sample, Jann N. Sarkaria, and Kathleen A. Gallo. "EGFR signals through a DOCK180-MLK3 axis to drive glioblastoma cell invasion." *Molecular Cancer Research* 15, no. 8 (2017): 1085-1095.

Mishra, Prajna, Subramanian Senthivinayagam, Velusamy Rangasamy, Gautam Sondarva, and Basabi Rana. "Mixed lineage kinase-3/JNK1 axis promotes migration of human gastric cancer cells following gastrin stimulation." *Molecular endocrinology* 24, no. 3 (2010): 598-607.

Moore, Amanda R., Scott C. Rosenberg, Frank McCormick, and Shiva Malek. "RAS-targeted therapies: is the undruggable drugged?." *Nature Reviews Drug Discover*y 19, no. 8 (2020): 533-552.

Moerland, Jessica A., Di Zhang, Lyndsey A. Reich, Sarah Carapellucci, Beth Lockwood, Ana S. Leal, Teresa Krieger-Burke, Bilal Aleiwi, Edmund Ellsworth, and Karen T. Liby. "The novel rexinoid MSU-42011 is effective for the treatment of preclinical Kras-driven lung cancer." *Scientific reports* 10, no. 1 (2020): 1-16.

Nheu, Thao V., Hong He, Yumiko Hirokawa, Kazuhiko Tamaki, Lore Florin, M. Lienhard Schmitz, Ikuko Suzuki-Takahashi et al. "The K252a derivatives, inhibitors for the PAK/MLK kinase family, selectively block the growth of HAS transformants." *The Cancer Journal* 8, no. 4 (2002): 328-336.

Okada, Masashi, Hiroyuki Takeda, Hirotsugu Sakaki, Kenta Kuramoto, Shuhei Suzuki, Tomomi Sanomachi, Keita Togashi, Shizuka Seino, and Chifumi Kitanaka. "Repositioning CEP-1347, a chemical agent originally developed for the treatment of Parkinson's disease, as an anti-cancer stem cell drug." *Oncotarget* 8, no. 55 (2017): 94872.

Parkinson Study Group. "The safety and tolerability of a mixed lineage kinase inhibitor (CEP-1347) in PD." *Neurology* 62, no. 2 (2004): 330-332.

Patil, Rajeshwari H., R. L. Babu, M. Naveen Kumar, KM Kiran Kumar, Shubha M. Hegde, Govindarajan T. Ramesh, and S. Chidananda Sharma. "Apigenin inhibits PMA-induced expression of pro-inflammatory cytokines and AP-1 factors in A549 cells." *Molecular and cellular biochemistry* 403, no. 1 (2015): 95-106.

Pérez, Efrén, William Bourguet, Hinrich Gronemeyer, and Angel R. de Lera. "Modulation of RXR function through ligand design." *Biochimica et Biophysica Acta (BBA)-Molecular and Cell Biology of Lipids* 1821, no. 1 (2012): 57-69.

Piantelli, Mauro, Cosmo Rossi, Manuela Iezzi, Rossana La Sorda, Stefano Iacobelli, Saverio Alberti, and Pier Giorgio Natali. "Flavonoids inhibit melanoma lung metastasis by impairing tumor cells endothelium interactions." *Journal of Cellular Physiology* 207, no. 1 (2006): 23-29.

Parkinson Study Group PRECEPT Investigators. "Mixed lineage kinase inhibitor CEP-1347 fails to delay disability in early Parkinson disease." *Neurology* 69, no. 15 (2007): 1480-1490.

Rana, Ajay, Kathleen Gallo, Paul Godowski, Shu-ichi Hirai, Shigeo Ohno, Leonard Zon, John M. Kyriakis, and Joseph Avruch. "The mixed lineage kinase SPRK phosphorylates and activates the stress-activated protein kinase activator, SEK-1." *Journal of Biological Chemistry* 271, no. 32 (1996): 19025-19028.

Rattanasinchai, C., B. J. Llewellyn, S. E. Conrad, and K. A. Gallo. "MLK3 regulates FRA-1 and MMPs to drive invasion and transendothelial migration in triple-negative breast cancer cells." *Oncogenesis* 6, no. 6 (2017): e345-e345.

Seo, Hye-Sook, Jin Mo Ku, Han-Seok Choi, Jong-Kyu Woo, Bo-Hyoung Jang, Yong Cheol Shin, and Seong-Gyu Ko. "Induction of caspase-dependent apoptosis by apigenin by inhibiting STAT3 signaling in HER2-overexpressing MDA-MB-453 breast cancer cells." *Anticancer research* 34, no. 6 (2014): 2869-2882.

Sever, Richard, and Christopher K. Glass. "Signaling by nuclear receptors." *Cold Spring Harbor perspectives in biology* 5, no. 3 (2013): a016709.

Shiohara, Masaaki, Marcia I. Dawson, Peter D. Hobbs, Nobukuni Sawai, Tsukasa Higuchi, Kenichi Koike, Atsushi Komiyama, and H. Phillip Koeffler. "Effects of novel RAR-and RXR-selective retinoids on myeloid leukemic proliferation and differentiation in vitro." *Blood* 93, no. 6 (1999): 2057-2066.

Shukla, Sanjeev, and Sanjay Gupta. "Apigenin: a promising molecule for cancer prevention." *Pharmaceutical research* 27, no. 6 (2010): 962-978.

Sudhakaran, Meenakshi, Michael Ramirez Parra, Hayden Stoub, Kathleen A. Gallo, and Andrea I. Doseff. "Apigenin by targeting hnRNPA2 sensitizes triple-negative breast cancer spheroids to doxorubicin-induced apoptosis and regulates expression of ABCC4 and ABCG2 drug efflux transporters." *Biochemical pharmacology* 182 (2020): 114259.

Tibbles, Lee Anne, Y. L. Ing, F. Kiefer, J. Chan, N. Iscove, J. R. Woodgett, and N. J. Lassam. "MLK‒3 activates the SAPK/JNK and p38/RK pathways via SEK1 and MKK3/6." *The EMBO journal* 15, no. 24 (1996): 7026-7035.

Villalobos-Ayala, Krystal, Ivannie Ortiz Rivera, Ciara Alvarez, Kazim Husain, DeVon DeLoach, Gerald Krystal, Margaret L. Hibbs, Kun Jiang, and Tomar Ghansah. "Apigenin Increases

SHIP-1 Expression, Promotes Tumoricidal Macrophages and Anti-Tumor Immune Responses in Murine Pancreatic Cancer." *Cancers* 12, no. 12 (2020): 3631.

Voss, Oliver H., Daniel Arango, Justin C. Tossey, Miguel A. Villalona Calero, and Andrea I. Doseff. "Splicing reprogramming of TRAIL/DISC-components sensitizes lung cancer cells to TRAIL-mediated apoptosis." *Cell death & disease* 12, no. 4 (2021): 1-12.

Wang, Limin, Kathleen A. Gallo, and Susan E. Conrad. "Targeting mixed lineage kinases in ER-positive breast cancer cells leads to G2/M cell cycle arrest and apoptosis." *Oncotarget* 4, no. 8 (2013): 1158.

Wang, Meina, Roy S. Herbst, and Chris Boshoff. "Toward personalized treatment approaches for non-small-cell lung cancer." *Nature medicine* 27, no. 8 (2021): 1345-1356.

Watanabe, Norihiro, Ryoichi Hirayama, and Nobuo Kubota. "The chemopreventive flavonoid apigenin confers radiosensitizing effect in human tumor cells grown as monolayers and spheroids." *Journal of radiation research* 48, no. 1 (2007): 45-50.

Way, Tzong-Der, Ming-Ching Kao, and Jen-Kun Lin. "Apigenin induces apoptosis through proteasomal degradation of HER2/neu in HER2/neu-overexpressing breast cancer cells via the phosphatidylinositol 3-kinase/Akt-dependent pathway." *Journal of Biological Chemistry* 279, no. 6 (2004): 4479-4489.

Xu, Lu, Yang Zhang, Kang Tian, Xi Chen, Rongxin Zhang, Xindi Mu, Yueguang Wu et al. "Apigenin suppresses PD-L1 expression in melanoma and host dendritic cells to elicit synergistic therapeutic effects." *Journal of experimental & clinical cancer research* 37, no. 1 (2018): 1-15.

Zhang, Junxia, Liqin Chao, Xianghua Liu, Yanmei Shi, Caili Zhang, Lingfei Kong, and Ruiqin Li. "The potential application of strategic released apigenin from polymeric carrier in pulmonary fibrosis." *Experimental lung research* 43, no. 9-10 (2017): 359-369.

Zhang, Di, Ana S. Leal, Sarah Carapellucci, Pritika H. Shahani, Jaskaran S. Bhogal, Samir Ibrahim, San Raban et al. "Testing novel pyrimidinyl rexinoids: a new paradigm for evaluating rexinoids for cancer prevention." *Cancer Prevention Research* 12, no. 4 (2019): 211-224.

Zhao, Ying, Hui Huang, Chang-Hao Jia, Ke Fan, Tao Xie, Zeng-Yan Zhu, and Mei-Lin Xie. "Apigenin increases radiosensitivity of glioma stem cells by attenuating HIF-1α-mediated glycolysis." *Medical Oncology* 38, no. 11 (2021): 1-10.

Zhou, Xiang, Tian Gao, Xiao-Gang Jiang, and Mei-Lin Xie. "Protective effect of apigenin on bleomycin-induced pulmonary fibrosis in mice by increments of lung antioxidant ability and PPARγ expression." *Journal of functional foods* 24 (2016): 382-389.

CHAPTER 3. Testing a novel NRF2 inhibitor to prevent invasion and migration using a 3D tumor spheroid invasion model

Introduction

As a malignancy of a vital organ, lung cancer metastasis has received comparably less investigation than metastasis in cancers of non-vital organs such as breast and skin. Lung cancer can metastasize elsewhere in the lung, as well as to the pleura, lymph nodes, liver, adrenal gland, bone, and brain [Popper 2016]. The overall relative five-year survival rate of lung cancer is 21.7%, comparatively low in relation to other cancers. However, the five-year survival rate of those with distant metastases is an abysmal 6.3%, compared to nearly 60% in those with localized disease [SEER, 2021]. Thus, understanding and interrupting lung cancer metastasis is critical to reducing mortality.

NRF2 axis alterations in LUAD

Nuclear Factor Erythroid 2-Related Factor 2 (NRF2) is a transcription factor encoded by the *NFE2L2* gene and is responsible for regulating cellular responses to oxidative stress. Under normal conditions, NRF2 is sequestered by Kelch-like ECH associated protein 1 (KEAP1), which mediates the degradation of NRF2 through Cul3 E3 ligase [Kansanen et al. 2013]. Under conditions of oxidative stress, KEAP1 undergoes the oxidation of cysteine residues leading to its release of NRF2, allowing NRF2 to translocate to the nucleus, bind antioxidant response elements (AREs), and initiate transcription of effector genes [Kansanen et al. 2013]. Molecular alterations in the NRF2 axis, such as KEAP1 inactivation (Figure 3.1A), *NFLE2L2* amplification, or CUL3 inactivation, occur in roughly 25% of NSCLC (Chapter 1; Figure 1.1). The role of NRF2 in cancer is complex; NRF2 plays an important role in preventing cancer initiation by combatting ROS-induced DNA damage and thus may prevent cancer initiation. Once cancer has been initiated, however, NRF2 upregulation promotes cancer progression by conferring resistance to cell death as well as reprogramming metabolism and redox balance [Satoh et al. 2013]. KEAP1 mutations vary in both the level of NRF2 activation [Wilson et al. 2021] and effects on cellular physiology [Probst et al. 2015]. Oncogenic KRAS has also been shown to increase transcription of *NFE2L2* [Tao et al. 2014] reinforcing the importance of NRF2 pathway activation in lung cancer.

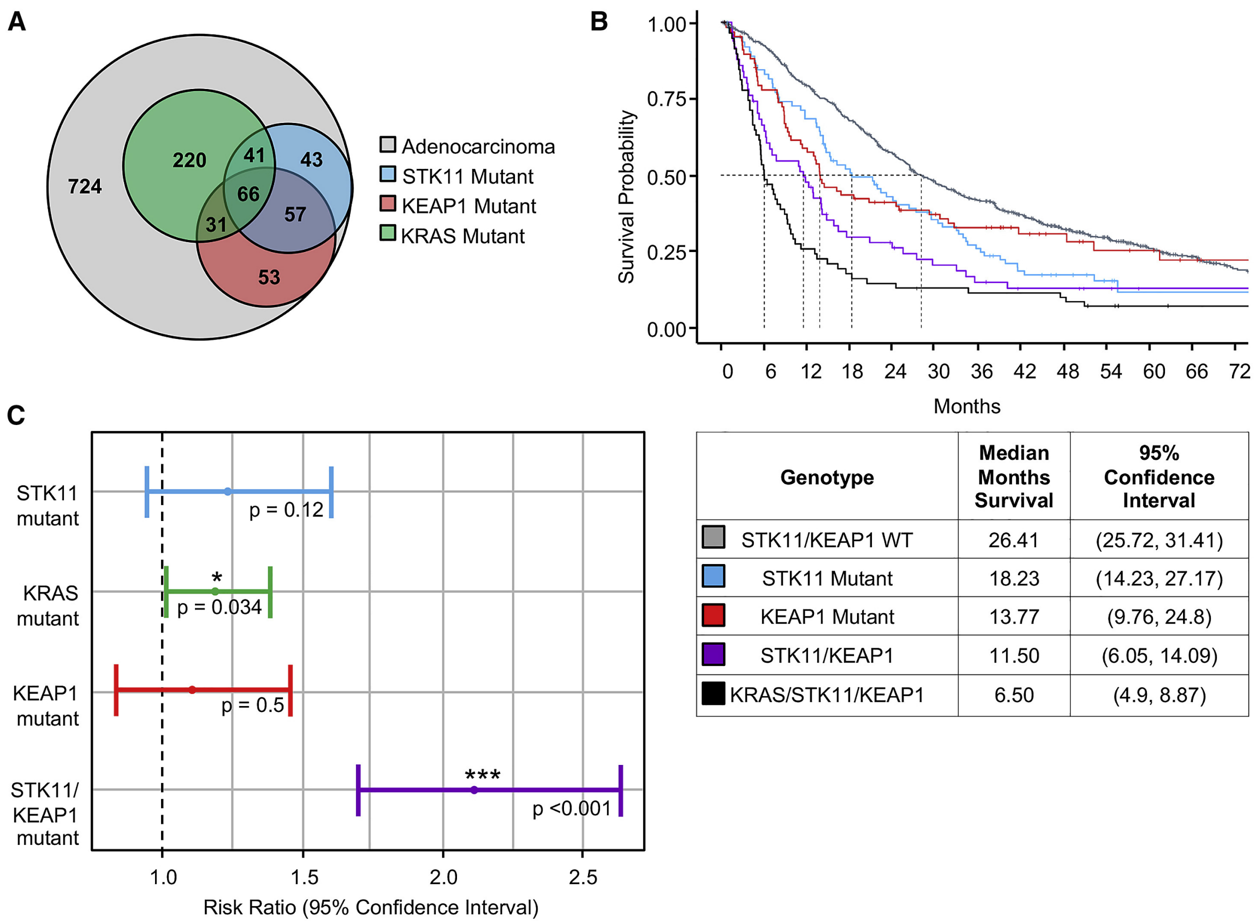

Genotype	Median Months Survival	95% Confidence Interval
STK11/KEAP1 WT	26.41	(25.72, 31.41)
STK11 Mutant	18.23	(14.23, 27.17)
KEAP1 Mutant	13.77	(9.76, 24.8)
STK11/KEAP1	11.50	(6.05, 14.09)
KRAS/STK11/KEAP1	6.50	(4.9, 8.87)

Figure 3.1. NRF2 pathway alterations in NSCLC. (**A**) Frequency of NRF2 and related pathway alterations (**B)** Co-occurrence of KEAP1 and STK11 molecular alterations in NSCLC. (**C**) Overall survival of LUAD patients comparing tumors with KEAP1 mutation, STK11 mutation, both, and neither. Reproduced from Wohlhieter et al. 2020 under Creative Commons Attribution Non-Commercial No-Derivatives License.

Metastasis & the NRF2/BACH1 axis

NRF2 has been implicated in the metastatic process at multiple levels. NRF2 induces EMT in cancer cell lines by downregulating E-cadherin [Arfmann-Knübel et al. 2015] and upregulating N-cadherin, the latter of which is achieved through the NRF2 target *NOTCH1* [Zhao et al. 2017]. Activation of NRF2 is correlated with activation of the migration promoting the RhoA/ROCK pathway [Zhang et al. 2016], and increases in MMP2 and MMP9, important matrix metalloproteases that degrade ECM [de la Vega et al. 2018]. Finally, reciprocal NRF2 activation between tumor cells and macrophages has been shown to induce EMT, indicating a key role for NRF2 in the tumor microenvironment [Feng et al. 2018]. The key NRF2-induced gene product *HMOX1*, heme oxygenase-1 (HO-1), metabolizes intracellular free heme, which also allows for accumulation of BACH1 protein [Igarashi et al. 2021].

A recent pair of publications found that BACH1, stabilized by NRF2 activation, drives formation of metastases in lung cancer under conditions of chronic antioxidant treatment [Anderson & Simon, 2019][Wiel et al. 2019][Lignitto et al. 2019]. Degradation of BACH1 is coordinated by the F-box protein FBXO22 of the E3 ubiquitin ligase complex, whose binding to BACH1 is stabilized by intracellular heme [Lignitto et al. 2019]. BACH1 itself inhibits *HMOX1* transcription, completing a negative feedback loop [Sun et al. 2002]. In pancreatic cancer (PDAC), BACH1 directly represses expression of the genes encoding Claudin 3 (*CLDN3*) and claudin 4 (*CLDN4)*, which are important for maintaining cell-cell tight junctions [Sato et al. 2020]. BACH1 regulates EMT-related transcription factors FOXA1 and SNAI2 in PDAC [Sato et al. 2020]. SNAI2 upregulation by BACH1 has also been observed in ovarian cancer [Han et al. 2019]. In NSCLC, BACH1 upregulates *GAPDH* and *HK2* to induce glycolysis-dependent metastasis [Wiel et al. 2019] However, the detailed mechanism linking glycolysis and metastasis is yet to be fully elucidated.

Ferroptosis

Evasion of programmed cell death is one of the original six hallmarks of cancer [Hanahan & Weinberg, 2001]. In addition to apoptosis, an iron-dependent death process known as ferroptosis has recently been identified as a relevant cell death mechanism in cancers. In the presence of overwhelming oxidative stress, such as in response to chemotherapy or when antioxidant defenses are impaired, lipid peroxidation and ferroptotic cell death can ensue [Dixon et al. 2012]. The cystine/glutamate antiporter, encoded by the *SCL7A11* gene, is a transcriptional target of NRF2 [Hassannia et al. 2019], and plays a key role in maintaining cellular glutathione (GSH) [Anandhan et al. 2020], the primary cellular antioxidant. NRF2 transcriptional targets also include the heme metabolism gene *HMOX1,* iron storage gene *FTH1,* and multiple iron transport systems, which further protect against oxidative damage and ferroptosis [Anandhan et al. 2020]. Thus, KEAP1 mutant LUADs, which show high NRF2 activity, are predicted to be resistant to ferroptosis.

Serine-threonine kinase 11 (STK11) is mutated in approximately 17% of LUAD (Figure 3.1A). Co-mutation of KEAP1 and STK11 occurs, which occurs in roughly 10% of LUAD (Figure 3.1A), profoundly negatively impacts overall survival (Figure 3.1B) as well as portending poor response to both checkpoint inhibitors and chemotherapy [Papillon-Cavanaugh et al. 2020]. A recent study provides evidence that loss of STK11 and KEAP1 synergistically protects KRAS mutant NSCLC cells from ferroptosis [Wohlhieter et al. 2020], a result confirmed through a genetically engineered mouse model that showed concomitant mutations of KEAP1, STK11, and KRAS dramatically reduces survival [Singh et al. 2021].

Pharmacologically targeting NRF2

Because of the dual nature of NRF2, with activation preventing cancer initiation in normal cells, but promoting survival of existing tumor cells by protecting them from cell death, both activators and inhibitors of NRF2 have garnered interest. Activators of NRF2 are plentiful and generally act by inhibiting KEAP1 directly or inhibiting the interaction between NRF2 and KEAP1 [Roblendinos-Antón et al. 2019]. Contrastingly, there are fewer inhibitors of NRF2, many of which are also ligands of other nuclear factors such as the glucocorticoid receptor (dexamethasone), the retinoid-α receptor (all-*trans*-retinoic acid) and retinoid-X receptor (bexarotene and other rexinoids). Brusatol, a plant-derived quassinoid, inhibits NRF2 by blocking protein translation, which inevitably leads to inhibition of other high turnover proteins [Roblendinos-Antón et al. 2019].

A screen conducted by Liby et al. using a *tert*-butylhydroquinone (tBHQ) stimulated ARE-luciferase reporter gene identified the novel compound MSU38225 as a NRF2 pathway inhibitor. This compound reduced total NRF2 in addition to blocking its nuclear localization. In combination with carboplatin, MSU38225 significantly lowered tumor burden in an *in vivo* xenograft model of A549 LUAD and reduced histological markers of proliferation along with intratumoral NRF2 protein expression [Zhang et al. 2021]. MSU-71, a derivative of MSU38225 modified for improved solubility, was shown to be more potent than MSU38225 in reducing viability of both A549 and NCI-H460 LUAD cells. Importantly, both cell lines harbor co-mutations of KEAP1, STK11, and KRAS, which portend poor survival (Figure 3.1B-C).

While MSU38225 and other NRF2 inhibitors have been investigated for their effects on tumor burden and cancer cell viability, the effects of NRF2 inhibitors on lung cancer metastatic potential have not been examined. This chapter investigates the effects of NRF2 pathway inhibitors on LUAD migration and invasion. This chapter details the application of an established 3D tumor spheroid invasion assay [Lim et al. 2020] to investigate the effects of MSU-71 on macrophage-induced LUAD invasion, as well as the adaptation of the model to human LUAD and macrophage cell lines.

Materials & Methods

Compounds & Cell Lines

MSU38225 and MSU-71 were synthesized by the lab of Aaron Odom (Michigan State University) and were obtained through the lab of Karen Liby (Michigan State University). Both compounds were dissolved in vehicle (DMSO) and were validated to be ≥98% pure through gas chromatography with flame ionization detection.

LLC1/LL2-luc cells were obtained from ATCC and RAW246.7-gfp cells were a gift from the lab of Sophia Ran (Southern Illinois University); both lines were maintained in DMEM (Gibco, cat. 11995065) supplemented with 10% FBS (Gibco cat. 26140079) and 500U/ml penicillin/streptomycin (Gibco cat. 15070063). ATCC lung adenocarcinoma cell lines A549, NCI-H23, and NCI-H1975 cells were a gift from the lab of Eran Andrechek (Michigan State University), NCI-H358 cells were obtained from American Tissue Culture Collection. These lines were maintained in RPMI-1640 (Gibco, cat. 21875034) supplemented with 10% FBS (Gibco cat. 26140079) and 500U/ml penicillin/streptomycin (Gibco cat. 15070063). THP-1 cells were obtained from ATCC (Michigan State University) and were maintained in RPMI-1640 (Gibco, cat. 21875034) supplemented with 5% low-endotoxin FBS (Gibco cat. 26140079) and 500U/ml penicillin/streptomycin (Gibco cat. 15070063). All cell lines were grown at 37°C and 5% CO_2.

Transwell Migration Assays

A549 cells were dissociated and resuspended in serum free medium (RPMI) and $5x10^4$ cells added to the upper chamber of each transwell (8µm pore size; VWR, cat. 10769-234). In the bottom chamber, medium containing 5% FBS was used as a chemoattractant. Treatments or vehicle control were added to both the upper and lower chambers. After allowing cells to migrate for 24h, transwell inserts were fixed with 3.7% formaldehyde, stained with DAPI (300 nM) and imaged with a BZ-X-800E All-in-one fluorescence microscopy system (Keyence, Osaka, Japan). Images were analyzed with Fiji (NIH, Bethesda, MD) by stacking all images, converting to 8-bit and binary (using threshold setting "moments"), removing outliers (2.0px, radius 50) and analyzing particles. The number of particles was taken as the number of migrated cells and was spot checked against unprocessed images to ensure analysis was accurate. See Appendix for Fiji image analysis macro script (Supplemental Information A1).

In transwell migration experiments where the effects of THP-1 cells on tumor cell migration were tested, 10^5 THP-1 cells were seeded in the bottom of a 24-well plate and differentiated into M0 macrophages with 100ng/ml PMA for 72h prior to the initiation of the migration assay. After differentiation, M0 THP-1s were rinsed three times with warm PBS and the migration experiment was conducted as indicated above.

Spheroid Generation

LLC1/LL2-luc, A549, H23, H358, or H460 cells were dissociated and resuspended at a density of 4 x 10^5 cells/ml in their respective complete growth medium supplemented with 0.24% methylcellulose (Thermo Fisher cat. S25427). On the lid of a petri dish, cells were carefully plated in 25μl drops containing 1000 cells for each spheroid at a spacing that prevented coalescence of drops. The lid was then inverted and placed on top of the petri dish containing 10 ml sterile H_2O. After incubation for 3 days, spheroids were ready for use and were transferred for embedding using a cut 200 μl-pipette tip.

Conditioned Media Generation

To generate RAW 264.7 macrophage conditioned medium (mCM), $4x10^6$ RAW246.7-gfp cells were seeded into a 10 cm plate in complete growth media (8 ml) and incubated for 48h. After conditioning, medium was centrifuged at 500*g* for 5 min to remove cellular debris. To generate THP-1 M0 conditioned media, $6x10^6$ THP-1 cells were seeded into a 10 cm plate in 10 ml of their growth medium and differentiated with 100 nM phorbol 12-myristate 13-acetate (PMA) for 48h. Once differentiated, THP-1 M0 macrophages were rinsed three times with PBS and 6ml of fresh growth medium was added. After conditioning for 48h, medium was centrifuged at 500*g* for 5 min to remove cellular debris. To generate THP-1/tumor cell co-culture medium, $3x10^6$ tumor cells were added to THP-1 M0s during conditioning.

Spheroid Embedding & Invasion Assay

In a 96-well plate, 30μl of Matrigel (Corning) was added to wells. The plate was then briefly vortexed to ensure full well coverage by the Matrigel and large bubbles were eliminated using a high-gauge needle. After incubation at 37°C for 60 min to polymerize Matrigel, an additional 30 μl of Matrigel was added to wells, followed promptly by the addition of the spheroid in 20μl media. After another 60min incubation, 100μl of medium (normal or mCM) with treatment or vehicle was added.

After spheroid embedding and treatment, spheroids were imaged (day 0 images), and then allowed to grow at 37°C and 5% CO_2. After three days of growth, spheroids were imaged again (day 3 images) and analyzed using Fiji (NIH, Bethesda, MD). Analysis was conducted by outlining the perimeter of the spheroids with free-draw tool in Fiji and analyzing the region of interest for area, perimeter, and circularity[4].

Results

Transwell migration assay

To test the effects of the novel NRF2 pathway inhibitor, MSU-71, on NSCLC cell migration, a transwell migration assay using 5% serum as chemoattractant was performed on A549 cells with vehicle, 10μM of previously published [Zhang et al. 2021] NRF2 pathway inhibitor MSU38225 or 10μM of the novel inhibitor MSU-71. Both compounds significantly reduced migration by approximately 75% ($p<.005$) (Figure 3.2A). To further investigate the novel compound, a dose response transwell migration experiment was performed with

[4] Circularity is defined as 4π (area÷perimeter^2)

MSU-71 at 1, 5, and 10 µM. MSU-71 reduced cell migration by more than 2-fold at 5µM concentration ($p=0.104$), and statistically significantly reduced migration by 80% in the 10µM treatment ($p<0.05$) (Figure 3.2B).

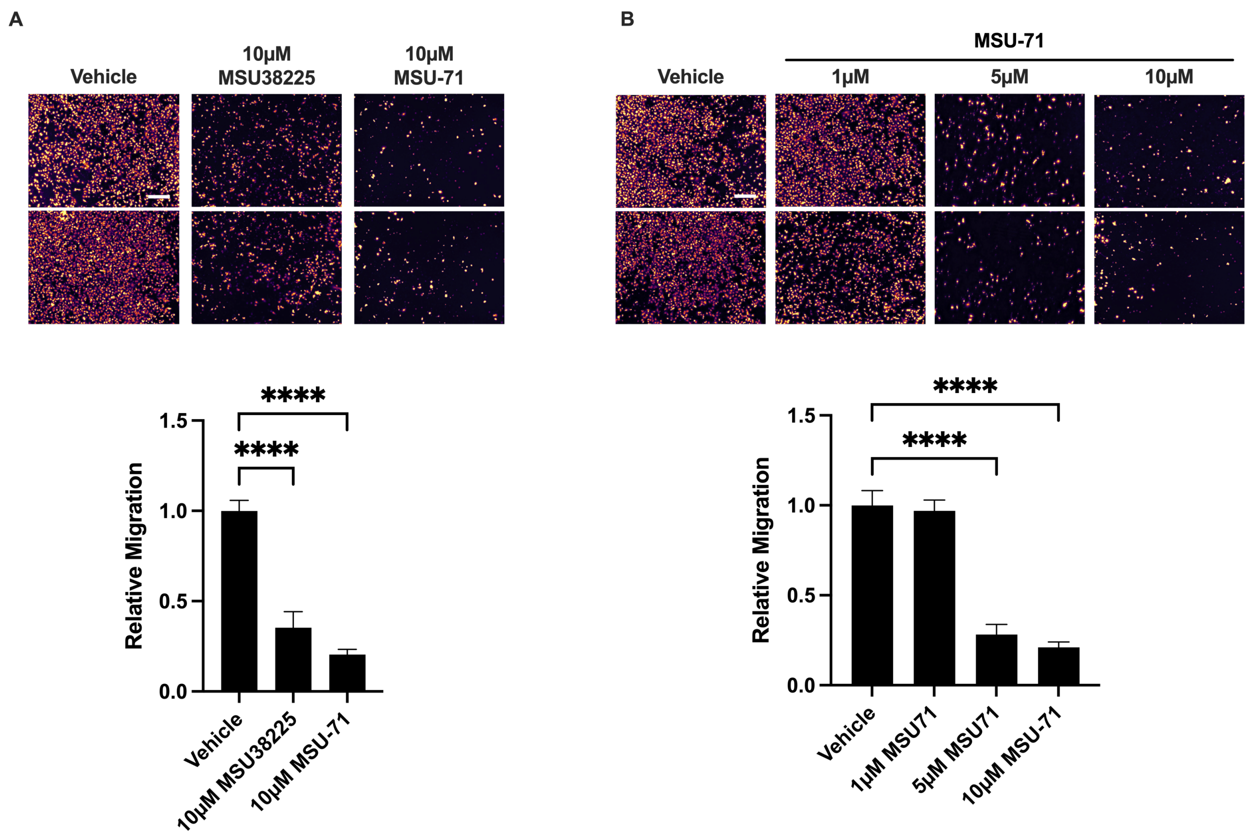

Figure 3.2. NRF2 pathway inhibitors reduce NSCLC transwell migration. A549 cells were seeded in serum-free medium with **(A)** 10µM of NRF2 pathway inhibitors MSU38225 or MSU-71; or **(B)** 1µM, 5µM and 10µM of MSU-71 in the top chamber of transwells. Media containing treatments and 5% FBS as a chemoattractant was used in the bottom chamber and cells were allowed to migrate for 24 h, at which point filters were fixed, unmigrated cells removed, and remaining cells were stained with DAPI, and imaged (9 fields per transwell insert, 2 representatives shown). Vehicle for both drugs was an equivalent volume of DMSO as the largest volume of treatment used. Scale bars = 200µm. n=2 transwell inserts for each condition, N=2-3 experimental replicates. Statistical analysis via one-way ANOVA with Dunnett post-test, **** $p<0.001$.

Spheroid invasion assay validation

To optimize initial conditions, spheroids were generated via the hanging drop method with either 1000 or 2000 cells per spheroid. It was determined that spheroids initiated with 1000 cells were optimal for measuring extent for growth and invasion over the assay time of 72 h (data not shown).

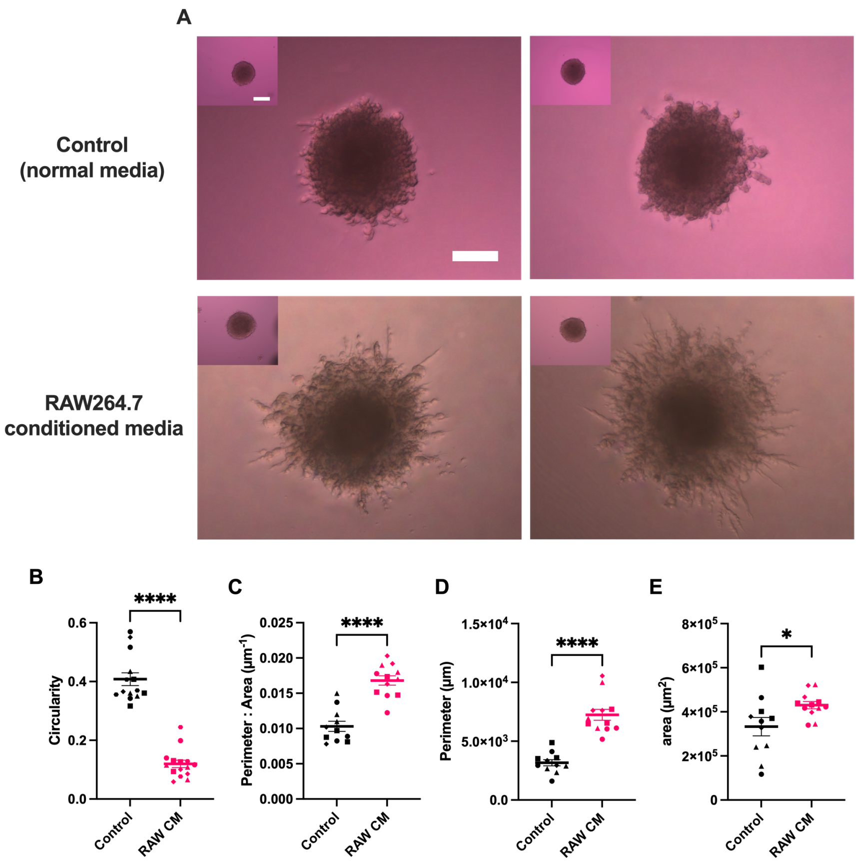

Figure 3.3. Validation of LLC1/LL2-luc spheroid invasion assay. Spheroids generated from LLC1/LL2-luc cells were embedded in Matrigel and treated with control (normal medium) or RAW264.7 conditioned medium. (**A**) Spheroids were imaged at the time of treatment (day 0, corner inset image) and at 3 days-post treatment (scale bar = 200µm). Two representative spheroids per treatment are shown. Images were then analyzed in Fiji for (**B**) circularity, (**C**) P:A ratio, (**D**) perimeter, and (**E**) area. Each datapoint indicates a single spheroid, with datapoints of the same symbol corresponding to spheroids within the same experimental replicate. n=2-3 spheroids per experiment for N=3 experiments. Statistical analysis via unpaired t-test, * $p<0.05$, **** $p<0.001$.

Spheroids were embedded in Matrigel and treated with either control (normal growth medium) or RAW264.7 conditioned media (mCM) and imaged. After three days of incubation, spheroids were imaged again (Figure 3.3A) and quantitative image analysis of circularity was performed as a measure of invasion. The circularity of mCM treated spheroids significantly decreased compared to control (Figure 3.3B), indicating a greater level of invasion. The perimeter:area (P:A) ratio, perimeter, and area of mCM treated spheroids all increased compared to control (Figure 3.3C-E). These data indicate that mCM can induce substantial spheroid invasion, which can be quantified as a decrease in circularity.

NRF2 inhibitor effect on invasion

To test the effects of novel NRF2 inhibitors on tumor spheroid invasion, spheroids were embedded and treated with 10 μM MSU38225, 10 μM MSU-71 or vehicle (DMSO) and imaged. After three days of incubation, spheroids were imaged again (Figure 3.4A). Consistent with results in Fig. 3.3, mCM treatment resulted in significantly increased invasion as measured by a decrease in spheroid circularity. Treatment with MSU38225 slightly increased circularity, and MSU-71 treatment completely blocked mCM-induced invasion (Figure 3.4B). Both compounds significantly reduced spheroid perimeter (Figure 3.4D), and MSU-71 significantly reduced spheroid area compared to mCM alone (Figure 3.4E). Taken together, these data indicate that MSU-71, and potentially MSU38225, are effective at decreasing spheroid invasion and that MSU-71 may also decrease spheroid viability.

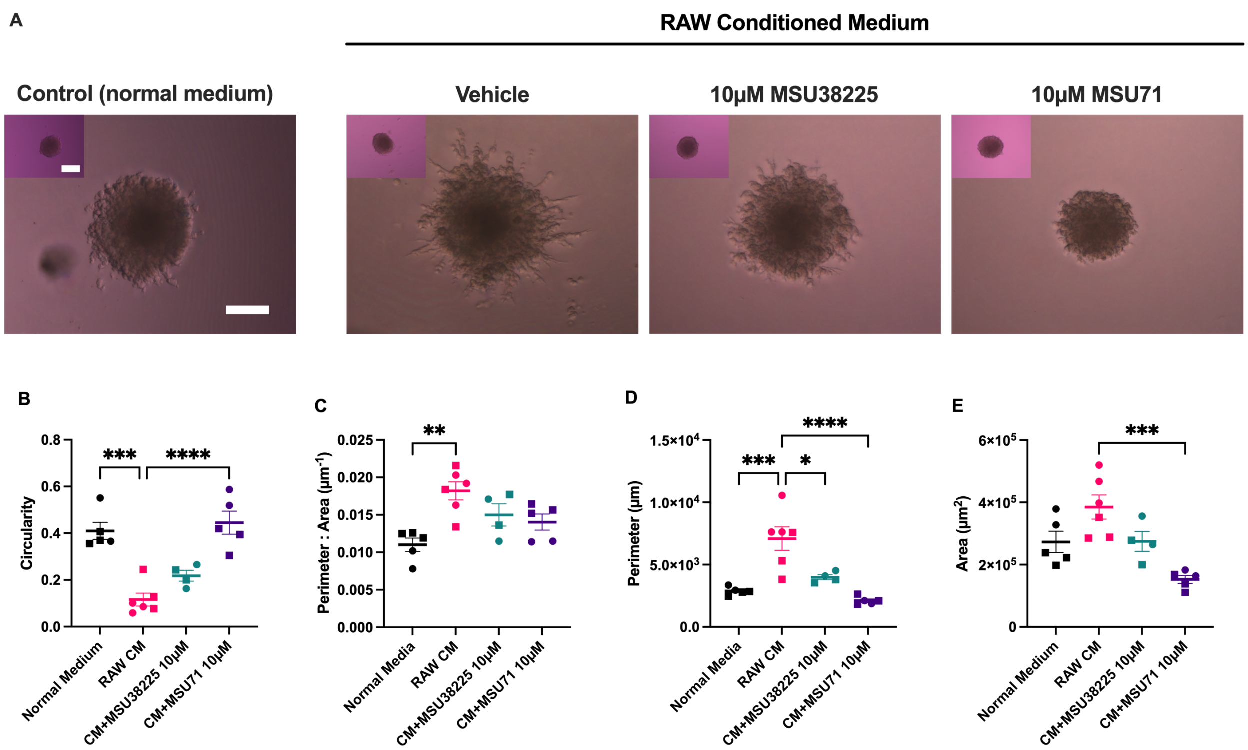

Figure 3.4. NRF2 inhibition blocks RAW CM-induced invasion of LLC1/LL2-luc spheroids. LLC1/LL2-luc spheroids were generated, embedded in Matrigel, and treated with control (normal medium), or RAW264.7 conditioned media ± NRF2 inhibitors MSU38225 or MSU-71. **A**) Spheroids were imaged at the time of treatment (day 0, corner inset image) and at 3 days-post treatment (scale bars = 200µm). Images were then analyzed in Fiji for circularity (**B**), P:A ratio (**C**), perimeter (**D**), and area (**E**). n=2-3 spheroids per experiment for N=2 experiments. Statistical analysis via one-way ANOVA with Tukey post-test, *p<0.05, **p<0.01, ***p<0.005 **** p<0.001.

Interestingly, treatment with MSU-71 decreased both invasion and size of spheroid, as determined by circularity and area, respectively. This supports the idea that NRF2 inhibition may reduce both viability and metastatic potential in lung cancer.

Adaptation for human 3D tumor spheroids

To adapt the LLC/LL2 tumor spheroid invasion platform to human cell lines, spheroids were generated from dissociated A549 cells via the hanging drop method. To generate macrophage conditioned media, the human monocyte-like line THP-1 was first differentiated by treatment with phorbol ester. After differentiation, CM was generated over 48h from THP-1 "M_0" macrophages (M_0 macrophage CM) or from a co-culture of A549 and THP-1 M_0s at a 1:2 ratio (tumor:macrophage), referred to as co-culture CM (co-culture CM). Spheroids were embedded and treated with control (RPMI+5% FBS), M_0 macrophage CM or co-culture CM and imaged (day 0). After three days spheroids were imaged again (Figure 3.5A) and analyzed in the same fashion as LLC1/LL2 spheroids (Figure 3.5B-E). M_0 macrophage CM induced invasion of A549 spheroids, as quantified by a significant decrease in spheroid circularity compared with control medium. This indicates that macrophage secreted factor(s) increased tumor spheroid invasion. In contrast to findings in the murine system, M_0 macrophage CM did not increase spheroid area compared with control, indicating the lack of a growth effect. The perimeter was increased, resulting in an increase in the P:A, another metric for invasiveness. Taken together, A549 spheroids display significant increases in invasion when treated with either M_0 macrophage CM or co-culture CM.

Discussion

The importance of NRF2 pathway alterations to LUAD metastasis has become increasingly apparent. NRF2 pathway alterations are present in about 15% of LUAD (Figure 1.1), primarily resulting from KEAP1 mutations that result in constitutive activation of NRF2. Importantly, oncogenic KRAS–present in up to 20% of lung cancers–can also increase NRF2 activity [DeNicola et al. 2011][Tao et al. 2014], indicating ever a greater fraction of lung cancers have upregulated NRF2 pathway. NRF2 has been connected to LUAD invasion, migration, and metastasis primarily through its relationship with BACH1 [Wiel et al. 2019]. The hypothesis investigated in this chapter is that the NRF2 pathway is critical for LUAD invasion. To explore this hypothesis, the impact of NRF2 pathways inhibitors on LUAD cell migration and macrophage-induced 3D tumor invasion was evaluated. The data show that MSU-71 profoundly blocks invasion, consistent with the ascribed roles for NRF2 in LUAD metastasis animal models. There could, however, be hitherto unidentified targets of MSU-71 that contribute to the effects observed. Further experiments examining the impact of MSU-71, or related compounds, on NRF2 targets that orchestrate metastasis, such as BACH1, will shed mechanistic light on these issues.

The role of NRF2 in the tumor microenvironment is less straightforward than its function in tumor cells [de la Vega et al. 2018]. NRF2 is involved in feedback loops between tumor cells and macrophages, wherein tumor cells elicit in macrophages an M2 phenotype and macrophages in turn elicit EMT of the tumor cells [Feng et al. 2018]. Macrophage conditioned medium has previously been used to promote invasion of LUAD tumor spheroids [Lim et al. 2020]. The studies presented in this chapter show that the addition of THP-1 macrophages to the bottom chamber of transwell migration assays significantly increases the migration of A549 cells (Figure A1). While NRF2 signaling in tumor cells is important for metastatic potential, it is unclear how NRF2 signaling in macrophages affects the metastatic phenotype. Myeloid-specific NRF2 ablation has been shown to increase lung metastases from subcutaneous 3LL tumors (line derived LLC1) [Hiramoto et al. 2014]. Thus, a rationale could be made for activation of NRF2 in macrophages as a therapeutic strategy in

LUAD. Drugs developed to modulate the physiology of only tumor associated macrophages could potentially be formulated for strategic drug delivery with nanoparticles, which are preferentially taken up by phagocytic macrophages [Walkey et al. 2012].

Spheroids can be readily formed from both the A549 and LLC1/LL2 lines for use in 3D invasion assays [Madajewski et al. 2015] [Takahashi et al. 2020]. A549, one of the most widely

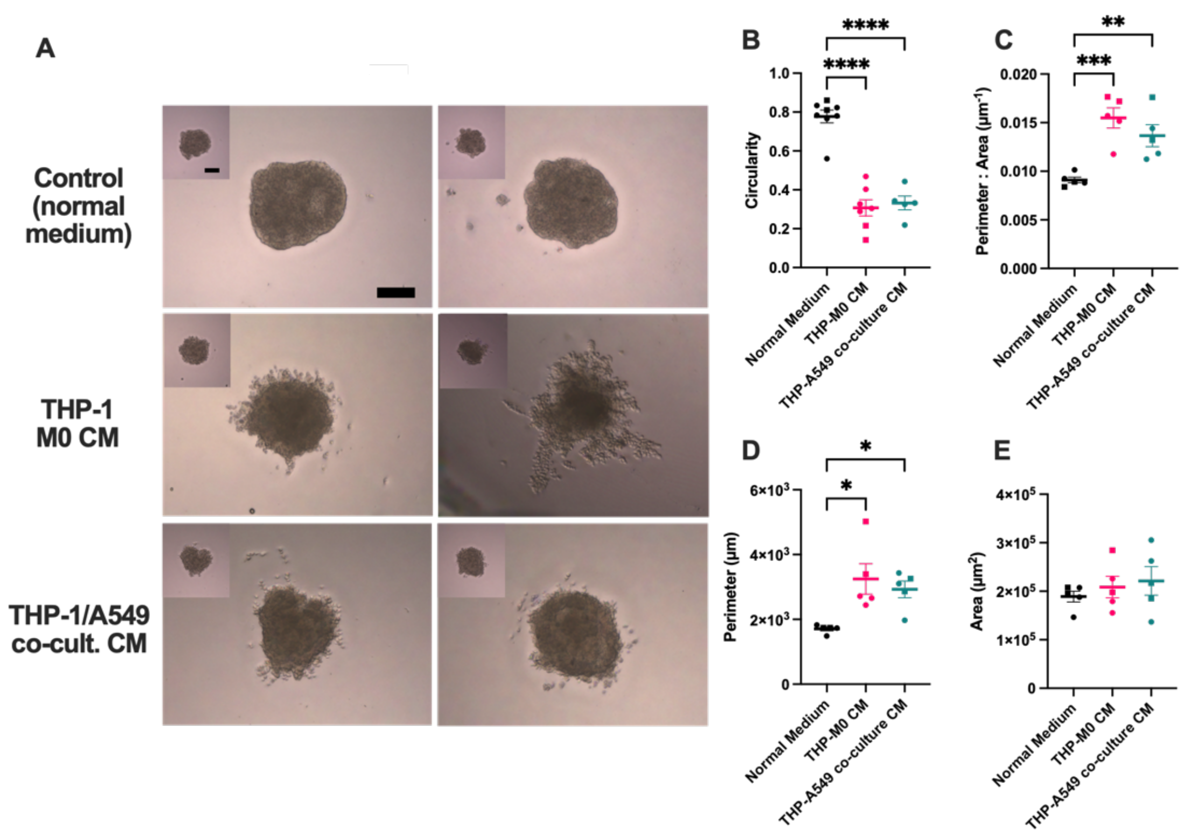

Figure 3.5. Spheroid invasion assay in a human lung adenocarcinoma line. A549 cells were used to generate spheroids, which were then embedded in Matrigel and treated with control (normal media), THP-1 M_0 CM, or THP-1/A549 co-culture CM. (**A**) Spheroids (two representatives per treatment shown) were imaged at the time of treatment (day 0, corner inset image) and at 3 days-post treatment (scale bars = 200µm). Images were then analyzed in Fiji for circularity (**B**), P:A ratio (**C**), perimeter (**D**), and area (**E**). Each datapoint indicates a single spheroid, with like shapes being from the same batch of spheroids/CMs. n=2-3 spheroids per experiment for N=2 experiments. Statistical analysis via one-way ANOVA with Tukey post-test, * $p<0.05$, ** $p<0.01$, *** $p<0.005$, **** $p<0.001$.

used human LUAD cell lines, has mutations in KRAS as well as in KEAP1, and STK11, allowing for the study of oncogenically upregulated NRF2. The murine LLC1/LL2 has become a valuable syngeneic model of KRAS mutant LUAD, and the luciferase-expressing line used here has utility for *in vivo* imaging systems (IVIS). While LLC1/LL2 cells have wildtype KEAP1, oncogenic KRAS is known to sufficiently upregulate NRF2 transcription via AP-1 as has been demonstrated in other engineered murine cell lines and *in vivo* mouse models [DeNicola et al. 2011][Tao et al. 2014].

A key feature of developing a quantitative invasion assay was selection of a metric that distinguishes invasion from growth. The collective cell migration seen in the LLC1/LL2 spheroids (Figure 3.3A) necessarily increases the perimeter of the spheroids; however, measurement of perimeter alone (Figure 3.3C) can also capture spheroid growth absent invasion. Taking this into consideration, *circularity* was selected as the optimal metric. Circularity—defined as $4\pi(\text{area}\div\text{perimeter}^2)$—captures the invasiveness of the spheroids while also controlling for non-invasive growth. Notably, a *decrease* of circularity corresponds to an *increase* of invasion since the perimeter increases more rapidly relative to the area (Figure 3.3B). A second metric, perimeter:area (P:A) ratio (Figure 3.3C), provides a second, more intuitive readout of invasion, where an increase in the value reflects an increase in invasion. Area (Figure 3.3E) can also be used as a measure of spheroid growth and viability, as change in spheroid diameter (ΔD) was in Chapter 2, assuming all spheroids start at the same size.

In this study, macrophage conditioned medium robustly induced LUAD 3D tumor spheroid invasion, which was effectively blocked by MSU-71. The components within the macrophage conditioned medium that are responsible for this effect are yet unidentified. In principle, secreted protein factors or metabolites could induce invasion. An interesting observation is that the mCM tended to be more acidic than control medium as judged by the color of the phenol red containing medium. In fact, the metabolites lactate and oxalate have been implicated in TAM-tumor cell feedback loops resulting in tumor cell EMT [Feng et al. 2018], and the BACH1 target genes *HK2* and *GAPDH*—both glycolytic enzymes—were identified as essential for NRF2-mediated metastasis [Wiel et al. 2019]. This is an interesting area that deserves further study, as it may increase our understanding of both NRF2 signaling and macrophage-mediated cancer metastasis.

While activators of NRF2 are numerous, direct inhibitors of NRF2 are limited. Brusatol, a phytochemical of the quassinoid family, inhibits NRF2 as well as many proteins with rapid turnover rates since it acts as a broad inhibitor of translation [Savage 2018]. Brusatol has been shown to reverse EMT [Aarthi 2019] and may modulate ferroptosis [Kuang et al. 2021]. To identify novel NRF2 pathway inhibitors, an ARE-luc reporter screen was conducted, and the initial hit compound from this project, MSU38225, has shown promise in preclinical models of lung cancer in combination with chemotherapy [Zhang et al. 2021].

MSU-71 was synthesized as a derivative of MSU38225 as part of an effort to develop NRF2 inhibitors with improved drug-like properties and was shown to be more potent than MSU38225 in decreasing viability of KEAP-1 mutant cell lines NCI-H460 and A549 (Liby and Odom labs, in preparation). This improved potency is also seen in the transwell migration assays where the inhibitory effect of MSU-71 on migration was greater than that of MSU38225

(Figure 3.2A). In the spheroid invasion model presented here (Figure 3.4), while the 10μM MSU38225 treatment trended toward decreased invasiveness of LLC1/LL2 spheroids, it did not reach statistical significance. However, 10μM MSU-71 completely blocked invasion, and additionally decreased spheroid size overall (Figure 3.4E), indicating that this improved compound may decrease viability or increase death of tumor cells in the lung spheroids. More investigation into the effects of MSU-71 needs to be conducted to fully decipher the mechanisms behind these phenomena.

Adapting the LLC1/LL2 spheroid invasion model to human cell lines required generation of mCM with human macrophages. The THP-1 cell line is a widely used human monocytic leukemia line. Rather than directly generating conditioned media as with RAW267.4 cells, THP-1 monocytes need to be first differentiated into macrophages with PMA, a protein kinase C (PKC) activator [Lund et al. 2016], which produces unpolarized macrophages (M_0). Macrophages exist as diverse and heterogeneous populations, and while tumor associated macrophages (TAMs) display markers associated with both classical (M_1) and alternative (M_2) subtypes, A549 cells have been shown to polarize THP-1 macrophages to a CD206+ M_2–like phenotype [Larianova et al. 2020][Guo et al. 2019].

This study marks, to the author's knowledge, the first instance wherein THP-1 conditioned media was used to elicit human NSCLC spheroid invasion. A549 spheroids became much more invasive when treated with both M_0 macrophage CM and co-culture CM (Figure 3.5), indicating that factors produced by both unpolarized macrophages and co-cultured tumor cells/macrophages are sufficient to induce a change in spheroid phenotype.

The invasion observed in these A549 spheroids was markedly different from the LLC1/LL2 spheroids, potentially indicating a loss of cell-cell junctions, rather than collective invasion. The human NCI-H23 spheroids did, however, undergo collective cell invasion (Figure A2), while the NCI-H358 (Figure A3), NCI-H460 (Figure A4), and NCI-1975 (Figure A5) spheroids had no observable invasion in any condition. Each of these cell lines harbor unique mutational profiles, which may influence their invasiveness in this model (Table A1). Matrigel has emerged as the standard ECM for 3D cell culture. However, Matrigel and other laminin-rich matrices generally restrict tumor cell invasion to lobopodial phenotypes, whereas collagen—the most abundant protein in the lung ECM [Götte & Kovalszky 2018]—is typically more permissive of invasion and mesenchymal phenotypes [Anguiano et al. 2017]. The addition of Matrigel to the culture medium of normally loosely adherent and epithelioid LLC1/LL2 cells indeed changes morphology to a more firmly adherent and mesenchymal phenotype (Figure A6). Further examination of the impact of ECM that reflects the lung TME on LUAD spheroid invasion would be worthwhile.

The results of these studies demonstrate the potential efficacy of MSU-71 in inhibiting lung tumor metastatic potential. While MSU-71 blocks NRF2 signaling, future studies will be required to identify specific targets of this compound and to elucidate the mechanism(s) by which it blocks migration and invasion. NRF2 promotes pro-metastatic genes through both BACH1 dependent and independent mechanisms (Figure 3.6). Expanding these studies by incorporating additional components and/or cell types of the lung tumor microenvironment could provide a more complete picture of the effects of NRF2 and MSU-71 (and other compounds) on lung cancer progression. Forthcoming pre-clinical mouse model studies with MSU-71 will provide further useful insights into its *in vivo* efficacy and ultimately its potential as a therapeutic in NRF2 driven LUAD.

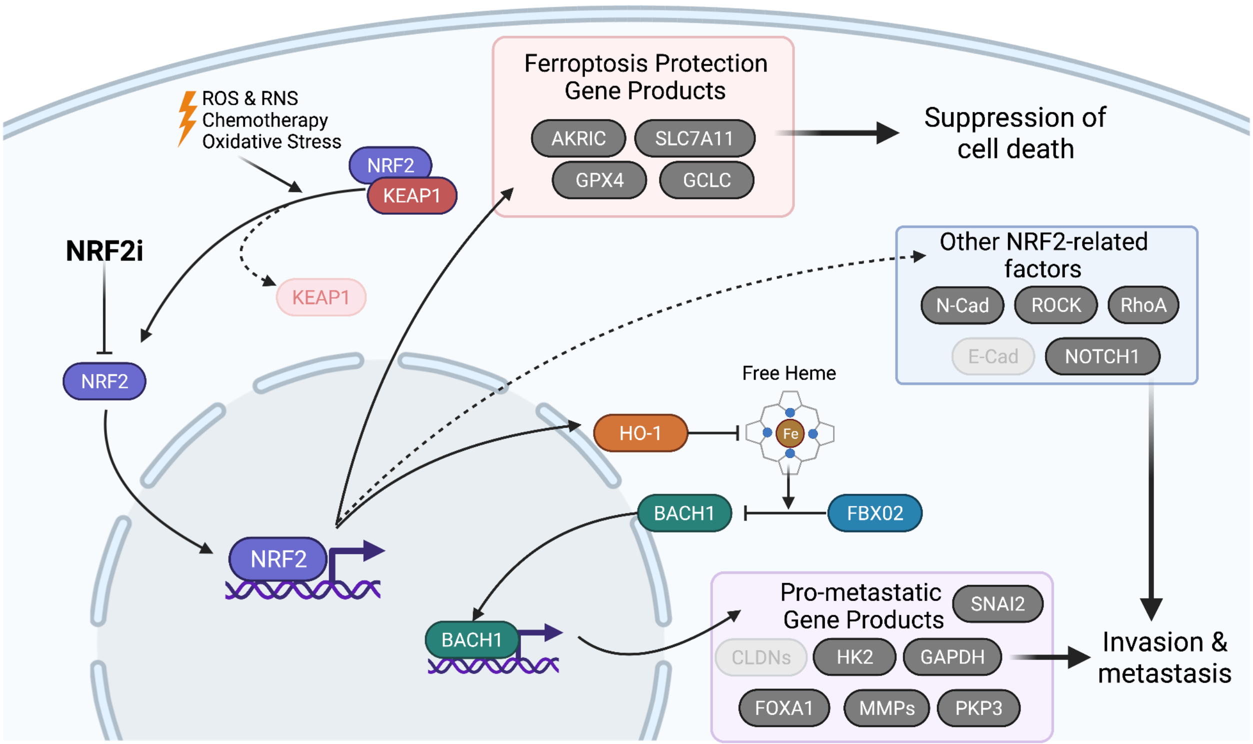

Figure 3.6. Mechanistic model of NRF2 inhibitors in NSCLC. NRF2, normally sequestered and marked for degradation by KEAP1, is liberated by reactive oxygen/nitrogen species (ROS/RNS), chemotherapy, or other oxidative stressors. NRF2 is also constitutively liberated by KEAP1 mutation. Transcriptionally active NRF2 promotes expression of genes involved in protection from ferroptosis, preventing cell death. NRF2 also promotes metastasis-associated gene expression, either directly, or by stabilization of BACH1 through HO-1.

APPENDIX

Table A1. Human NSCLC cell lines used in chapter 3

Cell Line	Common LUAD Mutations				NRF2 Pathway Mutations			
	TP53	*KRAS*	*EGFR*	*ALK*	*KEAP1*	*STK11*	*NFE2L2*	*CUL3*
A549	WT	**G12S**	WT	WT	**G333C**	**Q37***	WT	WT
NCI-H1975	**R273H**	WT	**T790M**	WT	WT	WT	WT	WT
NCI-H23	**M246I**	**G12C**	WT	WT	**Q193H**	**W332***	WT	WT
NCI-H358	**Deletion**	**G12C**	WT	WT	WT	WT	WT	WT
NCI-H460	WT	**Q61H**	WT	WT	**D236H**	**Q37***	WT	**T410I**

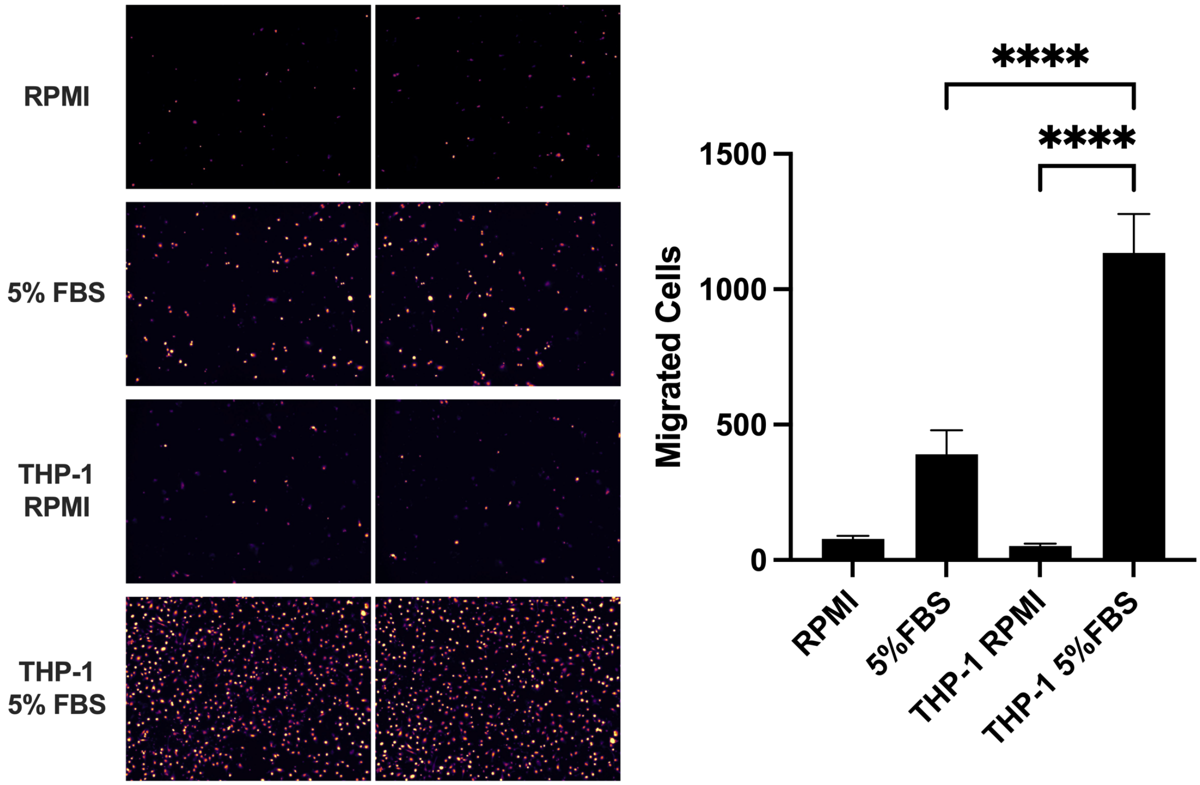

Figure A1. A549 transwell migration is enhanced by THP-1 macrophages. A549 cells were seeded in serum-free medium in the top chamber of transwells. Media containing 5% FBS, differentiated THP-1 macrophages, or the combination of both were used as chemoattractant in the bottom chamber and A549s were allowed to migrate for 24 h, at which point filters were fixed, unmigrated cells removed, and remaining cells were stained with DAPI, and imaged (9 fields per transwell insert). n=2 transwell inserts per experiment, N=2 experimental replicates. Statistical analysis via one-way ANOVA with Tukey post-test; **** p<0.001.

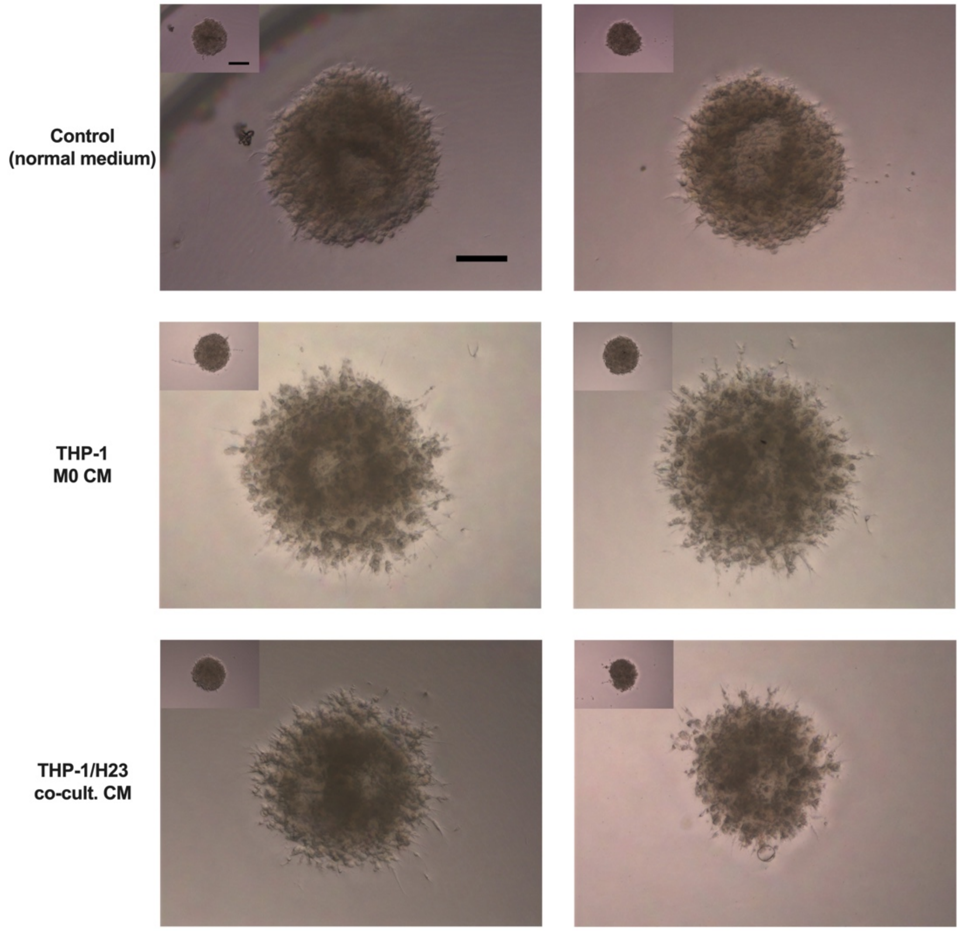

Figure A2. NCI-H23 spheroid invasion. NCI-H23 cells were used to generate spheroids, which were then embedded in Matrigel and treated with control (normal media), THP-1 M0 CM, or THP-1/NCI-H23 co-culture CM. Spheroids (two representatives per treatment shown) were imaged at the time of treatment (day 0, corner inset image) and at 3 days-post treatment (scale bars = 200μm).

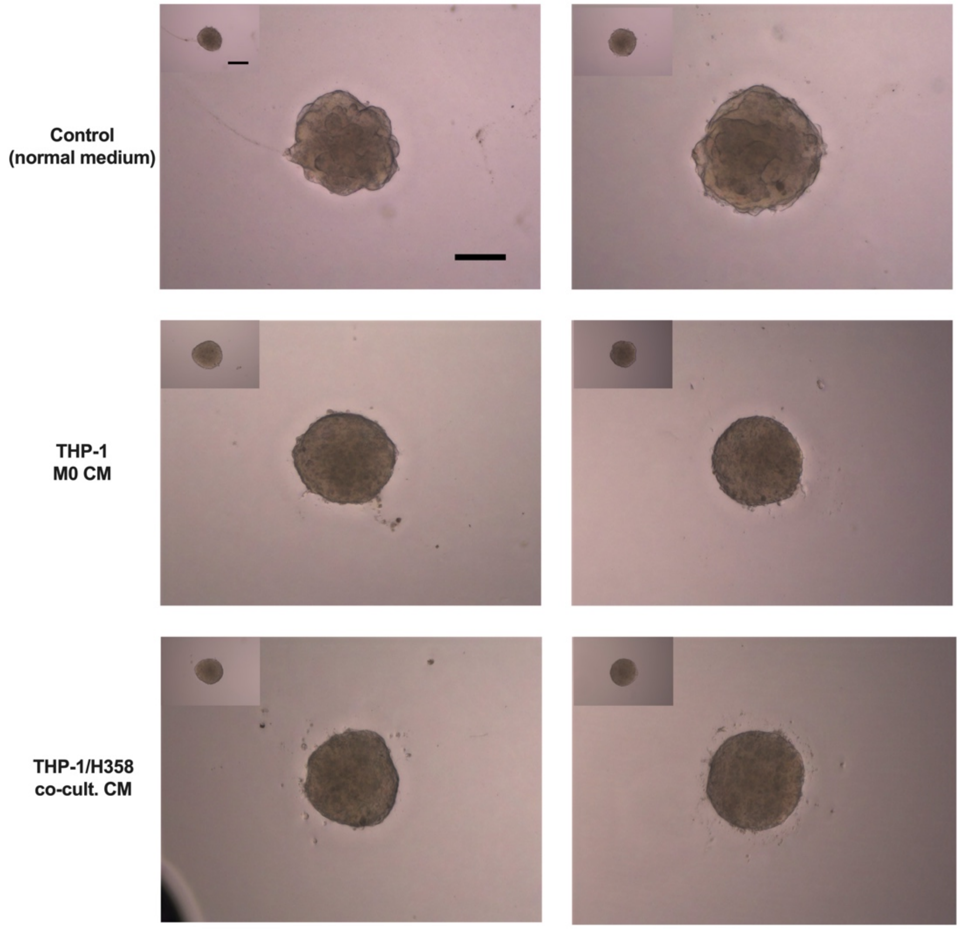

Figure A3. NCI-H358 spheroid invasion. NCI-H358 cells were used to generate spheroids, which were then embedded in Matrigel and treated with control (normal media), THP-1 M0 CM, or THP-1/NCI-H358 co-culture CM. Spheroids (two representatives per treatment shown) were imaged at the time of treatment (day 0, corner inset image) and at 3 days-post treatment (scale bars = 200μm).

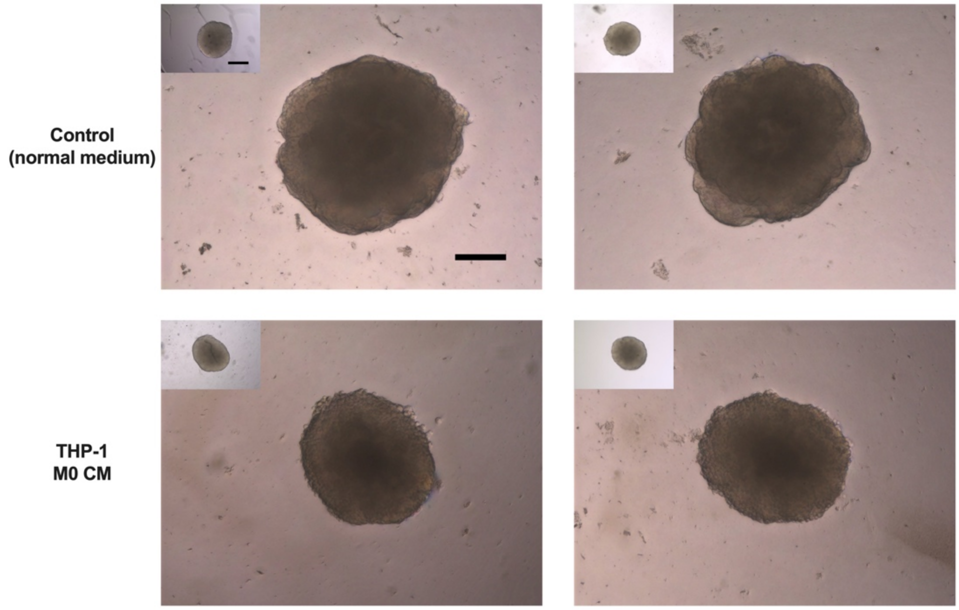

Figure A4. NCI-H460 spheroid invasion. NCI-H460 cells were used to generate spheroids, which were then embedded in Matrigel and treated with control (normal media), or THP-1 M0 CM. Spheroids (two representatives per treatment shown) were imaged at the time of treatment (day 0, corner inset image) and at 3 days-post treatment (scale bars = 200μm).

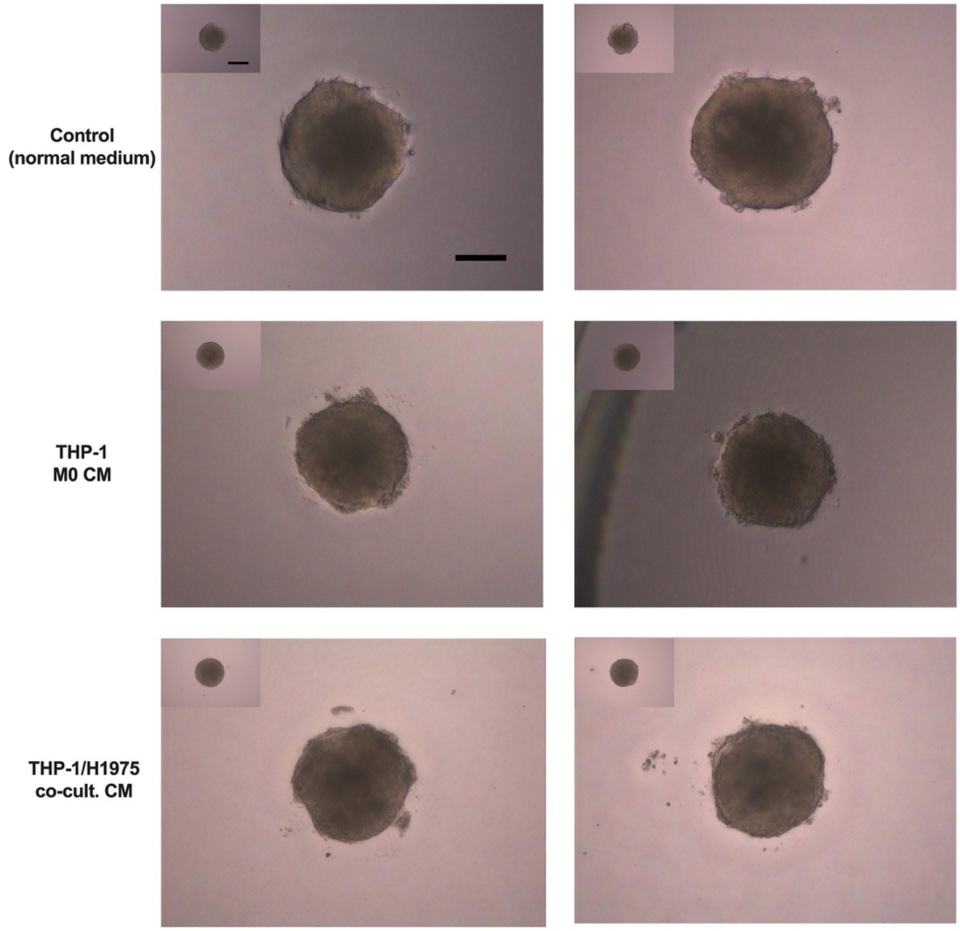

Figure A5. NCI-H1975 spheroid invasion. NCI-H1975 cells were used to generate spheroids, which were then embedded in Matrigel and treated with control (normal media), THP-1 M0 CM, or THP-1/NCI-H1975 co-culture CM. (**A**) Spheroids (two representatives per treatment shown) were imaged at the time of treatment (day 0, corner inset image) and at 3 days-post treatment (Scale bars = 200μm).

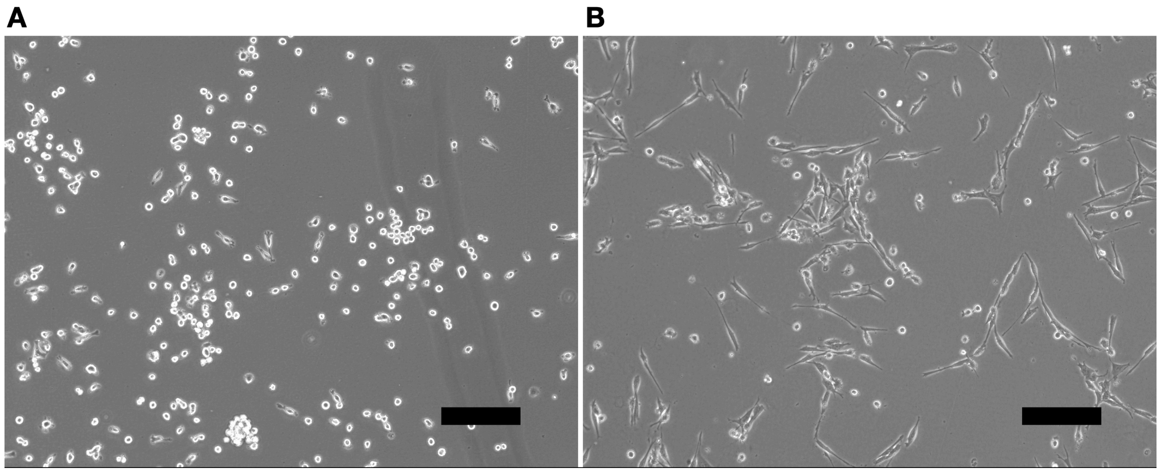

Figure A6. Matrigel changes morphology of LLC1/LL2 cells in 2D culture. 105 LLC1/LL2 were plated on a 35mm plate and allowed to loosely adhere overnight, at which point (**A**) normal growth medium or (**B**) medium supplemented with 5% Matrigel was added. After 24h, cells were imaged (Scale bars = 200μm).

Supplemental Information 1. Transwell migration analysis macro.

```
run("Images to Stack", "name=Stack title=[] use");

run("8-bit");

setAutoThreshold("Moments dark");

//run("Threshold...");

setOption("BlackBackground", false);

run("Convert to Mask", "method=Moments background=Dark calculate");

run("Watershed", "stack");

run("Remove Outliers...", "radius=2 threshold=50 which=Dark stack");

run("Analyze Particles...", "size=10-1000 pixel display summarize add in_situ stack");
```

REFERENCES

REFERENCES

Arfmann-Knübel, Sarah, Birte Struck, Geeske Genrich, Ole Helm, Bence Sipos, Susanne Sebens, and Heiner Schäfer. "The crosstalk between Nrf2 and TGF-β1 in the epithelial-mesenchymal transition of pancreatic duct epithelial cells." *PloS one* 10, no. 7 (2015): e0132978.

Aarthi, R. "Brusatol-as potent chemotherapeutic regimen and its role on reversing EMT transition." *Journal of Pharmaceutical Sciences and Research* 11, no. 5 (2019): 1753-1762.

Anandhan, Annadurai, Matthew Dodson, Cody J. Schmidlin, Pengfei Liu, and Donna D. Zhang. "Breakdown of an ironclad defense system: the critical role of NRF2 in mediating ferroptosis." *Cell chemical biology* 27, no. 4 (2020): 436-447.

Anderson, Nicole M., and M. Celeste Simon. "BACH1 orchestrates lung cancer metastasis." *Cell* 178, no. 2 (2019): 265-267.

Campbell, Joshua D., Anton Alexandrov, Jaegil Kim, Jeremiah Wala, Alice H. Berger, Chandra Sekhar Pedamallu, Sachet A. Shukla et al. "Distinct patterns of somatic genome alterations in lung adenocarcinomas and squamous cell carcinomas." *Nature genetics* 48, no. 6 (2016): 607-616.

de la Vega, Montserrat Rojo, Eli Chapman, and Donna D. Zhang. "NRF2 and the hallmarks of cancer." *Cancer cell* 34, no. 1 (2018): 21-43.

Dixon, Scott J., Kathryn M. Lemberg, Michael R. Lamprecht, Rachid Skouta, Eleina M. Zaitsev, Caroline E. Gleason, Darpan N. Patel et al. "Ferroptosis: an iron-dependent form of nonapoptotic cell death." *Cell* 149, no. 5 (2012): 1060-1072.

Feng, Rui, Yuji Morine, Tetsuya Ikemoto, Satoru Imura, Shuichi Iwahashi, Yu Saito, and Mitsuo Shimada. "Nrf2 activation drive macrophages polarization and cancer cell epithelial-mesenchymal transition during interaction." *Cell Communication and Signaling* 16, no. 1 (2018): 1-12.

Han, Wenyan, Yiqun Zhang, Cong Niu, Jieyu Guo, Jiajia Li, Xiangxiang Wei, Mengping Jia, Xiuling Zhi, Liangqing Yao, and Dan Meng. "BTB and CNC homology 1 (Bach1) promotes human ovarian cancer cell metastasis by HMGA2-mediated epithelial-mesenchymal transition." *Cancer letters* 445 (2019): 45-56.

Hanahan, Douglas, and Robert A. Weinberg. "The hallmarks of cancer." *Cell* 100, no. 1 (2000): 57-70.

Hassannia, Behrouz, Peter Vandenabeele, and Tom Vanden Berghe. "Targeting ferroptosis to iron out cancer." *Cancer cell* 35, no. 6 (2019): 830-849.

Hiramoto, Keiichiro, Hironori Satoh, Takafumi Suzuki, Takashi Moriguchi, Jingbo Pi, Tooru Shimosegawa, and Masayuki Yamamoto. "Myeloid lineage–specific deletion of antioxidant system enhances tumor metastasis." *Cancer Prevention Research* 7, no. 8 (2014): 835-844.

Igarashi, Kazuhiko, Hironari Nishizawa, Yuriko Saiki, and Mitsuyo Matsumoto. "The transcription factor BACH1 at the crossroads of cancer biology: From epithelial–mesenchymal transition to ferroptosis." *Journal of Biological Chemistry* 297, no. 3 (2021).

Kansanen, Emilia, Suvi M. Kuosmanen, Hanna Leinonen, and Anna-Liisa Levonen. "The Keap1-Nrf2 pathway: Mechanisms of activation and dysregulation in cancer." *Redox biology* 1, no. 1 (2013): 45-49.

Kuang, Feimei, Jiao Liu, Yangchun Xie, Daolin Tang, and Rui Kang. "MGST1 is a redox-sensitive repressor of ferroptosis in pancreatic cancer cells." *Cell Chemical Biology* 28, no. 6 (2021): 765-775.

Lignitto, Luca, Sarah E. LeBoeuf, Harrison Homer, Shaowen Jiang, Manor Askenazi, Triantafyllia R. Karakousi, Harvey I. Pass et al. "Nrf2 activation promotes lung cancer metastasis by inhibiting the degradation of Bach1." *Cell* 178, no. 2 (2019): 316-329.

Papillon-Cavanagh, Simon, Parul Doshi, Radu Dobrin, Joseph Szustakowski, and Alice M. Walsh. "STK11 and KEAP1 mutations as prognostic biomarkers in an observational real-world lung adenocarcinoma cohort." *ESMO open* 5, no. 2 (2020): e000706.

Popper, Helmut H. "Progression and metastasis of lung cancer." *Cancer and Metastasis Reviews* 35, no. 1 (2016): 75-91.

Probst, Brandon L., Lyndsey McCauley, Isaac Trevino, W. Christian Wigley, and Deborah A. Ferguson. "Cancer cell growth is differentially affected by constitutive activation of NRF2 by KEAP1 deletion and pharmacological activation of NRF2 by the synthetic triterpenoid, RTA 405." *PLoS One* 10, no. 8 (2015): e0135257.

Sato, Masaki, Mitsuyo Matsumoto, Yuriko Saiki, Mahabub Alam, Hironari Nishizawa, Masahiro Rokugo, Andrey Brydun et al. "BACH1 Promotes Pancreatic Cancer Metastasis by Repressing Epithelial Genes and Enhancing Epithelial–Mesenchymal Transition." *Cancer research* 80, no. 6 (2020): 1279-1292.

Satoh, Hironori, Takashi Moriguchi, Jun Takai, Masahito Ebina, and Masayuki Yamamoto. "Nrf2 prevents initiation but accelerates progression through the Kras signaling pathway during lung carcinogenesis." *Cancer research* 73, no. 13 (2013): 4158-4168.

Savage, Matthew Connor. "Toward understanding the inhibition of Nrf2 protein levels by reactive oxygen species or a histone deacetylase inhibitor." PhD diss., Villanova University, 2018.

SEER*Explorer: An interactive website for SEER cancer statistics [Internet]. Surveillance Research Program, National Cancer Institute. [Cited 2021 September 27]. Available from https://seer.cancer.gov/explorer/

Sun, Jiying, Hideto Hoshino, Kazuaki Takaku, Osamu Nakajima, Akihiko Muto, Hiroshi Suzuki, Satoshi Tashiro et al. "Hemoprotein Bach1 regulates enhancer availability of heme oxygenase‐1 gene." *The EMBO journal* 21, no. 19 (2002): 5216-5224.

Tao, Shasha, Shue Wang, Seyed Javad Moghaddam, Aikseng Ooi, Eli Chapman, Pak K. Wong, and Donna D. Zhang. "Oncogenic KRAS confers chemoresistance by upregulating NRF2." *Cancer research* 74, no. 24 (2014): 7430-7441.

Walkey, Carl D., Jonathan B. Olsen, Hongbo Guo, Andrew Emili, and Warren CW Chan. "Nanoparticle size and surface chemistry determine serum protein adsorption and macrophage uptake." *Journal of the American Chemical Society* 134, no. 4 (2012): 2139-2147.

Wiel, Clotilde, Kristell Le Gal, Mohamed X. Ibrahim, Chowdhury Arif Jahangir, Muhammad Kashif, Haidong Yao, Dorian V. Ziegler et al. "BACH1 stabilization by antioxidants stimulates lung cancer metastasis." *Cell* 178, no. 2 (2019): 330-345.

Wilson, Carter J., Megan Chang, Mikko Karttunen, and Wing-Yiu Choy. "KEAP1 Cancer Mutants: A Large-Scale Molecular Dynamics Study of Protein Stability." *International journal of molecular sciences* 22, no. 10 (2021): 5408.

Zhang, Chao, Hui-Jie Wang, Qi-Chao Bao, Lei Wang, Tian-Kun Guo, Wei-Lin Chen, Li-Li Xu et al. "NRF2 promotes breast cancer cell proliferation and metastasis by increasing RhoA/ROCK pathway signal transduction." *Oncotarget* 7, no. 45 (2016): 73593.

Zhang, Di, Zhilin Hou, Kelly E. Aldrich, Lizbeth Lockwood, Aaron L. Odom, and Karen T. Liby. "A novel Nrf2 pathway inhibitor sensitizes Keap1-mutant lung cancer cells to chemotherapy." Molecular *Cancer Therapeutics* (2021).

Zhao, Qiuyue, Aihong Mao, Ruoshui Guo, Liping Zhang, Jiawei Yan, Chao Sun, Jinzhou Tang, Yancheng Ye, Yanshan Zhang, and Hong Zhang. "Suppression of radiation-induced migration of non-small cell lung cancer through inhibition of Nrf2-Notch Axis." *Oncotarget* 8, no. 22 (2017): 36603.